Calhoun: The NPS Institutional Archive
DSpace Repository

Theses and Dissertations 1. Thesis and Dissertation Collection, all items

1966-05

Analysis and synthesis of a pure fluid state attitude control system.

Lewis, Jack W.

Massachusetts Institute of Technology

http://hdl.handle.net/10945/9436

Downloaded from NPS Archive: Calhoun

Calhoun is the Naval Postgraduate School's public access digital repository for research materials and institutional publications created by the NPS community. Calhoun is named for Professor of Mathematics Guy K. Calhoun, NPS's first appointed -- and published -- scholarly author.

Dudley Knox Library / Naval Postgraduate School
411 Dyer Road / 1 University Circle
Monterey, California USA 93943

http://www.nps.edu/library

NPS ARCHIVE
1966
LEWIS, J.

ANALYSIS AND SYNTHESIS OF A PURE FLUID STATE ATTITUDE CONTROL SYSTEM

by

Jack W. Lewis

Thesis Supervisor: Herbert H. Richardson
Date Submitted: May 20, 1966

Thesis
L608

ACCOPRESS®
GENUINE PRESSBOARD BINDER
CAT. NO. BF 2507 EMB

ACCO
CHICAGO,
LONDON,

OGDENSBURG, N.Y.
TORONTO,
MEXICO, D. F.

ANALYSIS AND SYNTHESIS OF A PURE FLUID STATE ATTITUDE CONTROL SYSTEM

by

Jack W. Lewis

SUBMITTED IN PARTIAL FULFILLMENT
OF THE REQUIREMENTS FOR THE DEGREE OF
NAVAL ENGINEER
AND THE DEGREE OF
MASTER OF SCIENCE IN MECHANICAL ENGINEERING

at the

MASSACHUSETTS INSTITUTE OF TECHNOLOGY
May, 1966

NPS ARCHIVE
966
EWIS, J.

~~Thesis
L608~~

ANALYSIS AND SYNTHESIS OF A PURE FLUID STATE ATTITUDE CONTROL SYSTEM

Library
U. S. Naval Postgraduate School
Monterey, California

by

Jack W. Lewis

Submitted to the Department of Naval Architecture and Marine Engineering on May 20, 1966, in partial fulfillment of the requirements for the Master of Science degree in Mechanical Engineering and the professional degree, Naval Engineer.

ABSTRACT

A pneumatic, pure fluid control system, capable of maintaining the angular position of an inertia load in a gravitational space, using only one moving part, was designed and built. The control system consisted of a vortex-sink angular rate sensor, a pendulum controlled flapper-nozzle angular position sensor, a summing amplifier and bistable reaction jets. The system was designed to operate in a bang-bang manner in order to reduce errors in a minimum amount of time.

A previous author's work on the vortex-sink angular rate sensor is extended to include information and data on proportional amplification of the output signal and the frequency response of the sensor. Methods for synthesizing the components into a working system are presented along with a theoretical analysis of the system's performance.

Results of experiments performed on the completed system showed that the reaction jets could be switched in a nearly optimal manner when responding to errors introduced on one side of the system, but, due to the unsymmetrical gain of the rate sensor, the errors introduced on the opposite side resulted in a certain amount of after end-point chattering.

Good correlation between theory and experiment led to the conclusion that the application of standard control system design techniques can be readily applied to the design of pure fluid control systems.

Thesis Supervisor: Herbert H. Richardson
Title: Associate Professor of Mechanical Engineering

ACKNOWLEDGMENTS

I wish to express my sincere thanks to Professor Richardson who first introduced me to the subject of pure fluid amplification and whose keen insight into the fundamentals of dynamic systems and fluid control helped me overcome the many problems encountered in this work. I wish also to mention that because of his lively ability as a professor, I first became interested in the field of control systems and that without the warm professor-student relationship experienced with him, I might never have been able to accomplish this work.

My thanks also to Messrs. James Sitomer, Stanley Goodwin and Paul Hinckley of the Instrumentation Laboratory who assisted me in gathering the data on the rate sensor.

Special thanks are due Mr. William Ribich who suggested the design of the position sensor used in this work and who is responsible for the competent photography contained herein.

I would like to thank Messrs. Adam Bell, Paul Blaiklock, Chester Nachtigal, Richard Sidell and David Wormley of the Design and Controls Division of the Mechanical Engineering Department for their friendliness and advice.

Mrs. Martha Buckley is responsible for the competent typing of this thesis.

This thesis was supported in part by the U.S. Air Force under contract AF 33(615)-2210 and sponsored by the Division of Sponsored Research of M.I.T.

TABLE OF CONTENTS

Abstract ii
Acknowledgments. iii
Table of Contents. iv
Table of Figures vi

Chapter

I. INTRODUCTION 1
1.1 General Introduction to Pure Fluid State Technology 1
1.2 Purpose and Scope of Thesis. 1
1.3 Discussion of the Proposed System to Attain the Design Objectives. 2

II. VORTEX ANGULAR RATE SENSOR ANALYSIS AND DESIGN 5
2.1 General Theory of Operation. 5
2.2 Rate Sensor Design and Design Procedure. 20
2.3 Signal Amplification 22
2.4 Rate Sensor Dynamics 32
2.5 Testing Procedure and Results. 34
2.6 Discussion of Results. 35
2.7 Conclusions and Recommendations. 43

III. ANGULAR POSITION SENSOR ANALYSIS AND DESIGN. 45
3.1 Criteria Used in Selecting Operating Principle . . 45
3.2 Position Sensor Description. 45
3.3 Discussion of the Dynamics of a Pendulum Augular Position Sensor. 47
3.4 The Influence of Acceleration on the Output Signal 51
3.5 Transfer Function. 54
3.6 Switching Curve Computer 57

IV. SIGNAL COMPARATOR. 59
4.1 General. 59
4.2 Experimental Analysis. 60
4.3 Discussion of Results and Conclusions. 60

V. DRIVING BISTABLE AMPLIFIERS WITH PROPORTIONAL AMPLIFIERS 63
5.1 Introduction to Input Control Impedances of Bistable Amplifiers. 63
5.2 Problem Statement and Objective of Experiments . . 65
5.3 Test Results and Conclusions 66

VI. POWER AMPLIFIER AND BISTABLE REACTION JETS ANALYSIS AND DESIGN 69
6.1 Determination of the Required Output Thrust 69
6.2 Introductory Theory of Staging Unvented Bistable Amplifiers. 70
6.3 Initial Experimental Design 72
6.4 Final Three Stage Amplifier Design. 79
6.5 Reaction Jet Cascade Dynamics and Transfer Function 82

VII. CONTROL SYSTEM SYNTHESIS, PERFORMANCE AND ANALYSIS. . . 86
7.1 System Synthesis. 86
7.2 System Performance. 91
7.3 System Analysis 100

APPENDIX
A RATE SENSOR CALCULATIONS 103
A.1 Rate Sensor Design Calculations 103
A.2 Calculation of First Stage Supply Pressure. . . . 104

B CALCULATION OF THE REACTION JET TIME DELAY CONSTANT . 106

C SYSTEM ANALYSIS. 110
C.1 Determining the Equation of the Switching Curve . 110
C.2 Limit Cycle Analysis. 112

D PHOTOGRAPHS OF COMPONENTS 121

BIBLIOGRAPHY. 123

TABLE OF FIGURES

Figure Page

1.1 Phase Plane Representation of an Inertia Load Being Driven by a Constant Torque 4
2.1 Vortex Angular Rate Sensor. 6
2.2 Sketch of the Vortex-Sink Angular Rate Sensor 9
2.3 Cross Section of Probe. 10
2.4 Ideal Pressure Distribution Around a Circular Cylinder. 12
2.5 Sketch of Probe in Operation. 14
2.6 Effect of Viscosity on the Pressure Distribution Around a Circular Cylinder. 19
2.7 Typical Proportional Pure Fluid Amplifier 26
2.8 Probe Boundary Pressure Versus No Load Flow 29
2.9 Probe Output Pressure-Flow Characteristics. 30
2.10 Rate Sensor Steady State Output 36
2.11 Rate Sensor Steady State Output 37
2.12 Rate Sensor Frequency Response. 38
2.13 Typical Vortex Rate Sensor Frequency Response Data. . . 39
3.1 Sketch of the Angular Position Sensor 46
3.2 Analytical Model of the Position Sensor 48
3.3 Sketch of the Position Sensor Mounted on the System . . 52
3.4 Typical Steady State Position Sensor Output Showing Approximation to the Ideal Switching Curve. 56
4.1 Typical Summer-Amplifier Test Results 61
5.1 Bistable Fluid Jet Amplifier. 64
5.2 Input Characteristics of a Bistable Amplifier 64
5.3 Effect of Biasing the Controls of a Bistable Amplifier on the Switching Pressures and Flows. 67
6.1 Control Volume for Determining the Output Thrust. . . . 73
6.2 Output Characteristics of the Two Stage Bistable Amplifier Without Driving Amplifier 77
6.3 Output Characteristics of the Two Stage Bistable Amplifier With Driving Amplifier. 78
6.4 Reaction Jet Thrust Versus Supply Pressure. 83
6.5 Reaction Jet Input Characteristics. 84
7.1 Steady State Angular Rate Sensor Output While Loaded into the Summer-Amplifier. 88
7.2 Block Diagram of Complete Control System. 90
7.3 System Circuit Diagram. 92
7.4 Complete Control System and Demonstration Model 93
7.5 System Response, Bang-Bang Control. 94
7.6 System Response, Bang-Bang Control, Reduced Hysteresis. 96
7.7 System Response, Bang-Bang Control, Without Rate Feedback. 97
7.8 System Response, Pulse Width Modulation Control 98

Figure Page

7.9 System Response, PWM Control, Without Rate Feedback. . 99

C.1 Idealized Contactor Servomechanism Controlling an Inertia Load. 111
C.2 Generalized Autonomous Control System Containing a Nonlinear Element. 111
C.3 Polar Plot of $G(j\omega)$ and $-1/K_{eq}$ Without Rate Feedback 116
C.4 Polar Plot of $G(j\omega)$ and $-1/K_{eq}$ With Rate Feedback 116
C.5 Bode Plots of Linear Transfer Function $G(j\omega)$. 118
C.6 Polar Plot of $G(j\omega)$ and $-1/K_{eq}$. 119

D.1 Vortex Rate Sensor Showing Details of Signal Amplification 121
D.2 Summer-Amplifier 121
D.3 Angular Position Sensor. 122
D.4 Power Amplifier Cascade and Reaction Jets. 122

CHAPTER I

INTRODUCTION

1.1 General Introduction to Pure Fluid State Technology

The basic concept of pure fluid amplification is that high energy fluid streams can be controlled by low energy streams. The concept was evolved at the Harry Diamond Laboratories of the U. S. Army Material Command, Washington, D. C. in 1959.

At the First Fluid Amplification Symposium held at the Laboratories in October of 1962, Brigadier General John G. Zierdt described the possible future of these components:

> This advance has removed many of the limitations on conventional military and commercial pneumatic systems and has enabled an extremely rapid extension of their capabilities. The use of low energy flow to direct and control high energy streams permits the design of pure pneumatic components, elements, and systems, capable of amplification, feedback, memory, logic functions, analogue computation, and digital computation. This, in turn, makes it possible to use pneumatic control systems, amplifiers, and computers where they could not be used before.

1.2 Purpose and Scope of Thesis

Since the inception of pure fluid amplification, much

work has been done in analyzing individual components. Recently the emphasis in the field has been turned to the development of complete systems. Although much work has been done along these lines, the quantitative data associated with such systems is scanty and inaccessible.

One objective of this thesis is to develop techniques that may be used in designing, analyzing and synthesizing these components into a working control system.

The specific objective is to develop a pneumatic control system, using as few moving parts as possible, capable of maintaining a commanded angular position of a pure inertia load. Should errors be introduced, the control system is to reduce these errors to near zero in the shortest possible time within the limitations of the prime move used.

Another design objective is to purposely make the system respond slowly so that the device may be used as an educational model demonstrating the working of individual components and the system as a whole.

1.3 Discussion of the Proposed System to Attain the Design Objectives

Minimum time control of a vehicle generally involves the use of the full force available from the prime mover in a bang-bang manner. For example, it is obvious that to move an automobile from a point, A, to another point, B, in a minimum amount of time, the operator should use maximum acceleration, at the right instant lock his brakes and slide into the

desired end point. The operator in this example would be using full driving force in one direction and full braking force in the other to achieve the minimum time objective.

In controlling an angular inertia load, it can be shown that minimum time movements are obtained by using full torque in one direction or the other[1*]. Figure 1.1 shows a phase plane portrait of an inertia load being driven by a constant torque, whose sense is either plus or minus, for various initial conditions.

It can be seen from Figure 1.1 that one curve exists, which, if used as a boundary to switch the sense of the torque, will allow the system to reduce any errors to zero in minimum time. In order to switch the sense of the applied torque at the proper instant, it is obvious that the control system must be able to 1) measure angular positions, 2) measure angular rate, 3) compute the coordinates of the switching curve, and 4) compare the values of angular rate and angular position with the values of the switching curve and switch the sense of the applied torque at the proper instant.

The remaining chapters of this thesis deal with the design of the components needed to accomplish the above mentioned functions and the synthesis of these components into a working system.

---

[*] Superscripts denote references in the Bibliography

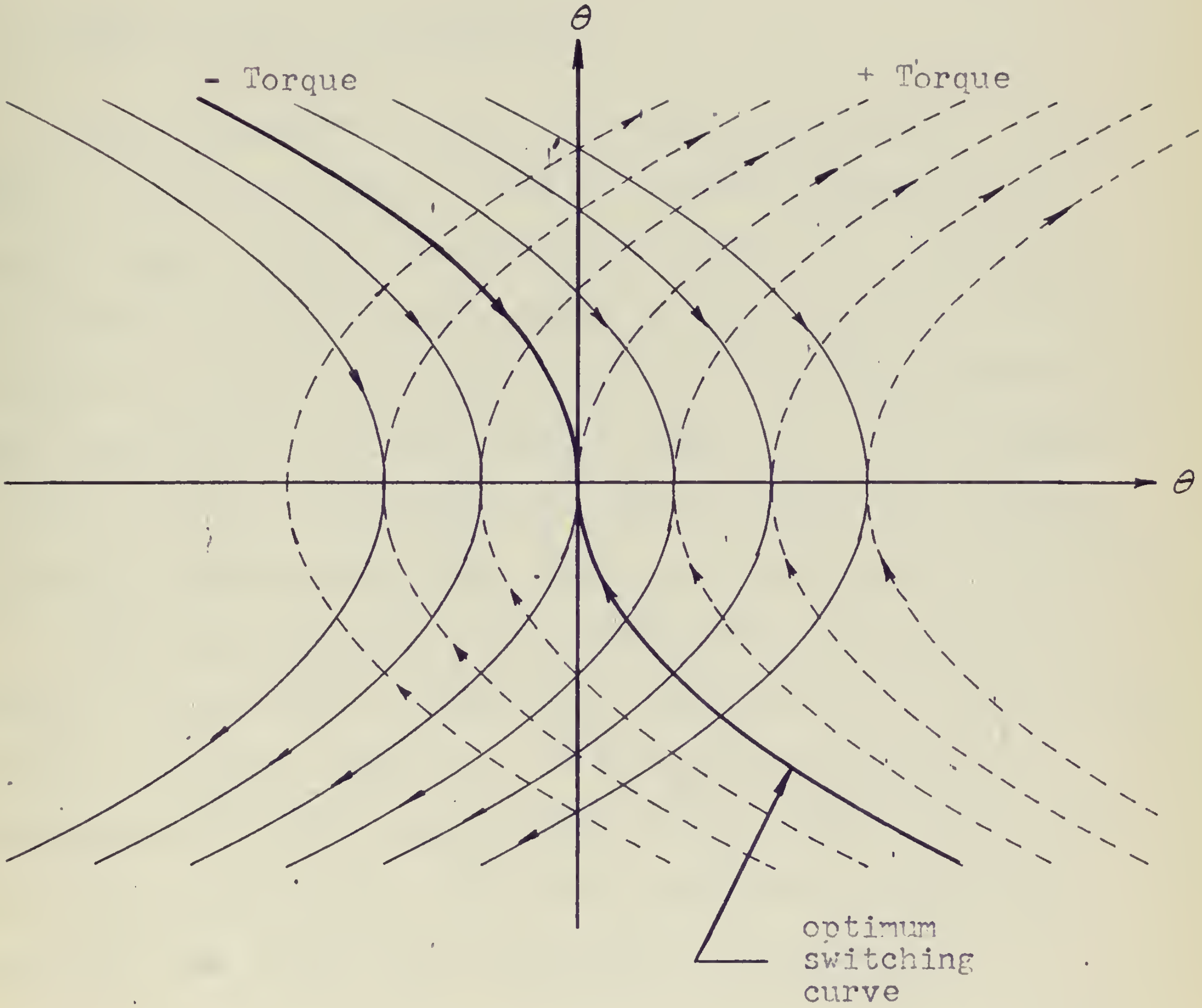

Figure 1.1

Phase Plane Representation of an Inertia Load being Driven by a Constant Torque

CHAPTER II

VORTEX ANGULAR RATE SENSOR ANALYSIS AND DESIGN

2.1 General Theory of Operation

The principles on which a vortex angular rate sensor operate are quite simple. Real difficulties quickly arise, however, when attempts are made at mathematical analysis of the complex flow which takes place in these devices or when attempts are made to obtain pressure or flow signals which are some function of the input angular rotation. It is primarily because of the latter difficulty that the methods of obtaining output signals have been, and still are, held confidential.

The basic operation of a rate sensor is depicted in Figures 2.1a and 2.1b. Figure 2.1a shows the flow state in the absence of angular rotation. In this case a particle of fluid passes from the supply plenum through the porous ring into the vortex chamber and out the exit hole. From mass continuity the radial flow velocity is described by

$$U_r = \frac{Q}{2\pi r h} \qquad (2.1)$$

where

Q = flow rate supplied to the sensor

r = any arbitrary radius

h = thickness of the vortex chamber

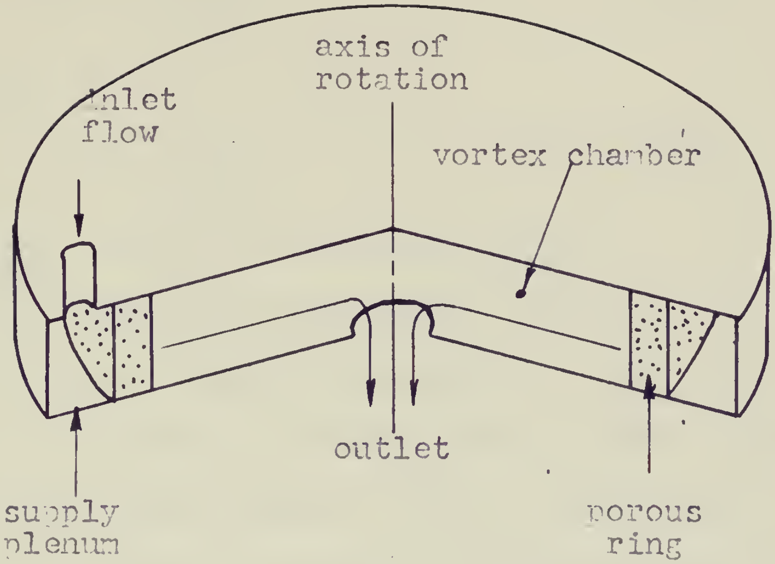

a) no angular rotation

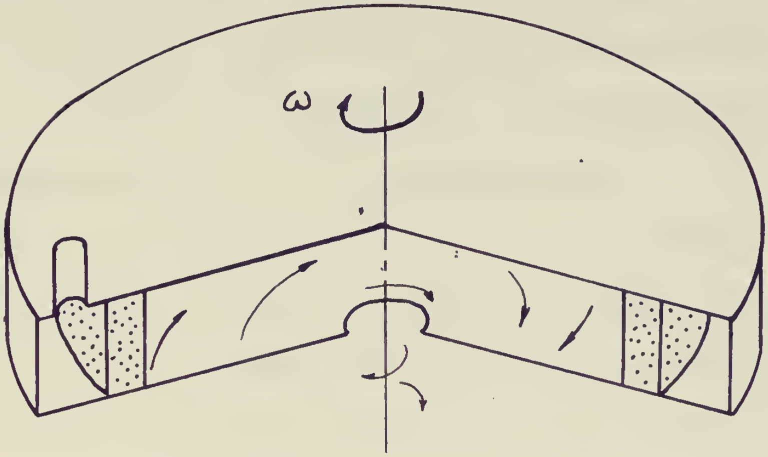

b) with angular rotation

Figure 2.1

Vortex Angular Rate Sensor

Thus just inside the porous ring, the radial velocity is given by

$$U_o = \frac{Q}{2\pi R_o h} \qquad (2.2)$$

and at the exit

$$U_e = \frac{Q}{2\pi R_e h} \qquad (2.3)$$

where Q and h are as given above
and R_e = radius of porous ring
R_o = exit hole radius

Figure 2.1b shows the flow condition when the sensor is rotated at a constant angular rate. In this case a particle of fluid entering the vortex chamber has the radial velocity given by equation (2.1) and a tangential component of velocity imparted to it while passing through the porous ring. In visualizing this tangential component, one must use a frame of reference other than the vortex chamber. Thus with respect to laboratory coordinates, the magnitude of the tangential component of velocity is given by

$$U_{to} = R_o \omega \qquad (2.4)$$

where U_{to} = magnitude of the tangential velocity
ω = magnitude of the input rotation

Hence, a particle of fluid of mass dm will have angular momentum given by $R_o\ U_{to}\ dm$. Conservation of Angular Momentum produces an expression for the tangential velocity (U_t) at an arbitrary radius (r):

$$r\ U_t\ dm = R_o\ U_{to}\ dm \qquad (2.5a)$$

$$U_t = \frac{R_o^2 \omega}{r} \qquad (2.5b)$$

For an ideal flow the familiar result of U_t approaching infinity is seen as r approaches zero.

Thus it can be seen that if a means can be devised to measure the amount of tangential velocity directly or indirectly at a particular radius, this velocity will change in proportion to the magnitude of ω as to the direction of rotation.

The method used to measure the amount of tangential velocity present in the vortex chamber of the rate sensor used in this control system was developed by Sarpkaya[4]. The analytical analysis about to be discussed is also given by Sarpkaya but is included here to maintain continuity of this chapter and to set the background for the extension of Sarpkaya's work which follows in the remaining articles*.

A schematic of the sensor developed by Sarpkaya is shown in Figure 2.2. This sensor differs from the one shown in Figure 2.1 in that two sink-tubes are attached to the exit holes of the vortex chamber. These sink-tubes serve the following purposes:

1) Tangential flow amplification - each tube can now be considered as a miniature elongated vortex chamber being fed from the top by a uniform radial flow on which is superimposed the tangential swirl flow from the main vortex chamber,

2) Directing radial flow - the tubes receive the flow from the main vortex chamber and direct it toward the probe,

3) The sink-tubes provide a housing for the probe.

The probe, shown in Figure 2.3, consists of a small circular cylinder divided into two chambers. Two small holes are drilled perpendicular to the center line of the probe and

---

* To further credit the work of Sarpkaya, most of his symbols are maintained throughout this chapter.

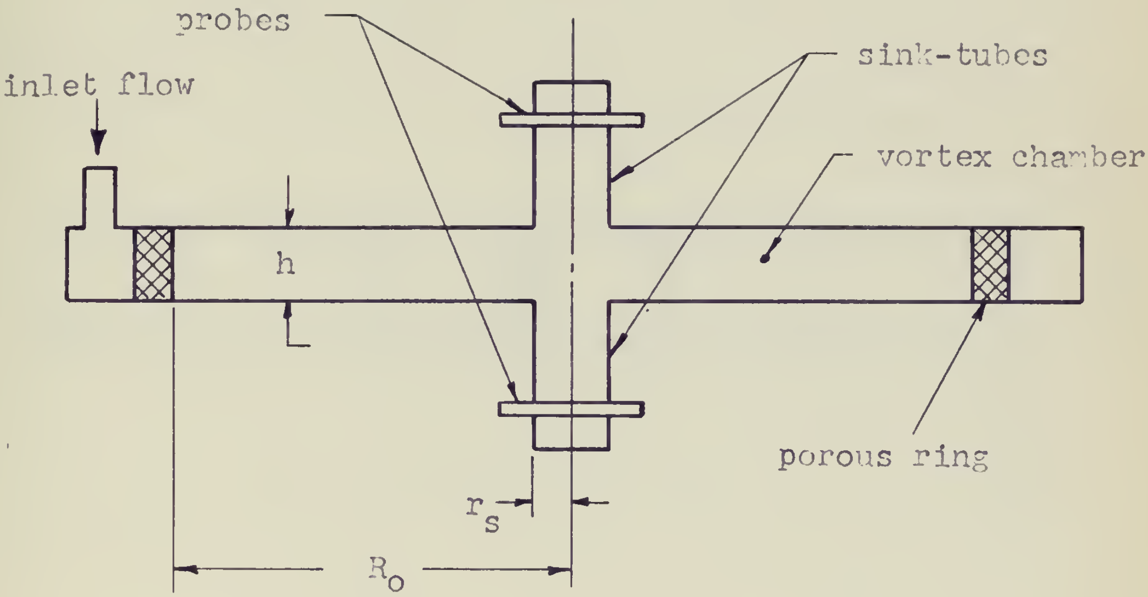

Figure 2.2

Sketch of the Vortex-Sink Angular Rate Sensor

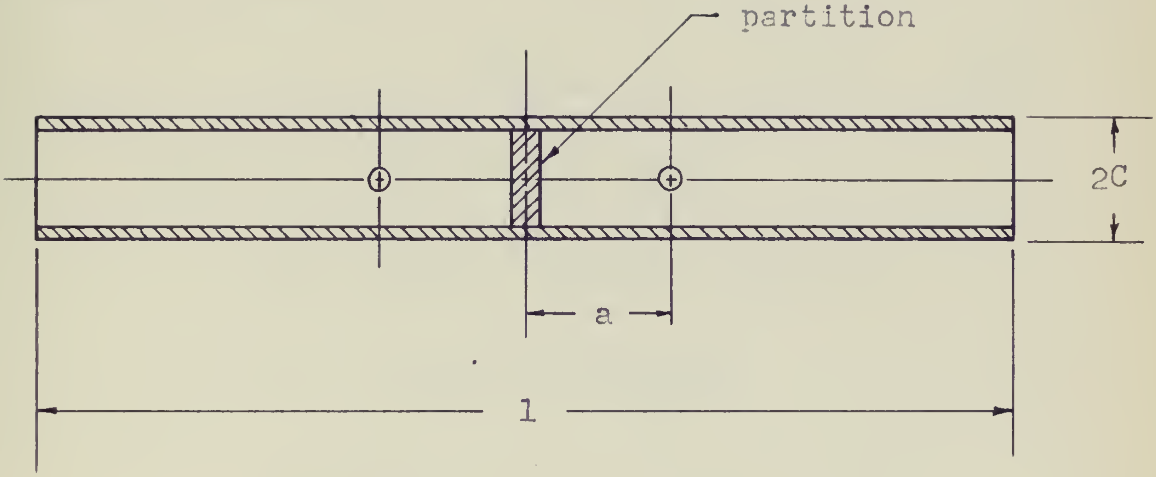

Figure 2.3

Cross Section of Probe

aligned along a straight line drawn on the surface of the cylinder between its ends. The probe is inserted into the sink-tube perpendicular to the axis of flow, as shown in Figure 2.2. The holes are set at an angle to the oncoming flow of fluid in the sink-tube.

The operation of this probe in sensing angular rotation is as follows: From potential flow theory the pressure distribution around a circular cylinder placed in a uniform flow field is given by

$$P_b = P_o + \frac{\rho U_s^2}{2} (1 - 4\sin^2\theta) \qquad (2.6)$$

where P_b = pressure in $\mathrm{lbf/in^2}$

P_o = static pressure in $\mathrm{lbf/in^2}$

ρ = density in $\frac{\mathrm{lbf\text{-}sec^2}}{\mathrm{in4}}$

U_s = axial sink velocity in in/sec

θ = angular position measured around the cylinder from the stagnation point.

A sketch of equation (2.6) is shown in Figure 2.4. In the absence of angular rotation of the device, the uniform radial velocity in the vortex chamber (U_r) turns into the sink-tube (now redesignated U_s), strikes the probes and then passes out of the sensor. Because both holes are aligned at the same angular position along the probe, equal pressures exist in each chamber. The output signal of the probe, however, is the difference between these two pressures. Since both

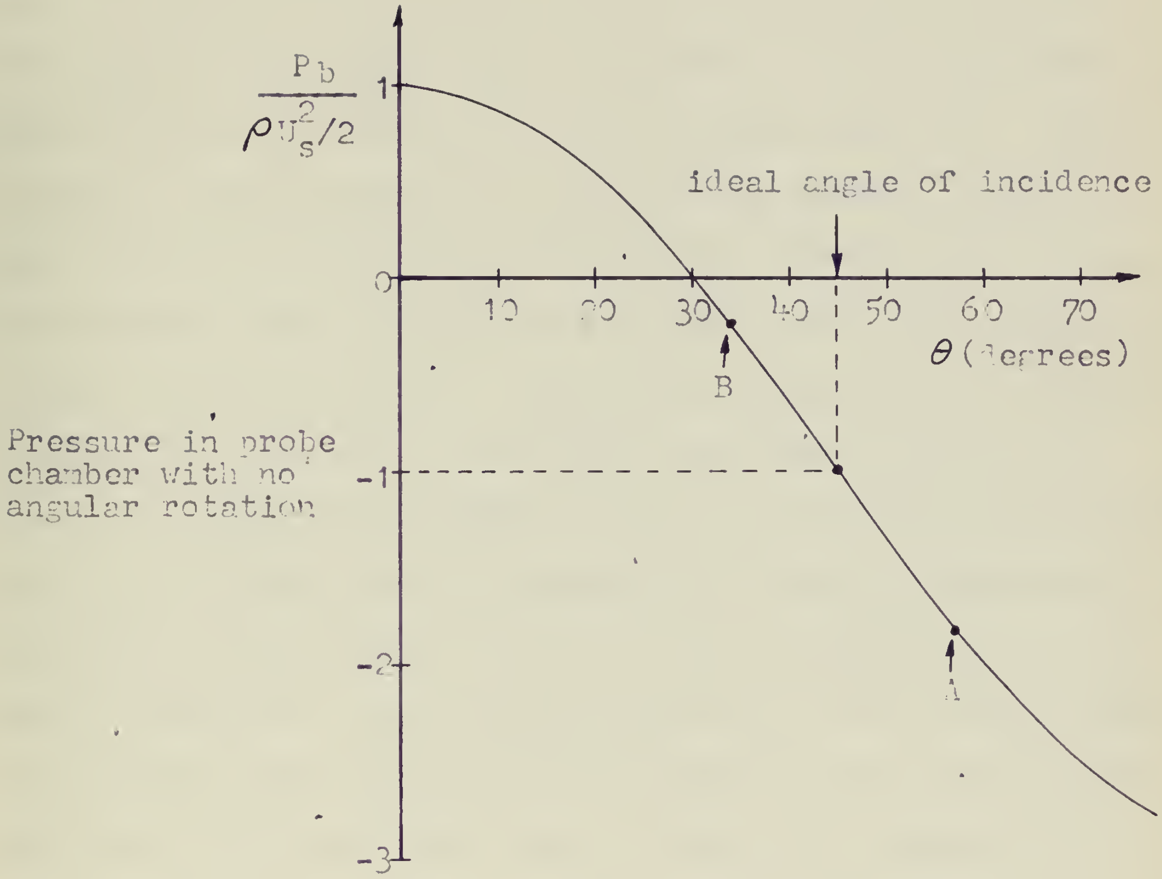

Figure 2.4

Ideal Pressure Distribution Around a Circular Cylinder

chambers are at the same pressure, no output signal (ΔP) exists.

Now let there exist angular rotation of the rate sensor. Figure 2.5 shows the velocity vectors in way of the probe. The tangential velocity (v_{po}) now present in the sink-tube has the effect at diverting the main axial sink flow. The top hole is thus placed in a uniform flow coming from an angle which is greater than that which existed without angular rotation. The bottom hole is placed in a flow coming from an angle which is smaller. Thus, the pressure in the chamber, to which the top hole is connected, decreases, (point A in Figure 2.4), while the pressure in the bottom chamber increases, (point B in Figure 2.4). A pressure differential now exists across the probe which is a function of the magnitude of the angular rotation. It is readily visualized that had the angular rotation been in the opposite direction that the reverse procedure would have taken place. Hence, the signal also senses direction of angular rotation as well as magnitude. It is assumed in this explanation that the relative magnitude of the sink-tube axial and tangential velocities are such that a long spiraling flow exists at the radius r_{po}.

To visualize the flow quantitatively and to obtain the function relating Δp and ω refer again to Figure 2.5. By inspection it can be seen that $\Delta\theta$, U_s, and v_{po} are related by:

$$\Delta\theta = \tan^{-1} \frac{v_{po}}{U_s} \qquad (2.7a)$$

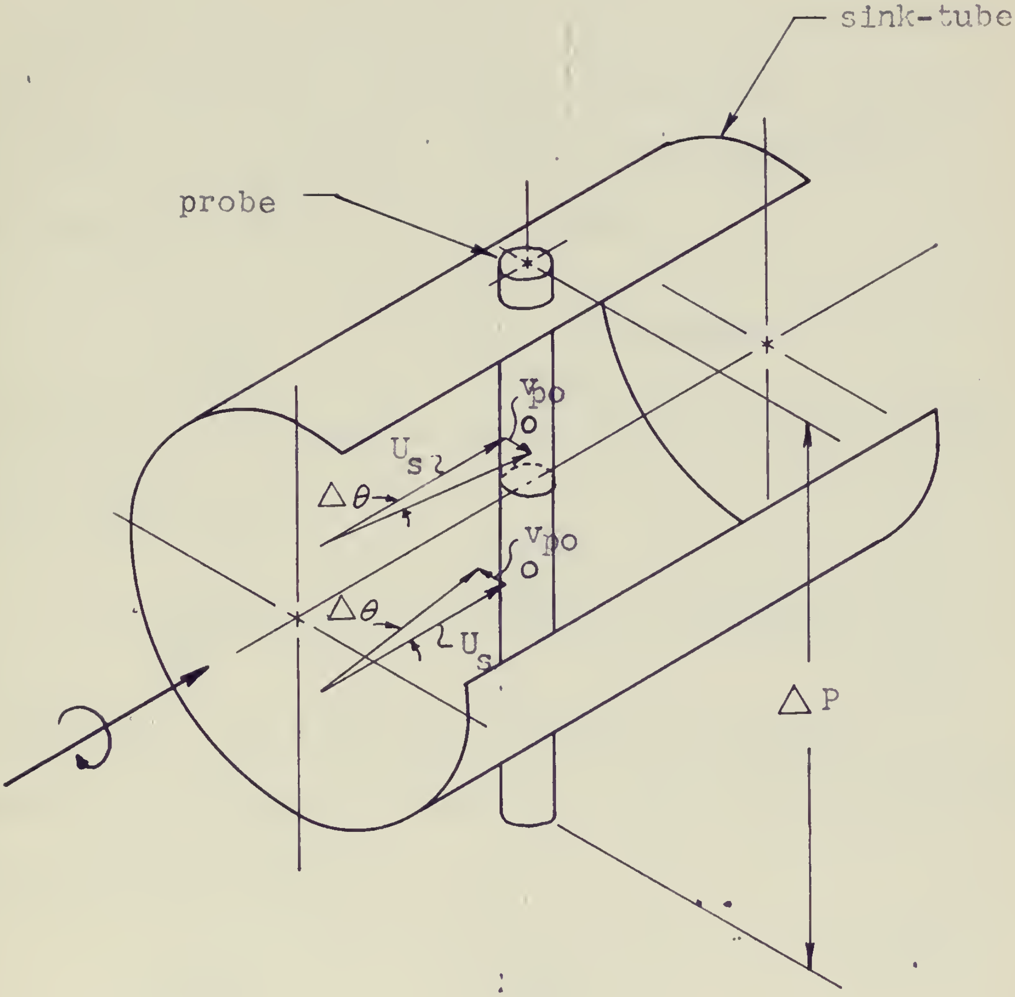

Figure 2.5

Sketch of Probe in Operation

If $\Delta\theta$ is a small angle then:

$$\Delta\theta = \frac{v_{po}}{U_s} \qquad (2.7b)$$

To obtain the maximum signal (ΔP) possible for a given ω, it is necessary to determine the maximum slope of the curve shown in Figure 2.4. Hence, differentiating equation (2.6) to obtain the slope gives:

$$\frac{\partial P_b}{\partial\theta} = -\frac{\rho U_s^2}{2}\, 8 \operatorname{Sin}\theta \operatorname{Cos}\theta \qquad (2.8)$$

Now the derivative of equation (2.8) set to zero will give the θ for maximum slope.

$$\frac{\partial^2 P_b}{\partial\theta^2} = -8\,\frac{\rho U_s^2}{2} \operatorname{Cos} 2\theta, \theta = \pi/4 \qquad (2.9)$$

Therefore, the probe holes should be located at a 45 degree angle to the oncoming flow. This value substituted into equation (2.8) gives

$$\frac{\partial P_b}{\partial\theta} = -4\left(\frac{\rho U_s^2}{2}\right) \qquad (2.10)$$

and in differential form for one hole:

$$|\Delta P| = 4\left(\frac{\rho U_s^2}{2}\right)\Delta\theta \qquad (2.11)$$

Equation (2.5b) gives the relation between the tangential velocity existing in the sink-tube and the input angular rotation. With new symbols, equation (2.5b) becomes:

$$v_{po} = \frac{R_o^2\,\omega}{r_{po}} \qquad (2.12)$$

Combining equations (2.7b), and (2.11), and (2.12) gives:

$$\frac{|\Delta P|}{\frac{\rho U_s^2}{2}} = 4\,\frac{R_o^2\,\omega}{U_s r_{po}} \quad \text{, for one hole} \qquad (2.13a)$$

Since two holes are being used equation (2.13a) becomes:

$$\frac{|\Delta P|}{\frac{\rho U_s^2}{2}} = 8\,\frac{R_o^2\,\omega}{U_s r_{po}} \qquad (2.13b)$$

This is the desired relationship between ΔP and ω in non-dimensional form. Note that for a given sensor and probe configuration, that R_o and r_{po} are fixed. Further, if the flow through the sensor is fixed, then U_s is constant. Thus it is seen that equation (2.13b) is of the form:

$$\Delta P = K\,\omega \qquad (2.14)$$

$$\text{where} \quad K = 8\,\frac{\rho U_s^2}{2}\,\frac{R_o^2\,\omega}{U_s r_{po}}$$

, a constant depending on geometry and flow.

Data given by Sarpkaya bear out the linearity of this equation over a substantial range of ω. As might well be expected, from inspection of Figure 2.4, linearity is preserved provided $\Delta\theta$ is small.

Thus far the equations derived to describe the operation of this rate sensor, are based on an idealized potential flow. It is now appropriate to consider the effects of viscosity on the operation of the sensor and the describing equations. Two major effects of viscosity will be noticed:

1) Viscosity will cause the vortex motion in the

vortex chamber and sink-tube to deviate from the ideal vortex given by equation (2.5b).

2) Viscosity will cause the flow around the probe to separate resulting in an alteration of the pressure distribution around the probe given by equation (2.6).

Effect 1) is studied in great detail by Sarpkaya, by analyzing the boundary layer equations in the chamber for the radial flow with small tangential flows superimposed on the main flow. The results show that viscosity reduces the strength of circulation as the flow travels from R_o to r_{po}. Sarpkaya introduces a factor he calls the viscous efficiency of the sensor defined as:

$$E = \frac{\Gamma_r}{\Gamma_o} \qquad (2.15)$$

where Γ_r = strength of vortex circulation at radius r

Γ_o = strength of vortex circulation at radius R_o

The viscous efficiency between the porous ring and the probe is:

$$E = \frac{\Gamma_{po}}{\Gamma_o} = \frac{v_{po}\, 2\pi\, r_{po}}{R_o \omega\, 2\pi\, R_o} = \frac{v_{po}\, r_{po}}{R_o^2 \omega} \qquad (2.16a)$$

from which

$$v_{po} = \frac{R_o^2 \omega}{r_{po}} E \qquad (2.16b)$$

With equation (2.16b) used in lieu of equation (2.12) and then combined with equations (2.7b) and (2.11), the new relationship between ΔP and ω becomes

$$\frac{|\Delta P|}{\frac{\rho U_s^2}{2}} = \frac{8 R_o^2 \omega E}{U_s r_{po}} \quad \text{for two holes.} \qquad (2.17)$$

Intuitively one might expect this efficiency to be relatively high provided the circulation is quite small. This is shown to be true by Sarpkaya in a plot of E versus Reynolds Number.

Effect 2) is an extremely important consideration which seems to have been neglected by Sarpkaya in his analysis of the sensor. Non ideal flow around the probe radically reduces the slope of ΔP versus θ in the vicinity of $\theta = 45^\circ$.

For the case of ideal flow around the probe, the nondimensional slope is given by equation (2.11).

$$\frac{|\Delta P| \Big/ \frac{\rho U_s^2}{2}}{\Delta \theta} \doteq 4 \qquad \begin{array}{l}(2.11)\\ \text{repeated}\end{array}$$

From actual measurements taken on the probe used in the sensor constructed by the author, this slope was found to vary between 2.58 and 3.17 for the flows considered. The effect of viscosity is more clearly shown in Figure 2.6 where nondimensional pressure distribution for two actual flows versus θ is shown along with that predicted by potential flow theory. Thus the relationship between ΔP and ω with the introduction of the new slope of ΔP vs $\Delta \theta$ becomes:

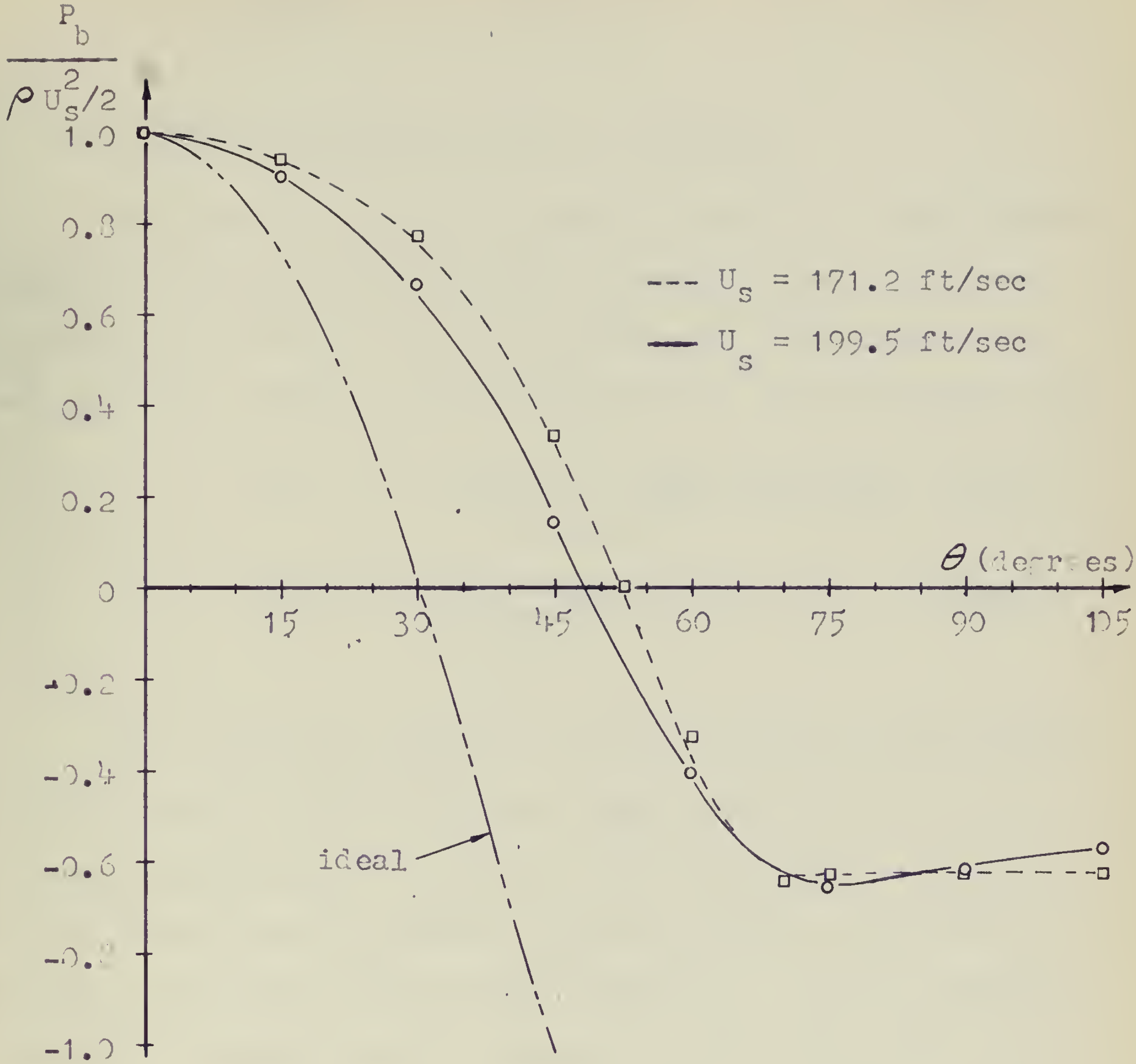

Figure 2.6

Effect of Viscosity on the Pressure Distribution

Around a Circular Cylinder

$$\frac{|\Delta P|}{\rho U_s^2/2} = \frac{5.16\, R_o^2 \omega E}{U_s\, r_{po}} \quad \text{for two holes.} \tag{2.18}$$

2.2 Rate Sensor Design and Design Procedure*

The author did not consider the effect of slope reduction due to viscosity of the ΔP versus θ curve, discussed at the end of article 2.1, until after the rate sensor had been designed. Hence, the equations used for the design were

$$\Delta P = 8\left(\frac{\rho U_s^2}{2}\right)\Delta\theta, \quad \text{two holes} \tag{2.19}$$

$$\Delta\theta = \frac{R_o^2 \ \omega E}{r_{po}\ U_s} \tag{2.20}$$

From the design specifications discussed in the introductory chapter to this thesis, ω_{max} was selected to be 70 degrees per second. In order that the output of the sensor be linear over the range $-\omega_{max} \le \omega \le \omega_{max}$, the value of $\Delta\theta$ must be constrained to stay within the linear portion of the ΔP versus θ curve. Analysis of the data given by Sarpkaya has shown that $\Delta\theta$ should not exceed roughly $\pm 3^\circ$ for linearity.

Inspection of equation (2.20) shows that R_o, r_{po}, E, and U_s are still to be determined. R_o was chosen on size considerations of the sensor and was selected to be three inches. The value of U_s will depend on the magnitude of the

---

[*] See Appendix A.1 for detailed numerical calculations in this section.

desired output signal ΔP and can be determined from equation (2.19). Once U_s is determined, Q can be calculated from the relationship

$$Q/2 = \left[\pi r_s^2 - 2c(2r_s) \right] U_s \qquad (2.21)$$

where r_s = radius of sink

c = radius of probe

In order to limit Q to a reasonable value, it is obvious that the magnitude of ΔP must be kept relatively small. For this design a value of ΔP = 0.1 psi to occur at $\omega = \omega_{max}$ was selected.

Having determined Q, the Reynolds Number can be determined from

$$Re = \frac{Q\ h/2}{\nu\ R_o^2} \qquad (2.22)$$

where $\nu = \frac{\mu}{\rho}$ = kinematic viscosity

h = thickness of vortex chamber

With the value of Re determined, the experimental data given by Sarpkaya on viscous efficiencies can be entered and a value of E determined.

Knowing all the values of the variables in equation (2.20) except r_{po}, allows one to solve for this variable. The position of the probe holes from the center of the sink-tube (distance a in Figure 2.3) can then be determined from the relationship

$$r_{po} = \sqrt{a^2 + \left(\frac{c}{\sqrt{2}}\right)^2} \qquad (2.23)$$

which can be verified by inspection of Figures 2.3 and 2.5. One word of caution must be made concerning a minimum value of r_{po}. Viscosity plays an increasingly important role as r approaches zero in a real vortex. If r_{po} is too large, full advantage is not made of the amplifying properties of the vortex. On the other hand, if it is made too small, viscosity rapidly decreases the strength of the vortex. This phenomena remains to be investigated more fully and is mentioned here only for design considerations.

The design data used in constructing the rate sensor is summarized in Table 1. The material used in construction was plexiglass. The porous ring was made of felt faced with fine wire screening which gave rigidity to the ring and acted as a flow straightener. The probe was constructed by cutting a 1 3/4 inch piece of number 19 gauge stainless steel hypodermic tubing in half and inserting a plug. The number 80 Drill Size holes were then drilled 0.095 inches apart. This construction allowed the holes to be aligned by rotating one side of the probe relative to the other.

2.3 Signal Amplification

The magnitude of the signal output (pressure and flow) by itself is too small to be used conveniently in the control

TABLE I

SUMMARY OF RATE SENSOR DESIGN DATA

Specified Data:

$\omega_{max} = 70^{\circ}/\text{sec}$

$R_o = 3$ in.

$\Delta P_{max} = 0.1 \ \text{lbf/in}^2$

$\Delta \theta_{max} = 3^{\circ}$

Arbitrarily Chosen Data:

$r_s = 0.1562$ in.

$c = 0.0212$ in. (#19 gauge hypodermic tubing OD x ID = 0.0425 x 0.0270 in)

probe hole diameter = 0.0135 in. (#80 Drill)

Derived Data:

$r_{po} = 0.0512$ in.

$a = 0.0475$ in.

$U_s = 171.2$ ft/sec

$Q = 9.05 \ \text{ft}^3/\text{min}$

$E = 0.50$

system loop and therefore must be amplified. The state of the art of pure fluid signal amplification, though not yet mature, is advanced to the point where a combination of experimental and analytical methods can be used to obtain reasonable signal amplification with tolerable signal to noise ratios.

The design problems faced at this stage of the development of the rate sensor are:

1) Given the output pressure-flow relations of the rate sensor probe, what are the supply pressure settings needed at each amplifier stage to insure linearity of the signal?

2) How many stages of amplification are needed to raise the pressure and flow to acceptable levels?

The last question could not be answered at this stage of the design for the rest of the systems components had not yet been designed. Therefore, it was decided to use two stages of amplification and after the amplifier stages were attached, to accept the output pressure-flow relations of the final amplification stage as the output characteristics of the sensor.

The first question, although a relatively straight forward design question, is covered only lightly in the literature.

The procedure used to obtain the supply pressure settings described below is by no means exact but it will let the designer set the pressures close to their optimum settings on the first try.

The amplifiers used to amplify the rate signal output were Corning Glass Work's Standard Size Proportional Amplifiers. The important dimensions of these devices are:

power nozzle width = w = 0.010 in.
control nozzle width = 1.5w
depth = 2.5w
receiver distance = 10w

Figure 2.7 is a sketch of the interaction region of a typical proportional amplifier which operates principly by momentum interaction. Following the development given by Dexter[5], the deflection of the power stream due to one control momentum only is determined as follows:

$$\tan\theta = \frac{V_t}{V_a}$$

where $V_t = \dfrac{\dot{m}_c V_c}{\dot{m}_c + \dot{m}_p}$

$$V_a = \frac{\dot{m}_p V_p}{\dot{m}_c + \dot{m}_p}$$

and $\dot{m}_p$ = mass flow rate of the power jet
$\dot{m}_c$ = mass flow rate of the control jet
V_c = velocity of the control jet
V_p = velocity of the power jet

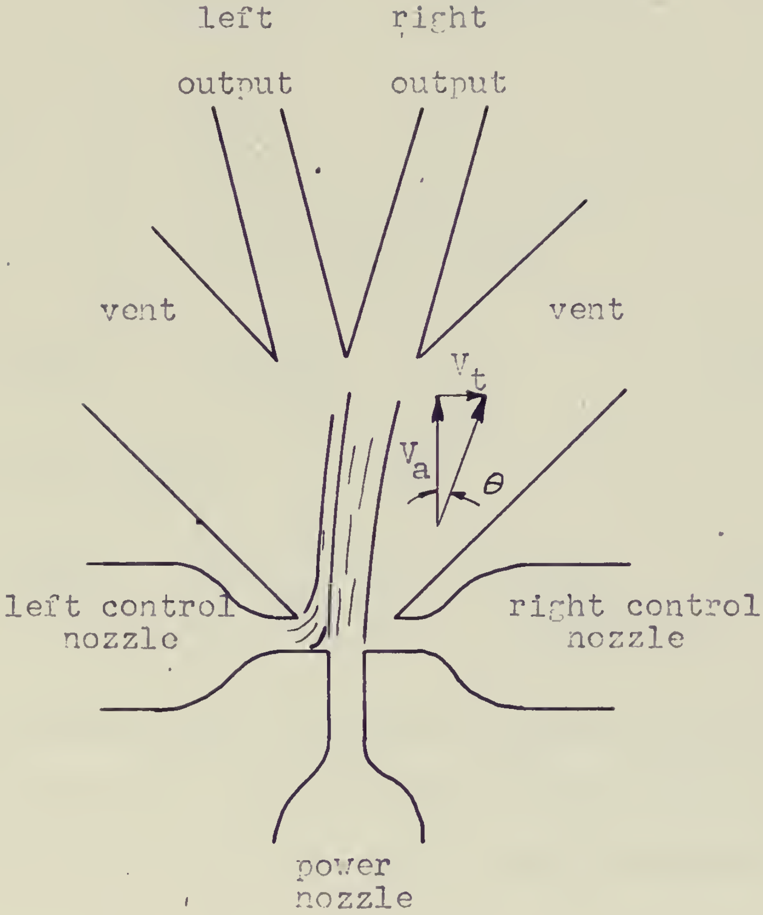

Figure 2.7

Typical Proportional Pure Fluid Amplifier

$$\therefore \tan\theta = \frac{\dot{m}_c \, V_c}{\dot{m}_p \, V_p}$$

but $\dot{m}v = \rho A V^2$

$$\therefore \tan = \frac{\rho A_c \, V_c^2}{\rho A_p \, V_p^2} = \frac{\rho \, d w_c \, V_c^2}{\rho \, d \, w_p \, V_p^2}$$

where d = depth

w_c = control nozzle width

w_p = power nozzle width

$$\therefore \tan\theta = \frac{w_c \, V_c^2}{w_p \, V_p^2} \qquad (2.24)$$

but $V^2 \doteq (2/\rho) P$

$$\therefore \tan\theta = \frac{w_c \; 2/\rho \; P_c}{w_p \; 2/\rho \; P_p} = \frac{w_c \, P_c}{w_p \, P_p} \qquad (2.25)$$

Reilly and Moynihan[18] indicate that the output of a proportional device will remain linear provided the deflection of the power jet at the receiver ports does not exceed one half the nozzle width. Thus:

$$\tan\theta \leq \frac{w_p/2}{L} \quad \text{for linearity}$$

where L = receiver distance

Combining this with equation (2.25) gives:

$$\frac{w_p}{2L} \geq \frac{w_c \, P_c}{w_p \, P_p} \quad \text{for linearity}$$

This result is readily extended to two control ports with the result:

$$\frac{w_p}{2L} \geq \frac{w_c\left(P_{cL}-P_{cR}\right)}{w_p\,P_p} \quad \text{for linearity} \qquad (2.26)$$

Having developed the basic equations of the amplifier, the output characteristics of the rate sensor probe must now be investigated. According to potential flow theory, if the probe is set so that the probe holes are at 45 degree angles to the oncoming flow, the pressure in the probe chambers is below ambient. Since the probe chambers are connected to the control ports of the first stage amplifier, this means that only the pressure differential existing in the two chambers and communicated to the first stage control ports is available for deflecting the jet. This is undesirable as it results in less gain when compared to operation with positive flow through both control ports. However, due to viscosity the ideal flow pattern is radically altered so that the pressure existing in the chambers when the flow angle is set to 45 degrees is positive.

The various flow rates to be expected out of either end of the probe, as the main sink flow is deflected, can be approximated by setting the sink flow at its operating value and turning the probe with respect to the flow. The results of such an experiment are shown in Figure 2.8.

The output pressure-flow characteristics for a given P_b are shown in Figure 2.9. An infinite number of such curves exist since P_b varies with $\Delta\theta$.

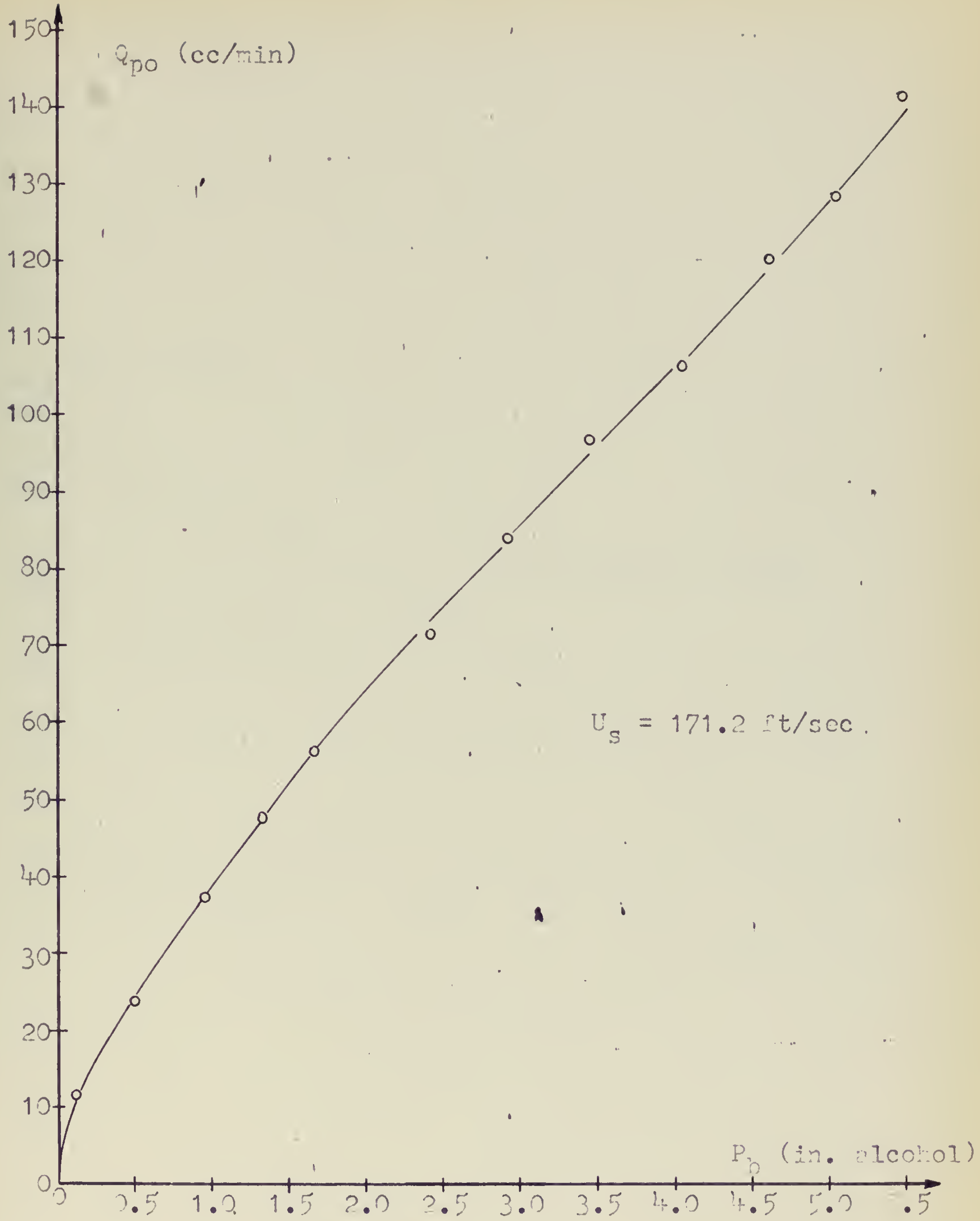

Figure 2.8

Probe Boundary Pressure versus No Load Flow

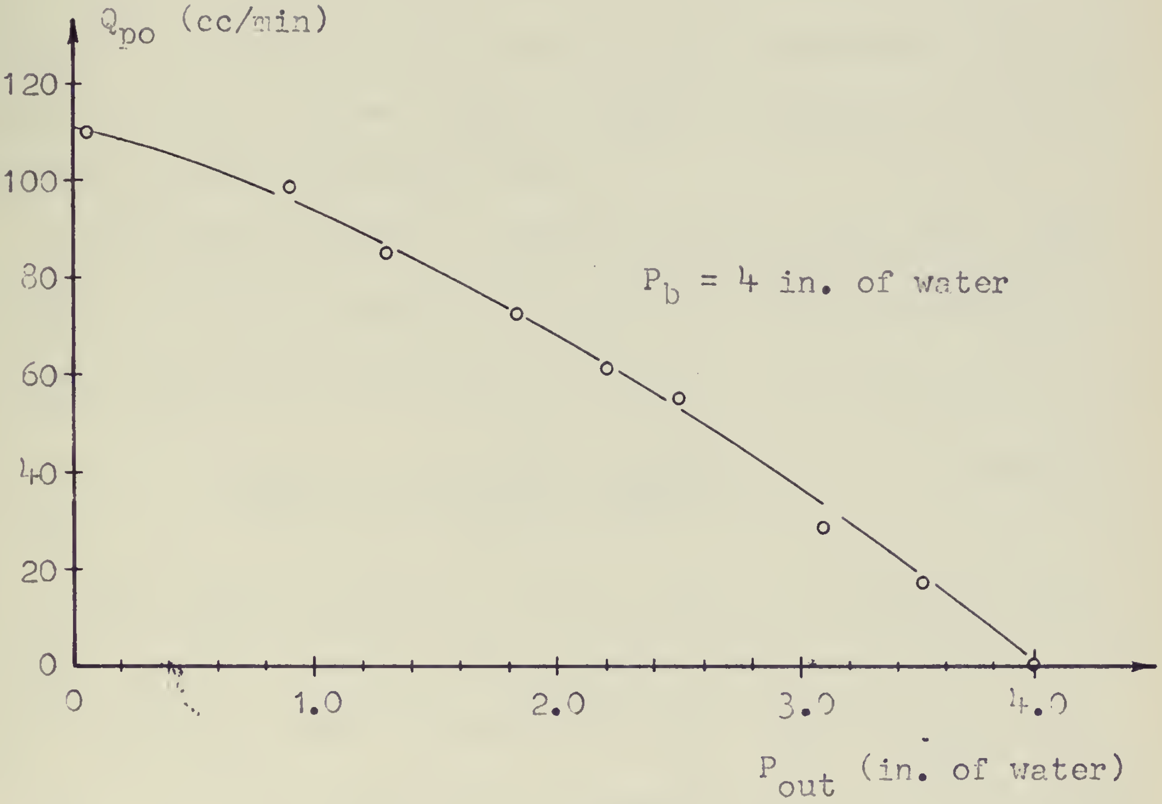

Figure 2.9

Probe Output Pressure-Flow Characteristics

The procedure initially used to set the first stage supply pressure (P_{pl}) was to determine the output pressure-flow relationship for maximum ΔP and superimpose the input characteristics of the first stage amplifier to determine $(P_{cL} - P_{cR})_{max} = \left|\Delta P_c\right|_{max}$. Then, from equation (2.25), the supply pressure was determined. However, when this procedure was followed, it was found that, because the control port area of the first stage amplifier was so large compared to the probe hole area (nearly three times as large), the input impedance of the amplifier was nearly zero.

Circumventing this problem, equation (2.24) was used in lieu of (2.25). With the constraint placed on tan θ and for two control port operation, equation (2.24) becomes:

$$\frac{w_p}{2L} \geq \frac{w_c \, (V_{cL}^2 - V_{cR}^2)_{max}}{w_p \, V_p^2} \qquad (2.27)$$

From measurements of the flow rate occurring at the expected maximum pressure just outside the probe hole, $(V_{cL}^2 - V_{cR}^2)_{max}$ was obtained from $V_{cL}^2 - V_{cR}^2 = \frac{1}{A_c^2}(Q_{cL}^2{}_{max} - Q_{cR}^2{}_{min})$ which then allowed V_p to be obtained from equation (2.27)

To obtain P_p the following relationship was used:

$$Q_p = C_{dp} \quad A_p \quad \sqrt{2/\rho \;\, P_p} \qquad (2.28)$$

where $Q_p = A_p V_p$

C_{dp} = discharge coeficient of the power nozzle which was determined from the design data sheet published by Corning glass Works.

From the calculations in Appendix A.2, P_{p1} was determined to be 7.7 inches of water.

The second stage pressure was set using information given in the design data sheet published by Corning Glass Works for these amplifiers. This sheet states that for maximum gain the control bias level pressure should be one tenth the power jet pressure*.

The bias level of the second stage controls was determined by setting the first stage supply pressure at 7.7 inches of water and measuring the pressure in the line connecting the output of the first stage and the control port of the first stage. This procedure resulted in an initial setting of P_{p2} equal to 5 psi.

2.4 Rate Sensor Dynamics

This rate sensor is characterized dynamically by 1) a pure time delay resulting from the time it takes for the fluid particles containing tangential momentum to reach the probe, 2) a first order lag due to the resistances of the probe holes and control nozzles of the first stage amplifier and the volume connecting them, and 3) the dynamics of the staging amplifiers and the lines used in interconnection.

The transport delay is the most significant. It may

---

* This procedure used in setting the first stage pressure resulted in a $P_{p1} = 1.95$ inches of water and hence was not used.

be approximated by the time it takes for the sensor to completely renew the supply of fluid in the vortex chamber[2] and sink-tubes. Thus:

$$\tau = \frac{V}{Q} \quad \text{seconds} \qquad (2.29)$$

where V = total volume

Q = flow rate given by equation (2.23)

The total volume (V) is given by:

$$V = \pi R_o^2 h + 2\pi r_s l_p$$

where R_o, h and r_s are as before

l_p = distance to probe measured along the axis of the sink-tube

For the geometry and flow rates of this device, the value of τ is 0.0556 seconds.

The time constant of the first order lag referred to in item 2) was found to be extremely small and was neglected in arriving at the transfer function of the rate sensor.

The dynamics of the staging amplifiers are discussed by Belsterling and Tsui[6] and Boothe[7]. These works show the devices to respond very much faster than the time delay of this rate sensor. In addition, the design data sheet for these amplifiers indicate that the frequency gain is over 1000 cps, well out of the range of the rate sensor.

Thus the transfer function relating the output (ΔP) to the input angular rate (ω) is given by:

$$\frac{\Delta P}{\omega} = K_1 e^{-S\tau_1}$$

where K_1 = steady state gain

τ_1 = pure time delay given by equation (29)

S = Laplace operator d/dt

2.5 Testing Procedure and Results

The rate sensor was made into a self contained package by attaching the staging amplifiers directly to one side of the vortex chamber. The sensor was equipped with a manifold allowing air to be supplied with only one line. This manifold pressure was then reduced to the required pressures needed at the vortex chamber supply plenum and power jets of the staging amplifiers. Variable resistors were used to set the pressures and were constructed from tapered dowel pins through which holes were drilled. Photographs of the assembled rate sensor are shown in Figures 7.4 and D.1 . A differential pressure to electric transducer was attached to the outputs of the second stage amplifier and the assembled device was tested on a rate table at the Instrumentation Laboratory of the Massachusetts Institute of Technology.

The testing procedure consisted of the following:

1) Steady state test over the range $1.10 \leq \omega \leq 1.15$ radians per second with the output loaded by orifices approximating the size of the control parts of an amplifier similiar to those used on the rate sensor for signal amplification.

2) Steady state test over the same range with the output flow equal to zero; i.e., infinite load.

3) Frequency response test at discrete frequencies up to 4.67 cps.

4) Steady state test while the device was being simultaneously rotated about its sensing axis and an arbitrary axis.

The test results for the first three tests are shown in Figures 2.10, 2.11, 2.12, and 2.13.

2.6 Discussion of Results

The results of the steady state rate tests show the following:

1. The very small signals available from the probe can indeed be amplified into reasonable signals.
2. The output of the sensor is not quite linear over the range tested.
3. The gain of the sensor with clockwise rotation is significantly larger than the gain with counter clockwise rotation when the bias is subtracted out of the results.
4. The gain increases continually as the input rate is increased.
5. The dog leg effect produces a highly undesirable rapid change of gain in the counter clockwise direction.

In an attempt to explain the last four items, accurate flow and pressure measurements were taken on each side of the probe as the angle of incidence of the probe holes with the oncoming flow was varied. Originally, in aligning the

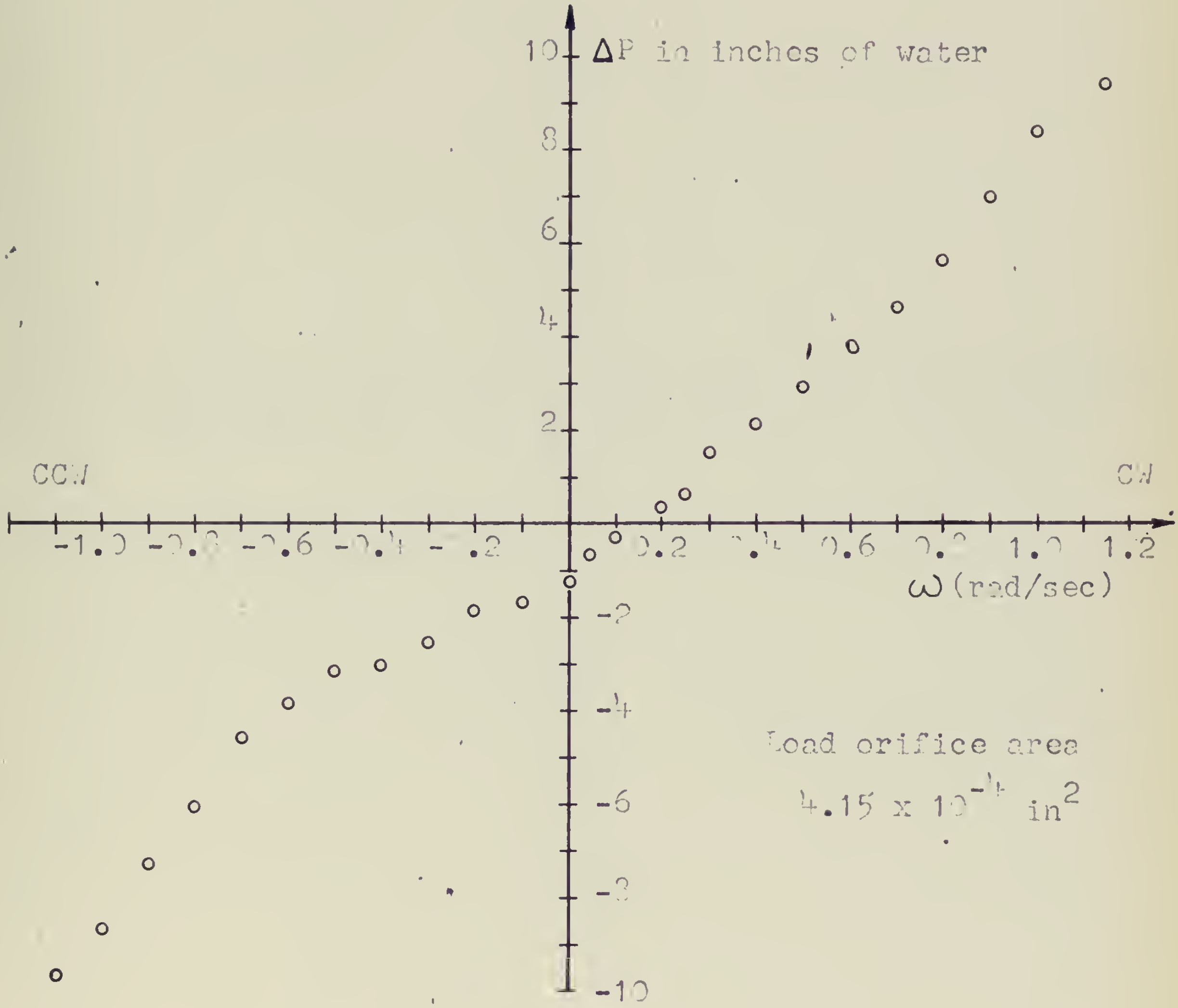

Figure 2.10

Rate Sensor Steady State Output

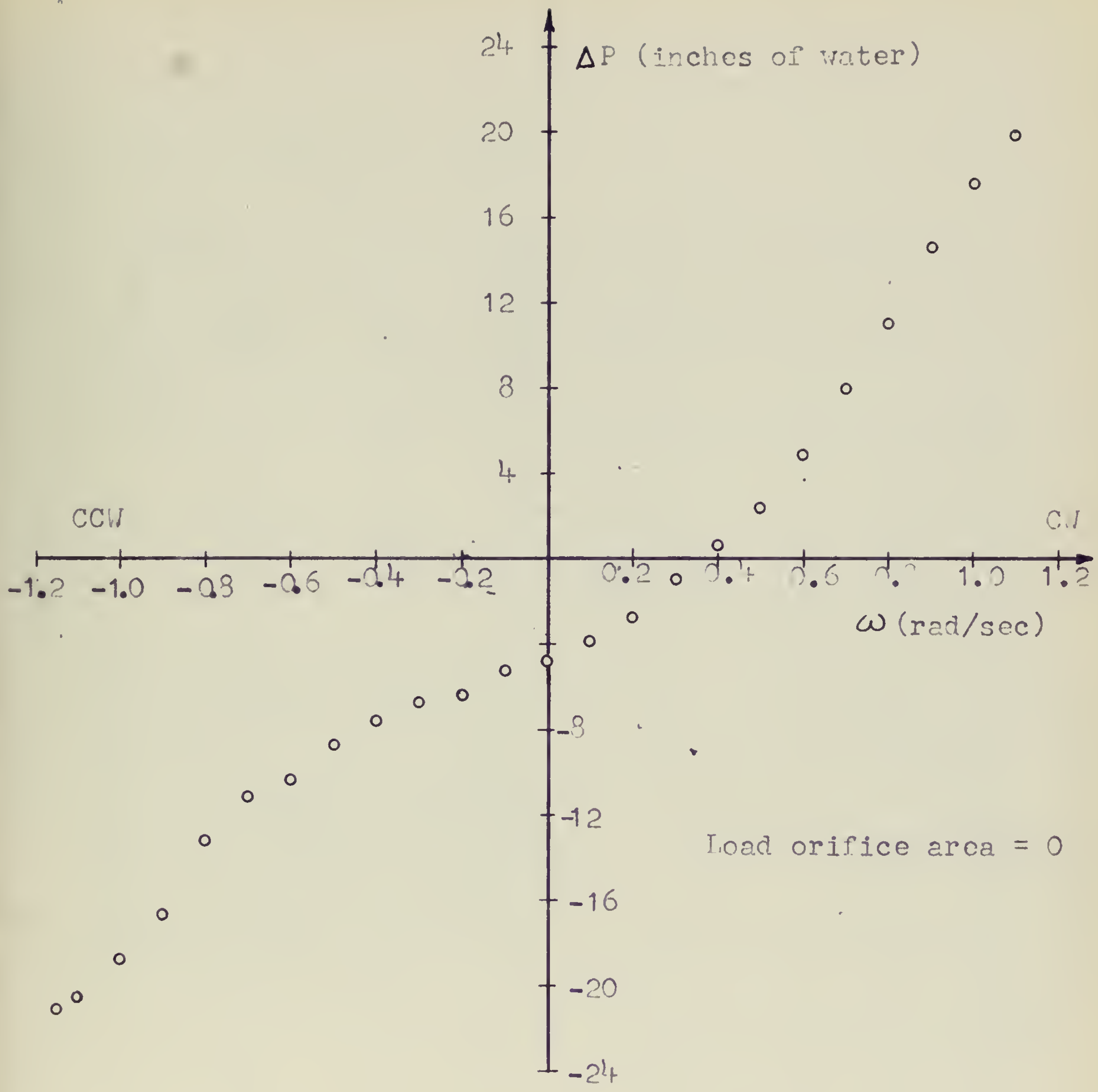

Figure 2.11

Rate Sensor Steady State Output

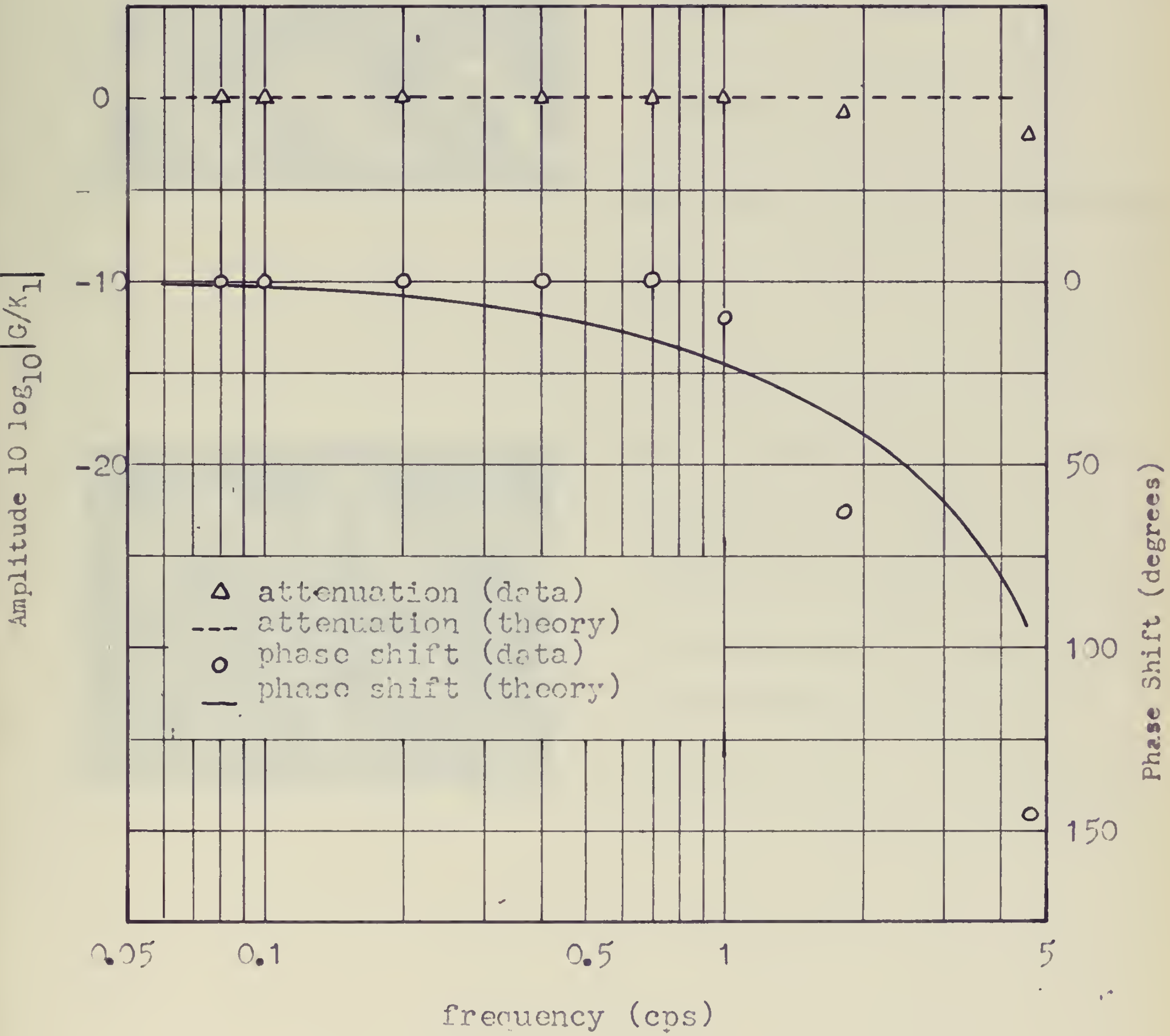

Figure 2.12

Rate Sensor Frequency Response

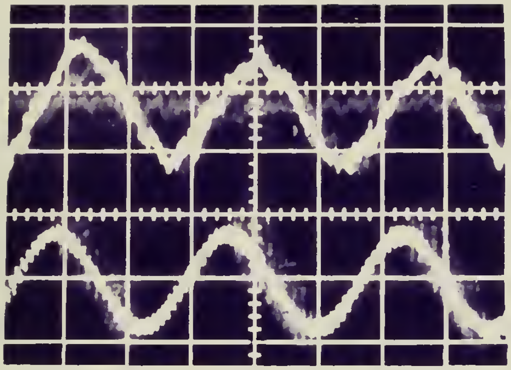

Output Signal

Frequency = 1.83 cps

Sweep = 0.2 sec/cm

Amplitude Ratio = -1.41 db

Phase Shift = 62°

Input Signal (ω_{max} = 0.98 rad/sec)

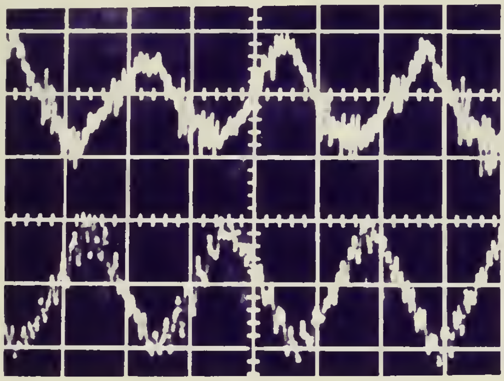

Output Signal

Frequency = 4.67 cps

Sweep = 0.1 sec/cm

Amplitude Ratio = -3.93 db

Phase Shift = 145°

Input Signal (ω_{max} = 1.02 rad/sec)

Figure 2.13

Typical Vortex Rate Sensor Frequency Response Data

probe holes (the turning of one probe hole with the other held fixed), only the dead-ended pressures were used, taking the probe holes as being aligned when the pressures were equal.

As was pointed out in article 2.3, signal amplification is essentially dependent on the flows coming from the probes. When these flows were measured, it was found that equal dead-ended probe pressures resulted in radically different flows indicating that, although the holes were supposedly of the same area, they were behaving as if they were not.

The probe was removed from the sensor and observed under a 50 power microscope. This showed that during the machining process, the drill had been allowed to cut a trough into the entrance to one of the holes. The effect of this trough was apparently to catch more flow from the main stream resulting in different orifice characteristics.

The effect of having the two probe holes producing different flows for equal boundary pressures was as follows: It has previously been shown that, as the sink-tube axial velocity is deflected, the pressure outside the probe holes increases or decreases depending on the sense of angular rotation and the probe hole in question. As the pressure outside the probe hole which gives less flow for a given pressure is reduced, a point is reached where the flow approaches zero. By referring to Figure 2.8, it can be seen that, as the flow approaches zero, the relation between the pressure outside the hole and the resulting flow becomes highly non-linear.

This highly non-linear flow region produces the dogleg effect noted above. This effect is not present when the direction of rotation is reversed for, as the boundary pressure outside the hole which gives the greater flow for a given pressure is reduced, the non-linear portion of the curve is avoided*. At the same time, the other probe hole is experiencing increasing pressure and hence this combination produces no dogleg effect. Thus, to remove the effect, the probe hole without the trough was altered to give approximately the same pressure-flow characteristics as the other probe hole.

To explain the difference in the maximum signal output between clockwise and counter clockwise rotation, one has only to realize that the positioning of the probe holes with respect to the center line of the sink-tube is critical. If the holes are off center the slightest amount, the output will be decreased on one side and increased on the other resulting in different peak outputs.

The effect of the gain continually increasing with increasing ω can be partly explained by realizing that deflection of the first stage power jet is roughly proportional to $(\Delta q)^2$. Generally the output pressure of a proportional amplifier is given by

$$\Delta P_o = K_1 \Delta P_c$$

$$\text{but} \quad \Delta P_c = K_2 (\Delta q^2)$$

---

* At least over the range of rotations tested.

$$\text{hence} \quad \Delta P_o = K_3 (\Delta \alpha)^2$$

Now as shown in Figure 2.8, $\Delta \alpha$ is approximately proportional to ω over a substantial range of operation, making the output pressure generally proportional to the square of ω. This of course is only approximate but does roughly explain the increasing gain of the device. In fact, if the output pressure is converted to flow using the output characteristics of the second stage amplifier, one finds the output flow quite linear with respect to ω.

Although accurate verifications of the explanations given for items 2, 3, 4, and 5 above were not accomplished due to inaccessibility of the rate table, the explanations given were partially verified and showed that the dogleg had been removed but that only slight improvement was made in balancing the outputs by centering the probe.

The zero input bias signal was found to be only partly due to the unequal flows from the probe. The amplifiers themselves are biased when the control flows are zero. This can be reduced somewhat by proper arrangement of the cascade so that the output bias of one tends to cancel the output bias of the next stage. However, adjusting orifices generally must be placed somewhere in the cascade to remove the bias.

The results of the frequency response tests verified the pure time delay nature of the dynamics of this sensor. The experimental phase data is approximate at the low frequencies because the method used to obtain the data (the input and

output were recorded on permanent recording paper and were compared in order to measure phase) could not discern small phase shifts. The amplitude data, however, is quite accurate.

Lissajous figures on an osciloscope could not be used to obtain frequency response data because the output noise moved the figures around the scope precluding any measurements*.

The best data was obtained by taking pictures of the oscilloscope traces and measuring phase and attentuation data from these. The rapid increase in phase verifies the existence of a pure time delay. The deviation from theory in phase shift and attenuation is probably due to volumes in the lines connecting the first and second stage amplifiers and the volume and resistance of the orifices between the output of the second stage amplifier and the pressure transducer.

The results of the last test showed the output signal did not change while the sensor was being simultaneously rotated about its sensing axis and an arbitrary axis.

2.7 Conclusions and Recommendations

Throughout the development of this rate sensor little attempt has been made at optimization. The objective was to develop a rate sensor capable of being used in a control system. To this end the following conclusions are drawn:

---

* The noise of fluidic proportional amplifiers is of a peculiar nature. Although high frequency noise is prevalent as shown in Figure 2.13, a more disturbing very low frequency noise is present which causes the signal to wander and make unexpected excursions which appear almost as steady state bias changes.

1. Use of the design procedure suggested in article 2.2 will allow the designer to theoretically design a rate sensor peculiar to his applications.

2. The steady state gain of the unamplified signal may be predicted analytically but due to the low input impedance of the type of amplifier used, the amplified gain will have to be determined experimentally.

3. The dynamics of the sensor may be determined to a reasonable degree of accuracy by theory.

4. The output of the sensor is very dependent on the accuracy of the machining of the probe holes and alignment in the sink-tube.

5. Noise of the very low frequency type is a serious problem causing unexpected wandering of the DC level of the signals.

6. Contrary to the results of Sarpkaya, it was found that closing one of the sink-tubes and keeping the flow constant, resulted in an increased output signal for a given ω. Since this equivalently means nearly the same signal with less power consumption, the author recommends that sensors of this type be built with only one sink-tube and, as recommended by Sarpkaya, that the end opposite the sink-tube be designed to streamline the flow into the sink-tube.

CHAPTER III

ANGULAR POSITION SENSOR ANALYSIS AND DESIGN

3.1 Criteria Used in Selecting Operating Principle

Angular position of the system can be obtained by analog[8] or digital[3,9] integration of the angular rate signal available from the vortex rate sensor. Digital integration would possibly involve developing a pressure sensitive oscillator and some form of digital-to-analog converter, both of which are beyond the time limitations of this thesis. Since a linear position signal over a large range of angular positions for demonstration purposes was desired, analog integration was ruled out since very large volumes would have been required to "store" the position signal. Furthermore, the state of the art of pure fluid analog computation[7] is such that up-down integration is inaccurate.

3.2 Position Sensor Description

Because of the problems mentioned above, it was decided to use a moving part position sensor consisting of a pendulum set between a pair of flapper nozzle valves to obtain a differential pressure signal that is a function of angular position. A schematic of this sensor is shown in Figure 3.1 and a photograph of the final design is shown in Figure D.3. The

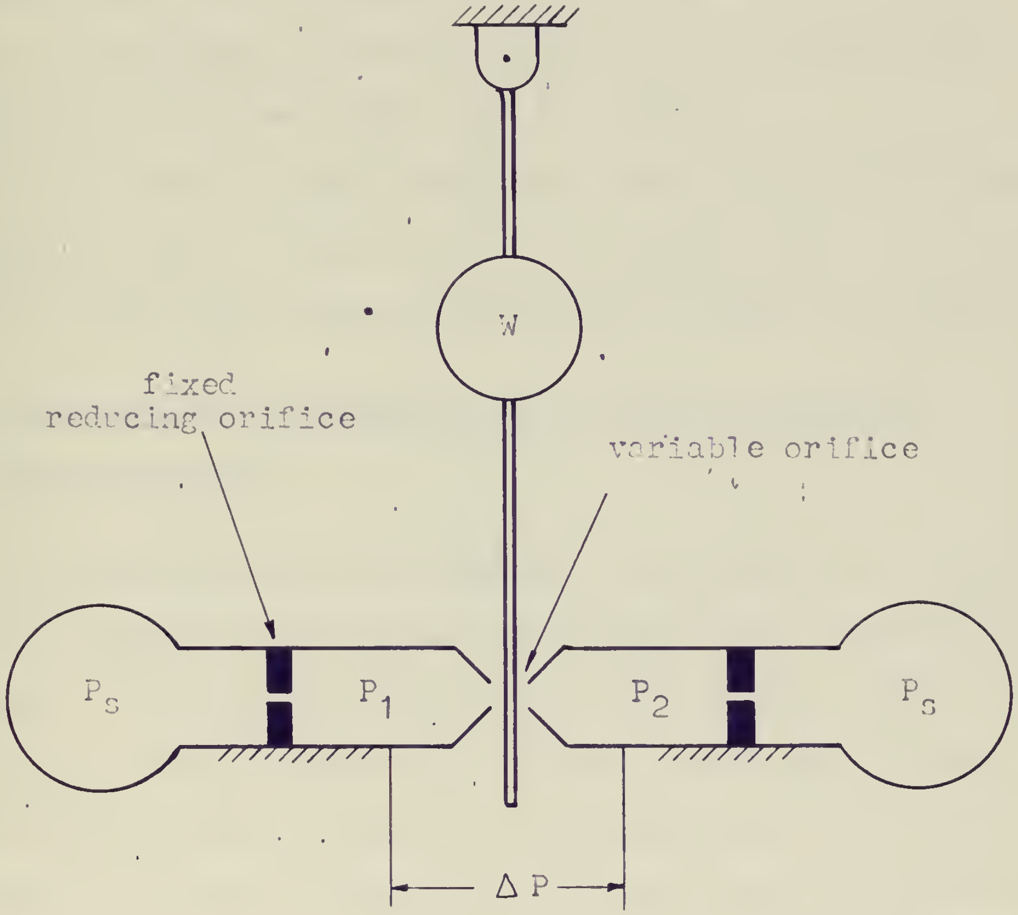

Figure 3.1

Sketch of the Angular Position Sensor

device is designed so that as the sensor rotates, the pendulum trys to return to a vertical position. In so doing, it widens the gap on one side and closes the gap on the other until the moments caused by the flow forces from the nozzles, balance the moment due to the weight of the pendulum. When this occurs a differential pressure exists in the chambers and constitutes the output signal of the sensor.

It is readily seen that the output differential pressure signal varies as the sine of the angular position and that the sensor also senses direction of angular position.

3.3 Discussion of the Dynamics of a Pendulum Angular Position Sensor

If the bearing which supports the pendulum is relatively free of damping, the angular position of the pendulum is unstable and the slightest perturbation will start the device oscillating. In the bang-bang control envisioned for the final system, this oscillation is undesirable. To understand the reasons for this instability, a linear model of the system can be constructed to describe the behavior of the system when the angular position of the pendulum is small. Figure 3.2 shows an analytical model of the sensor. Summing moments about the pivot point gives the following differential equation:

$$\frac{W}{g} l_w^2 \ddot{\theta} + b l_b \dot{\theta} + (K l_n + W)\theta = T_d(t)$$

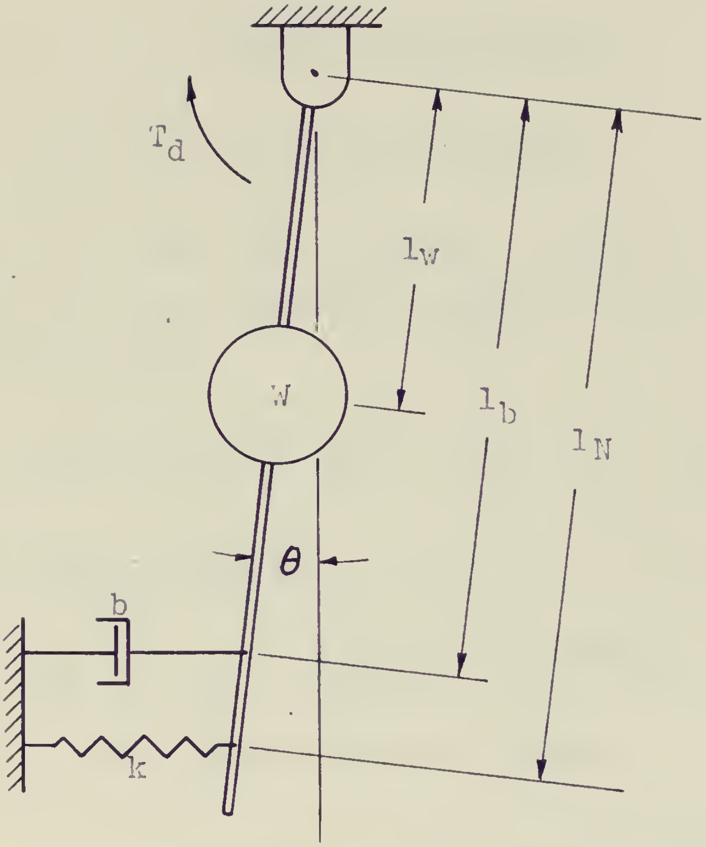

Figure 3.2

Analytical Model of the Position Sensor

where $\dot{\theta}$ = $d\theta/dt$

$\ddot{\theta}$ = $d^2\theta/dt^2$

bl_b = equivalent viscous damping

k = equivalent spring constant of the flapper nozzle valves

T_d = a disturbance torque

Neglecting the term $W\theta$, since it is much smaller than $kl_n\theta$, and introducing the symbols $J = \frac{W}{g} l_w^2$, $B = bl_b$, $K = kl_n$, and $s = d/dt$ gives

$$\left[Js^2 + Bs + K\right]\theta = T_d \qquad (3.1)$$

The spring force $K\theta$ is given by

$$K\theta = (P_1A - P_2A)l_n = \Delta PAl_n$$

where P_1 = pressure in one chamber

P_2 = pressure in the opposite chamber

rearranging gives

$$K = Al_n \frac{\Delta P}{\theta} \qquad (3.2)$$

The linearized transfer function between ΔP and θ is, in general, a first order lag of the form[10].

$$\frac{\Delta P}{\theta} = \frac{C_1}{\tau s+1} \qquad (3.3)$$

Substituting equation (3.3) into (3.2) gives

$$k = \frac{Al_nC_1}{\tau s+1} = \frac{C_2}{\tau s+1} \qquad (3.4)$$

If this equation is substituted into equation (3.1) the result is

$$\left[Js^2 + Bs + \frac{C_2}{\tau s+1} \right] \theta = T_d$$

From this the transfer function between θ and T_d is

$$\frac{\theta}{T_d} = \frac{\tau s + 1}{J\tau s^3+(J+B\tau)s^2+ Bs+C_2}$$

The characteristic equation of this transfer function is

$$\left[J\tau s^3 + (J + B\tau)\, s^2 + Bs + C_2 \right]$$

The Routh stability criterion for linear systems gives the condition for stability as

$$B(J+B\tau) > J\tau C_2$$

or

$$B > \frac{\sqrt{J^2 + 4J\tau^2C_2} - J}{2\tau} \qquad (3.5)$$

where the positive sign for the radical has been chosen since the damping can not be negative. If equation (3.5) is rewritten as

$$B > 1/2 \left[\sqrt{\left(\frac{J}{\tau}\right)^2 + 4JC_2} - \frac{J}{\tau} \right]$$

it can be seen that the value of C_2 is the important parameter determining the stability of the system. As C_2 increases, B must be made correspondingly larger. From equation (3.4), C_2 is the value of the steady state spring constant of the flapper-nozzle valves. Thus, as this spring constant increases, the magnitude of the damping must be increased.

Initially, to introduce damping into the system, the ball bearing used to support the pendulum was packed with heavy grease. This did not introduce a sufficient amount of damping into the system. The problem was finally solved by placing two small squeeze film dampers on either side of the pendulum and adding a minute amount of grease to aid in the damping process*.

3.4 The Influence of Acceleration on the Output Signal

The output signal of this sensor will be influenced by the angular acceleration of the device to which it is attached. Figure 3.3 is a sketch showing the position sensor mounted on the system and offset from the axis of rotation by a distance r.

If the sensor is given an angular acceleration α,

---

* Over most pressure settings the air in the squeeze film dampers provided sufficient damping. However, if the chamber pressures were made too high then the size dampers used were inadequate.

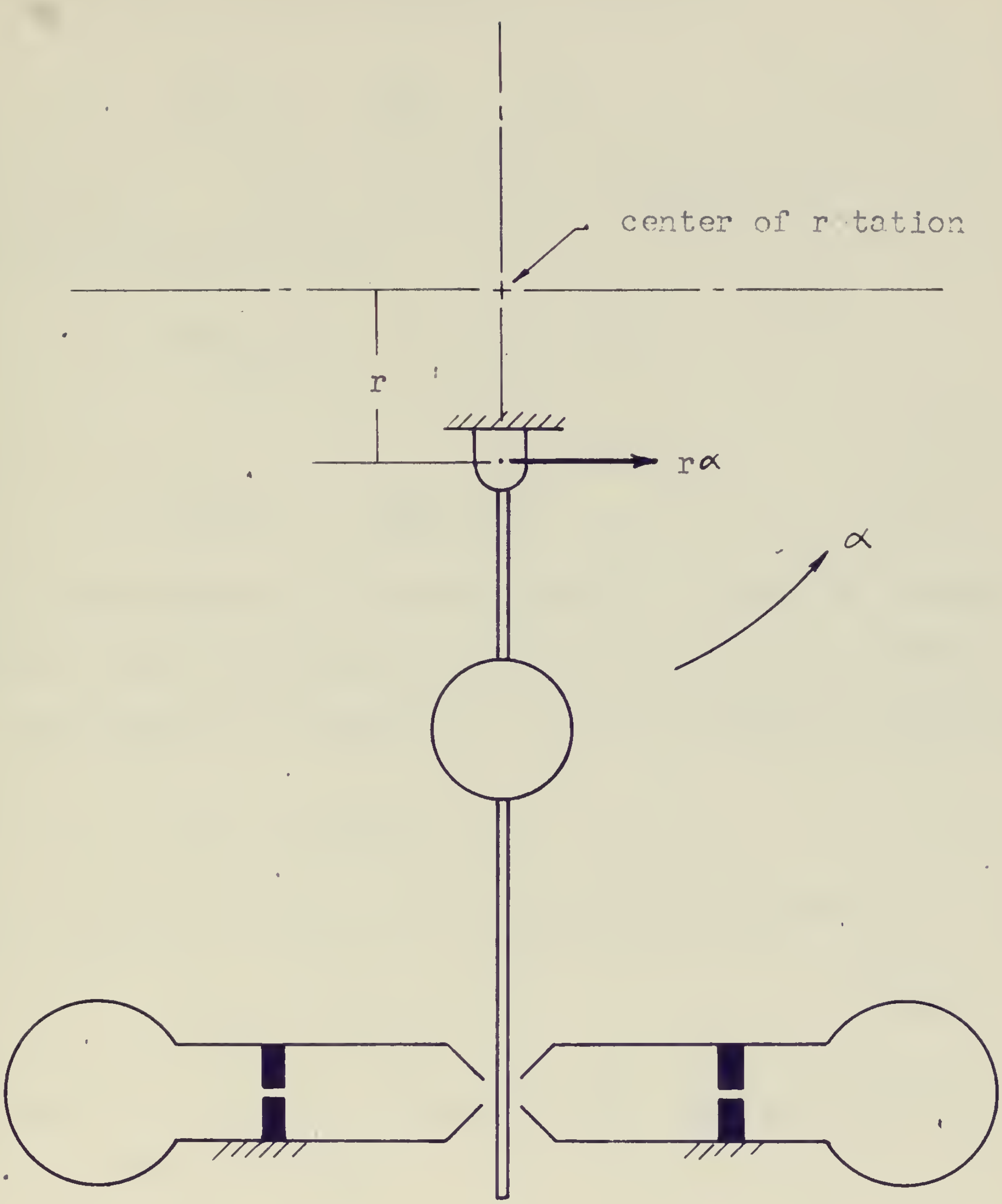

Figure 3.3

Sketch of the Position Sensor Mounted on the System

then the end of the pendulum receives a linear acceleration $r\alpha$. The torque on the pendulum is given by

$$T_{LA}^{*} = \frac{w}{g} r\alpha \qquad (3.6)$$

This torque must be balanced by the pressure forces on the end of the pendulum giving

$$\Delta P_{LA} A l_n = \frac{w}{g} r\alpha$$

or

$$\Delta P_{LA} = \frac{wr}{gAl_n} \alpha \qquad (3.7)$$

This ΔP corresponds to an error signal. It may be reduced by making r small assuming the other parameters are fixed.

The moment of inertia (I) of the pendulum is given by

$$I = \frac{w}{g} l_w^2$$

Thus the resulting torque on the pendulum is given by

$$T_{AA} = \frac{w}{g} l_w^2 \alpha \qquad (3.8)$$

This torque too must be balanced by the pressure forces on the end of the pendulum giving

$$\Delta P_{AA} A l_N = \frac{w}{g} l_w^2 \alpha$$

or

$$\Delta P_{AA} = \frac{w l^2_w}{gAl_n} \alpha \qquad (3.9)$$

---

* Subscripts LA and AA refer to linear acceleration and angular acceleration respectively.

This ΔP also represents an error in measuring angular position. The total error signal is the sum of the two differential pressures given by equations (3.7) and 3.9)

$$\Delta P_{error} = \left(\frac{wr}{gAl_n} + \frac{wl^2_w}{gAl_n} \right) a \qquad (3.10)$$

This pressure error may be converted into an equivalent angular position error by the equation

$$\theta = \text{Sin}^{-1} \left(\frac{\Delta P \, Al_n}{wl_w} \right) \qquad (3.11)$$

which is obtained by a steady state torque balance on the pendulum when at an angle θ from the vertical. Substitution of the value of ΔP from equation (3.10) into equation (3.11) will give the error in terms of angular position. Primarily because the accelerations to be dealt with in this system are quite small, substitution of the actual values into equations (3.10) and (3.11) showed that the maximum probable error would be less than one degree. If this system were to be made into a very fast high torque system, this type of position sensor would probably be undesirable unless the designer wished to have acceleration feed back in the system.

3.5 Transfer Function

Because the amount of damping added to the system to make it stable is difficult to determine, it was decided to connect the output signal into a pressure to electric transducer and experimentally determine the transfer function. By observing step responses on an oscilloscope, the system dynamics

can readily be determined.

The procedure was as follows:

1) The output signal was connected to the transducer and loaded into orifices which approximated the size to be expected at the control ports of the summing device.

2) The output signal was then displayed on an oscilloscope.

3) The pendulum was given an initial deflection and then released.

The response of the pendulum was observed to be essentially that of a first order lag. By measuring the time it took the signal to decay to 36.8 percent of its initial value, gave a close approximation to the time constant of the sensor. By averaging a large number of such measurements the time constant of the system was found to be 0.04 seconds. This time constant was found to be much larger than the time constant associated with the flapper-nozzle chambers*. Apparently, the measured time constant is essentially that of the mass-damping time constant of the system.

A typical steady state output curve is shown in Figure 3.4 from which the steady state gain may be measured.

The transfer function, relating the output pressure signal to the input angular position signal for small valves of θ, is given by

---

* The time constant due to the volume of the flapper nozzle chambers and connecting lines was found to be 0.008 seconds. The calculations are not shown here as they can be found in any standard reference such as reference 10.

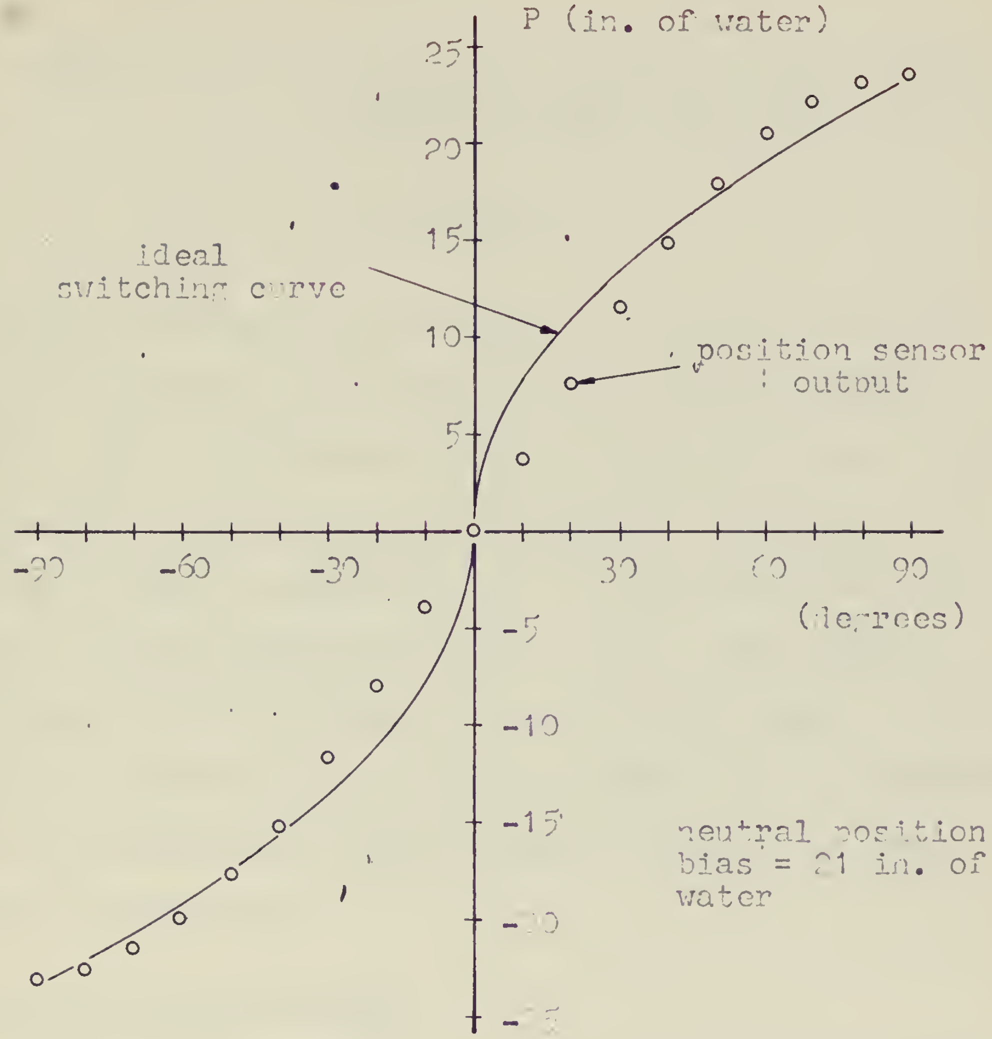

neutral position bias = 21 in. of water

Figure 3.4

Typical Steady State Position Sensor Output

Showing Approximation to the Ideal Switching Curve

$$\frac{\Delta P}{\theta} = \frac{K_2}{\tau_2 S+1} \qquad (3.12)$$

where K_2 = gain to be determined from a plot similar to Figure 3.4 once the final system pressures have been set

τ_2 = 0.04 seconds

Before concluding this chapter it is to be noticed that little information has been given concerning design procedures. This was purposely done as such procedures are more adequately covered in the literature[10]. However, the designer must keep in mind the over all system and the relationship of each component to the others. For example, it is obvious that the output of the position signal is to eventually be compared with the rate signal. It is therefore reasonable to assume that these signals should be of the same order of magnitude.

3.6 Switching Curve Computer

As shown in Appendix C.1, the ideal switching curve for this system is a parabola passing through the origin. The slope of this curve is infinite at the origin. Since it was planned to generate the switching curve by operating on the output signal of the position sensor, this meant that as θ varied slightly from its zero position an infinite gain would be required. Because of this consideration and the fact that the output signal of the rate sensor is not dependable at very low angular rates, the output of the position

sensor, without modification, was used as the switching curve.

Such a sine curve output can be adjusted to approximate a parabola over a large range of position signals as shown in Figure 3.4. The approximation is poor when θ is small, however, and thus, it is to be expected that "linear switching" will take place when the errors introduced into the system are small.

CHAPTER IV

SIGNAL COMPARATOR

4.1 General

The method[11] selected to algebraically sum the pressure signals from the rate sensor and position sensor consists of adding additional sets of controls to a proportional amplifier and having the power jet deflect in accordance with the vector sum of their momentums*. A stream interaction proportional amplifier, operating on this principle, is available from Corning Glass Works** and has two sets of control ports. The design data sheet accompanying this amplifier does not indicate that the second set of controls can be used for summing and, therefore, gives no data on the gain of these ports. In fact, the ports are not equipped with fittings and, therefore, had to be adapted for use in this control system. A photograph of this "summer-amplifier" is shown in Figure D.2. The vertical controls are the secondary controls and were adapted for use by inserting hypodermic tubing into the holes and then cementing the tubing into place.

---

* Other methods of summing signals, using no moving parts, are available and could have been used in this system.

** Catalog Number FD2511-2-1211 September, 1965

4.2 Experimental Analysis

A silhouette of the amplifier described above is given in the design data sheet. From this silhouette, it was found that the width of the secondary control ports is less than the width of the primary ports. In addition, the secondary ports are not perpendicular to the power jet. Because of these geometrical differences, it is obvious that if the same pressure differential is applied to both sets of controls ports, the power jet will be deflected a greater amount by the primary control ports. As a consequence of this greater deflection, the output pressure will be larger. Therefore, the primary control ports will exhibit a greater gain.

To determine the difference in the gain of these two sets of control nozzles, a number of tests were performed on the amplifier. The tests consisted of 1) systematic variation of the control port bias levels about the levels expected from the outputs of the rate and position sensors, 2) systematic variation of the supply pressure, and 3) at any particular bias level and supply pressure setting, recording the gains of the two sets of control ports.

Typical data from these tests for one particular combination of supply pressure and bias level settings is shown in Figure 4.1 During all these tests, the output of the summer-amplifier was loaded into a manometer.

4.3 Discussion of Results and Conclusions

The results of these tests showed that the gain ratio of the two pairs of control ports did not remain constant as

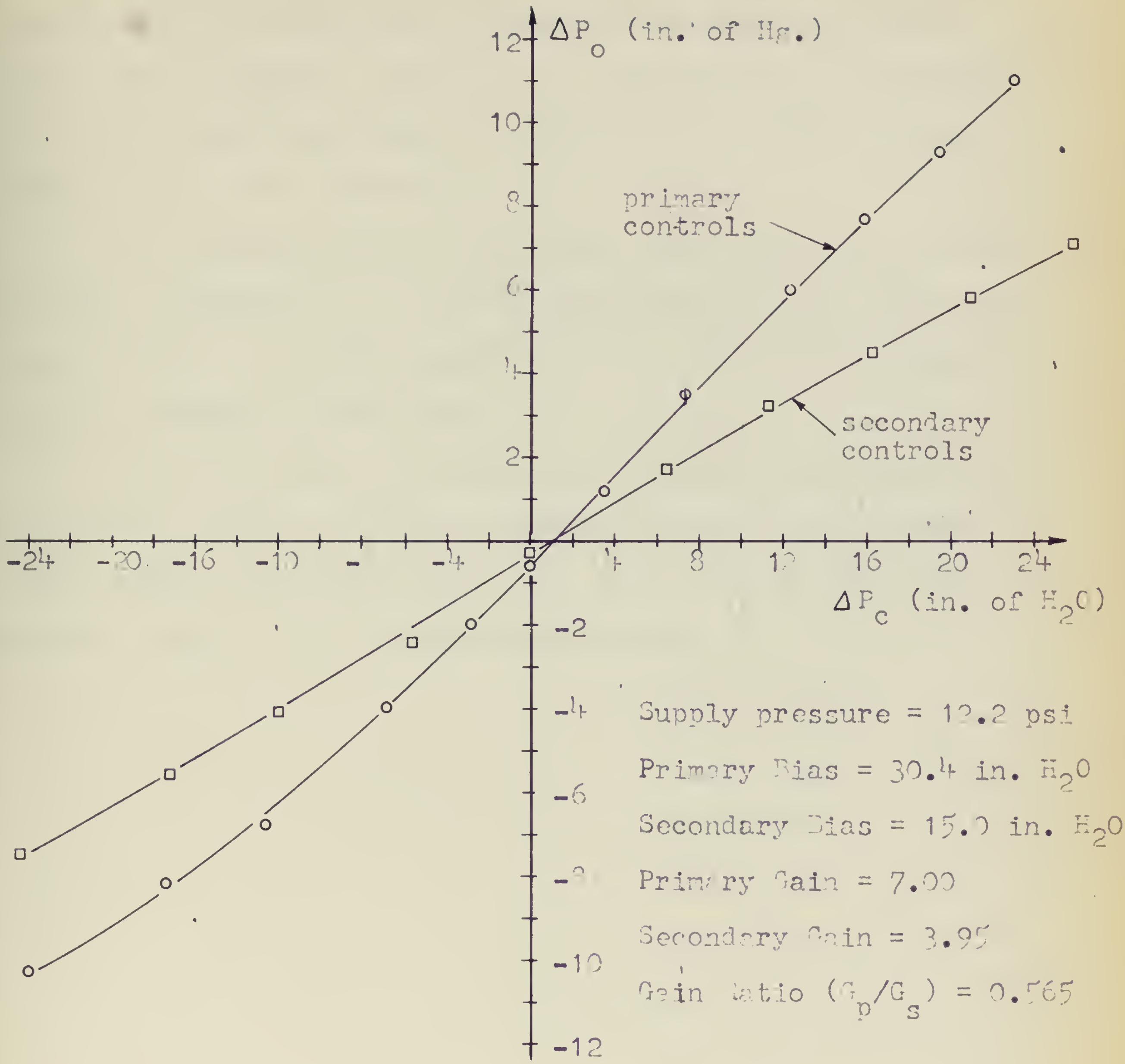

Supply pressure = 12.2 psi

Primary Bias = 30.4 in. H_2O

Secondary Bias = 15.0 in. H_2O

Primary Gain = 7.00

Secondary Gain = 3.95

Gain Ratio (G_p/G_s) = 0.565

Figure 4.1

Typical Summer-Amplifier Test Results

the control bias level or as the supply pressure was changed. However, for any given set of control bias pressures and a given supply pressure, the ratio of the gains of the two control ports could repeatedly be obtained after signals were introduced and then removed.

The results further showed that once the ratio of gains had been determined at a particular setting of bias levels and supply pressure that the algebraic sum of two control signals could accurately be predicted.

From the results of these tests, it was concluded that this device could be used as a summing device with accurate and predictable results if the bias levels of the input signals and the power jet pressure were known.

CHAPTER V

DRIVING BISTABLE AMPLIFIERS WITH PROPORTIONAL AMPLIFIERS

5.1 Introduction to Input Control Impedances of Bistable Amplifiers[12]

In Figure 5.1 a typical bistable fluid jet amplifier is shown with the power jet attached to the left boundary wall. In this condition, the entrainment flow through the left control port is greater than that through the right when both control ports are open to the atmosphere. If the left control port is sealed from the atmosphere while the right port is left open and a plot of the left control pressure and flow is made, a plot similar to Figure 5.2 will be obtained. This graph shows that as the left control pressure is increased above atmospheric pressure, a point is reached where the jet is supplied all the entrainment flow it can take. It then becomes separated from the left wall and switches to the right. When this occurs, the flow suddenly decreases due to a different pressure in the interaction chamber and now presented to the left control port. If the left control port pressure is then decreased, a point is reached where the jet will switch back to the left side.

If the amplifier has perfectly symetrical control ports, the "stream-on-right" curve will represent the pressure-flow characteristics at the right control port when the stream is

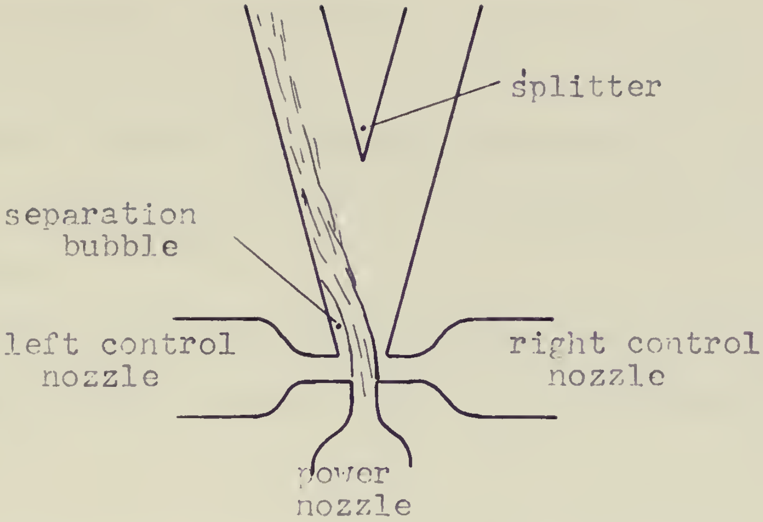

Figure 5.1

Bistable Fluid Jet Amplifier

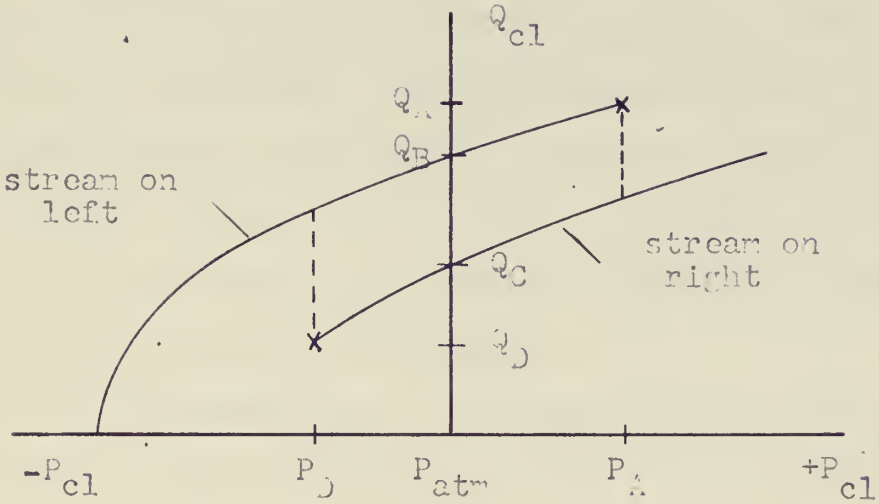

Figure 5.2

Input Characteristics of a Bistable Amplifier

attached to the left wall. From the graph it is seen that the flow differential required for switching from left to right is $Q_A - Q_C$ and the pressure differential required is $P_A - P_{atm}$. Similarly the flow differential to switch from right to left is $Q_B - Q_D$ and the required pressure differential is $P_{atm} - P_D$. The two sets of flow and pressure differentials are not neccessarily equal.

The effect of loading on the output legs of these devices is generally to decrease the flow and pressures required for switching.

5.2 Problem Statement and Objective of Experiments

Because of the nature of operation of proportional amplifiers, the useful signals from these devices are elevated about a bias pressure level greater than atmospheric. It was not clear what the effect of this bias level would be on the switching characteristics of a bistable amplifier being driven by a proportional amplifier. This information was necessary before undertaking the design of the bistable reaction jets in order that the pressure differential required at the controls of the proportional amplifier, to effect switching of the reaction jets, might be minimized.

The test procedure was to bias the control ports of a memory device* at various pressure levels above atmospheric and then measure the pressures and flows required to effect switching at these elevated levels.

---

* A memory device was selected for these tests as this is the type of device used for the first stage of the reaction jets discussed in the next chapter.

During the tests the output legs were loaded into an orifice whose area was approximately 0.75 times the receiver areas of the device.

5.3 Test Results and Conclusions

The memory device selected for these tests was a Corning Standard Size Load Insensitive device*.

A graph of representative results is shown in Figure 5.3. It can be seen that the effect of the bias level is to radically increase the flow and pressure differential required for switching.

During these tests it was found that the input characteristics of each control port were quite different. Therefore, to more accurately show the flow and pressure differentials required for switching, the pressure-flow relations for both legs are plotted.

When a bias level is present at the control ports of a bistable amplifier, the power jet is being supplied more flow than it can entrain. In this condition the bias flow is attempting to operate the device in a proportional manner. However, due to the close proximity of the bounding walls, the jet will still reduce the pressure slightly on one side and attach itself to that wall. This increased pressure differential required for switching can not be tolerated in this system as it represents a large hysteresis in the

---

* Catalog No. FL 2212-2-1211

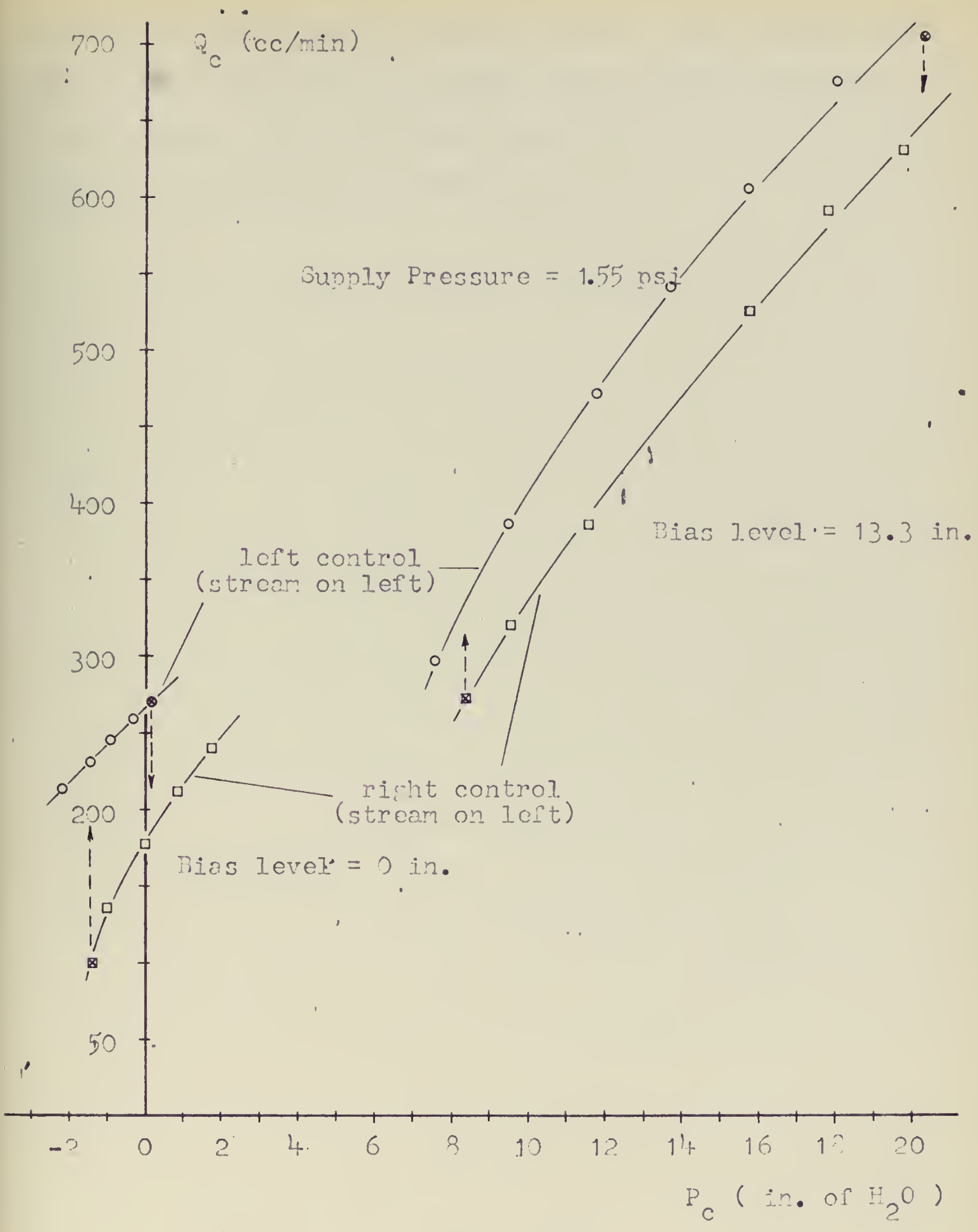

Figure 5.3

Effect of Biasing the Controls of a Bistable Amplifier on the Switching Pressures and Flows

switching of the bistable reaction jets. This problem, however, can be eliminated by making the bistable amplifier large enough so that the entrainment flow of the power jet is just equal to the bias level flow.

CHAPTER VI

POWER AMPLIFIER AND BISTABLE REACTION JETS ANALYSIS AND DESIGN

6.1 Determination of the Required Output Thrust

So far little mention has been made of the dynamics of the system to be controlled. As mentioned in the introductory chapter, the system was to approximate an ideal inertia load. The dynamics of such a system are given by

$$T = J\ddot{\theta} \qquad (6.1)$$

where T = the applied torque to the system

J = polar moment of inertia

θ = angular displacement

$\cdot$ = differentiation with respect to time

If this equation is integrated once with respect to time and the initial angular rate is assumed to be zero, one obtains

$$\dot{\theta} = \omega = \frac{T}{J} t \qquad (6.2)$$

Integrating equation (6.2) with respect to time and setting the initial angular displacement to zero gives

$$\theta = \frac{T}{J} \frac{t^2}{2} \qquad (6.3)$$

From the design considerations discussed in the introductory chapter, it was desired that the system respond fairly slowly and be able to receive large angular displacements. On the basis of these considerations, it was decided that the parameter T/J should be such that if the system starts from rest under full acceleration, it must be traveling at an angular velocity equal to 1.1 radians per second at the end of 45 degrees of angular displacement.

If equation (6.3) is solved for t and substituted into equation (6.2) the result upon rearranging is

$$\frac{T}{J} = \frac{\omega^2}{2\theta} \tag{6.4}$$

Substituting the values of ω and θ into this equation gives $T/J = 0.772\ \text{sec}^{-2}$. From equation (6.3) the time to travel 45°, with this T/J ratio, is 1.424 seconds.

Having determined the T/J ratio, an estimate of the system's final polar moment of inertia was made by accurately determining the polar moment of inertia of the rate sensor and multiplying the result by a factor of three to account for the remaining equipment to be added to the system. The J so calculated was found to be 7.5 in-ozf-sec^2 which results in a required torque of 5.79 in-ozf. If the lever arm is assumed to be 5.79 inches, then the thrust required is one ozf.

6.2 Introductory Theory of Staging Unvented Bistable Amplifiers[12, 13, 14]

This system was to develop the required thrust by using the change of momentum in a reaction jet. Since the

power available from the output legs of the summer-amplifier was too small to develop the required thrust, this signal had to be amplified.

Compagnuolo[13] has shown that this power amplification can be efficiently accomplished by staging bistable amplifiers in ascending order of size with each stage operating at the same supply pressure. He has pointed out that in order to make such a cascade, two design principles must be adhered to:

1) For maximum pressure recovery, the splitter distances must be kept small, preferably in the core region* of the power jets which in general is approximately six nozzle widths down stream.

2) In order that the units be capable of being loaded, each stage must have a high degree of stability which implies moving the splitter down stream to over approximately twelve nozzle widths.

At the present state of the art, a bistable unit can not possess both the characteristics of high pressure recovery (high efficiency) and high stability. As the splitter is moved down stream, the pressure which can be recovered, falls rapidly. If the splitter is moved up stream, then the ability to operate under load (stability) falls off rapidly.

---

* The core region of the power jet is that region in which the velocity of the jet has not been reduced from its value at the power nozzle due to viscous friction with the surrounding fluid.

Compagnuolo suggests that since the last stage is the most important for maximum efficiency that it be made with the splitter located in the core region of the power-jet. This stage can then be held into the load by making the preceeding stages high stability devices. The result is that the overall cascade exhibits high efficiency and stability under load.

In general the instantaneous flow gain of high stability devices is approximately ten. This means that it is possible to increase the size of the power nozzle of each stage by roughly a factor of ten. It should then be possible to have flow gains in a three stage device of at least 1000 and, if the efficiency of the cascade is good, power gains of greater than 5000.

6.3 Initial Experimental Design

Figure 6.1 shows an output leg of a bistable amplifier turned through a 90 degree angle. If a control volume is drawn as shown and the momentum equation for steady state operation is written for the x-direction, the resulting thrust due to the exiting jet is found to be:

$$T = \rho A_e V_e^2 \tag{6.5}$$

Assuming uniform velocity over the exit area, equation (6.5) can be rewritten as

$$T = \rho \frac{Q_e^2}{A_e} \tag{6.6}$$

From this last equation, knowing the thrust desired and

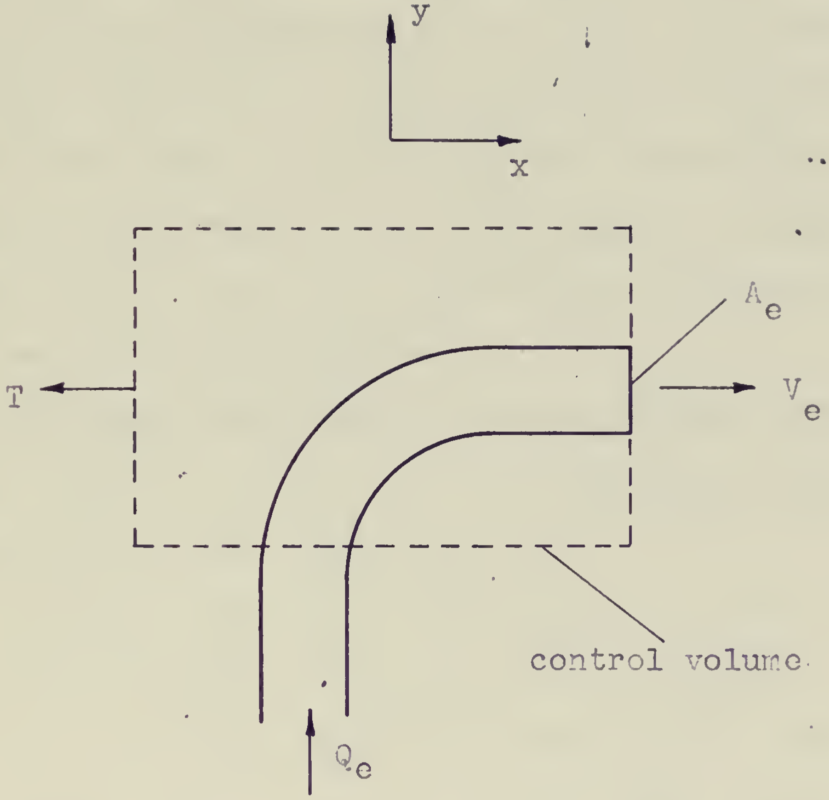

Figure 6.1

Control Volume for Determining the Output Thrust

assuming a reasonable value for the exit area, one can determine the flow required to develop the desired amount of thrust.

If one further knows the differential flow required for switching the first stage, then the flow gain needed can be readily determined.

It was shown in the preceeding chapter that it is desirable to have the entrainment flow of the first stage approximately equal to the output bias flow of the driving proportional amplifier. This entrainment flow depends on the geometry of the amplifier and the supply pressure.[12] It can be seen that if sufficient experimental data were available that it would be possible to

1) determine the supply pressure required for a chosen first stage amplifier design from the entrainment flow versus supply pressure characteristics and

2) with the supply pressure chosen as above, determine the differential flow required for switching.

It would then be a simple matter to determine the flow gain required and the number of amplification stages needed.

Lacking any such quantitative data, a preliminary two stage bistable amplifier was constructed in order to obtain the following information: (listed also are the reasons this information was desired)

1) Entrainment flows of a first stage design at various supply pressures to determine the supply pressure setting to match the output flows of the summer-amplifier.

2) Stability under load of the unit to check the set-

ting of the splitter distances, wall set back distences, etc.

3) Output pressure-flow relationships to determine the optimum loading for maximum torque output.

4) The number of stages required to develop the desired torque.

5) The thrust output for various supply pressures and loads.

The important dimensions of the amplifiers used in this initial design are as follows:*

First Stage

Power nozzle width = w = 0.020 in.
Control nozzle width = w
Wall setback = 3w
Splitter distance = 14w
Aspect ratio = h/w = 1.5w
Receiver width = 3w

Second Stage

Power nozzle width = w = 0.0625 in.
Control nozzle width = w
Wall setback = 1.4w

---

* Many of the dimensions given here, such as wall setback and receiver width, are based on carefully considered data given in references 12, 13, and 14. Time and space limitations do not allow a full discussion of the effects of varying these parameters.

Splitter distance = 6w

Aspect ratio = 1.535w

Receiver width = 1.5w

The devices were made out of plexiglass using a pantograph engraving machine.

The results of tests performed on this initial design showed that at a supply pressure of two psi the entrainment flow in the attached side was approximately 0.04 SCFM. This flow was approximately equal to the no load output flow of the summer-amplifier when operating at the supply pressure expected for final design setting.

This device was quite stable provided the output load was relatively small. Typical output curves for the device are shown in Figures 6.2 and 6.3. In Figure 6.2 the device is not being driven by an external signal and therefore cannot be heavily loaded. The overload area represents conditions under which the second stage power jet commences to oscillate. In Figure 6.3 the device is being driven by another bistable amplifier. It is apparent that the device can now be more heavily loaded before the overload region is reached.

In order to determine the value of the exit nozzle area for maximum thrust, a number of nozzle load curves were drawn on a plot similar to Figure 6.3. It was found that maximum thrust output of one nozzle corresponded closely to the point of maximum power transfer between the amplifier cascade and the nozzles. Since loading decreases the flow

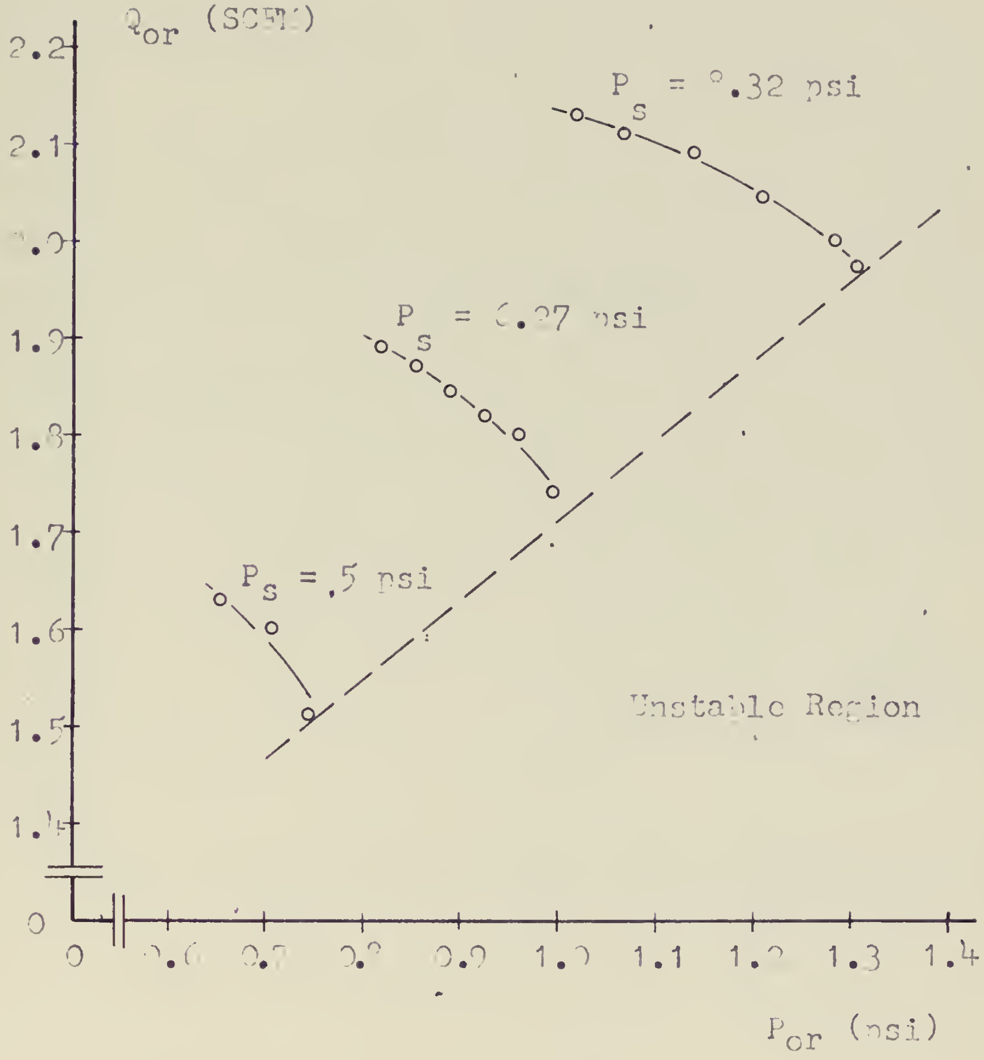

Figure 6.2

Output Characteristics of the Two Stage Bistable Amplifier

Without Driving Amplifier

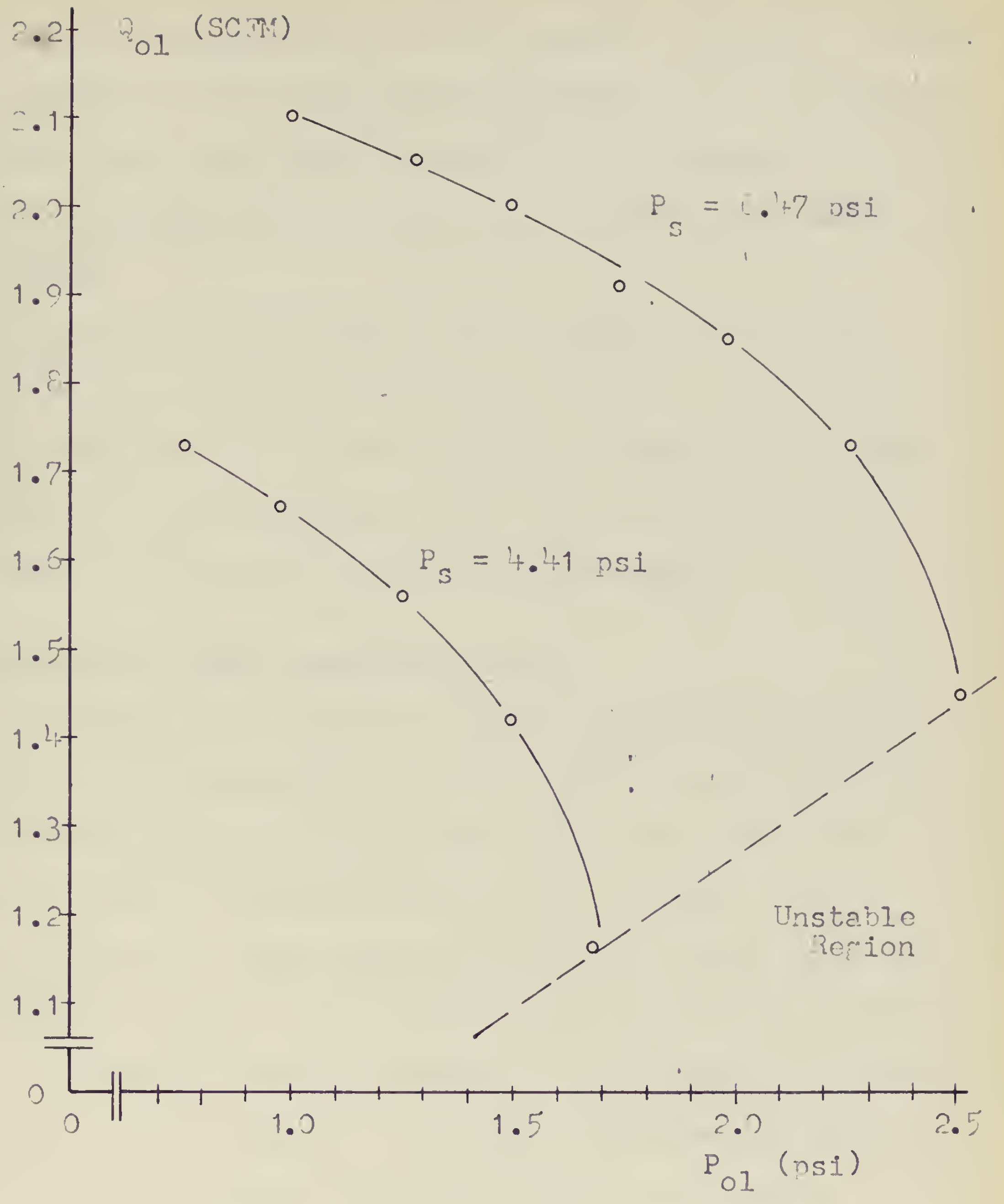

Figure 6.3

Output Characteristics of the Two Stage Bistable Amplifier
With Driving Amplifier

out of one leg, part of the flow is diverted into the other leg where it develops thrust in the opposite direction. Therefore, considering the total thrust developed from the device, it was found that the point of operation for maximum total thrust lay slightly up the output curve toward the region of higher flows.

The results also showed that in order for this two stage device to develop an ounce of thrust that the supply pressure would have to be over ten psi. Since this was incompatible with the entrainment flow desired, the final design would have to have at least three stages.

6.4 Final Three Stage Amplifier Design

In order to use the data gained from the two stage amplifier to full advantage, it was decided to use these first two stages in the final design and alter them only slightly in order to accommodate the third stage. This further allowed the power nozzle area of the third stage to be calculated from the data obtained on the two stage device.

The procedure used to determine the dimensions of the third stage are as follows: Assuming incompressible flow*, the flow from the third stage power nozzle is given by

$$Q_{j3} = C_d \, A_{j3} \sqrt{\frac{2}{\rho} \, P_s} \qquad (6.7)$$

---

* This assumption is reasonably valid as the final device was to operate at two psi.

where Q_{j3} = flow from third stage power nozzle

A_{j3} = area of third stage power nozzle

C_d = discharge coefficient

Similarly the second and first stage flows are given by:

$$Q_{j2} = C_d \, A_{j2} \sqrt{\frac{2}{\rho} \, P_s} \qquad (6.8)$$

$$Q_{j1} = C_d \, A_{j1} \sqrt{\frac{2}{\rho} \, P_s} \qquad (6.9)$$

The desired thrust is given by

$$T = \frac{\rho \, 0.8 \left(\sum_{n=1}^{3} Q_{jn} \right)^2}{A_{j3}} \qquad (6.10)$$

where it is assumed that the load orifice areas are equal to the areas of the third stage power jet and the factor 0.8 is to account for leakage flow out the opposite leg.

From the two stage amplifier, numerical values are known for equations (6.8) and (6.9). Furthermore, since P_s is known and assuming a value for c_d, equation (6.7) reduces to

$$Q_{j3} = (\text{Constant}) \, A_{j3} \qquad (6.11)$$

If the numerical values of equations (6.8) and (6.9) are substituted into equation (6.10) along with equation(6.11), a quadratic equation in A_{j3} is obtained. Solving this quadratic equation gives the third stage nozzle area. Since all dimensions of the third stage are determined from the

nozzle width, assuming an aspect ratio for the third stage will allow the nozzle width to be determined and hence specify the other dimensions of the third stage.

Following the above procedure resulted in the following dimensions for the final design:

First Stage

Power nozzle width = w_1 = 0.020 in.
Control nozzle width = $1.5w_1$
Wall setback = $3.0w_1$
Splitter distance = $18w_1$
Receiver width = $4w_1$
Aspect ratio = $1.5w_1$
Nozzle area = 0.0006 in.^2

Second Stage

Power nozzle width = w_2 = 0.0625 in.
Control nozzle width = w_2
Wall setback = $2.5w_2$
Splitter distance = $14w_2$
Receiver width = $3w_2$
Aspect ratio = $1.535w_2$
Nozzle area = 0.00655 in.^2

Third Stage

Power nozzle width = w_3 = 0.125 in.
Control nozzle width = w_3
Wall setback = $2w_3$

Splitter distance	$6w_3$
Receiver width	$1.4w_3$
Aspect ratio	$2.08w_3$
Nozzle area	0.0325 in.^{2}

A photograph of this device is shown in Figure D.4.

The circular chambers are vortex impedance matchers[15] modeled after those used by Compagnuolo[13].

In Figure 6.4 is shown the output thrust of the amplifier cascade versus supply pressure and input flow rate. The output flow of this final design oscillates due to the loading conditions unless the cascade is being driven by an external signal.

Figure 6.5 shows the input impedance characteristics for the right control port when the first stage power stream is attached to the right wall. The supply pressure is 1.96 psi.

6.5 Reaction Jet Cascade Dynamics and Transfer Function

The reaction jet cascade is characterized by two phenomena which are important when the device is placed in the control loop of the final system:

1) A hysteresis loop is present in the switching of the thrust from one side to the other

2) There is a finite time delay between the time a switching signal is received at the control ports until the thrust developed is switched from one side to the other.

The hysteresis loop is due to the characteristics of

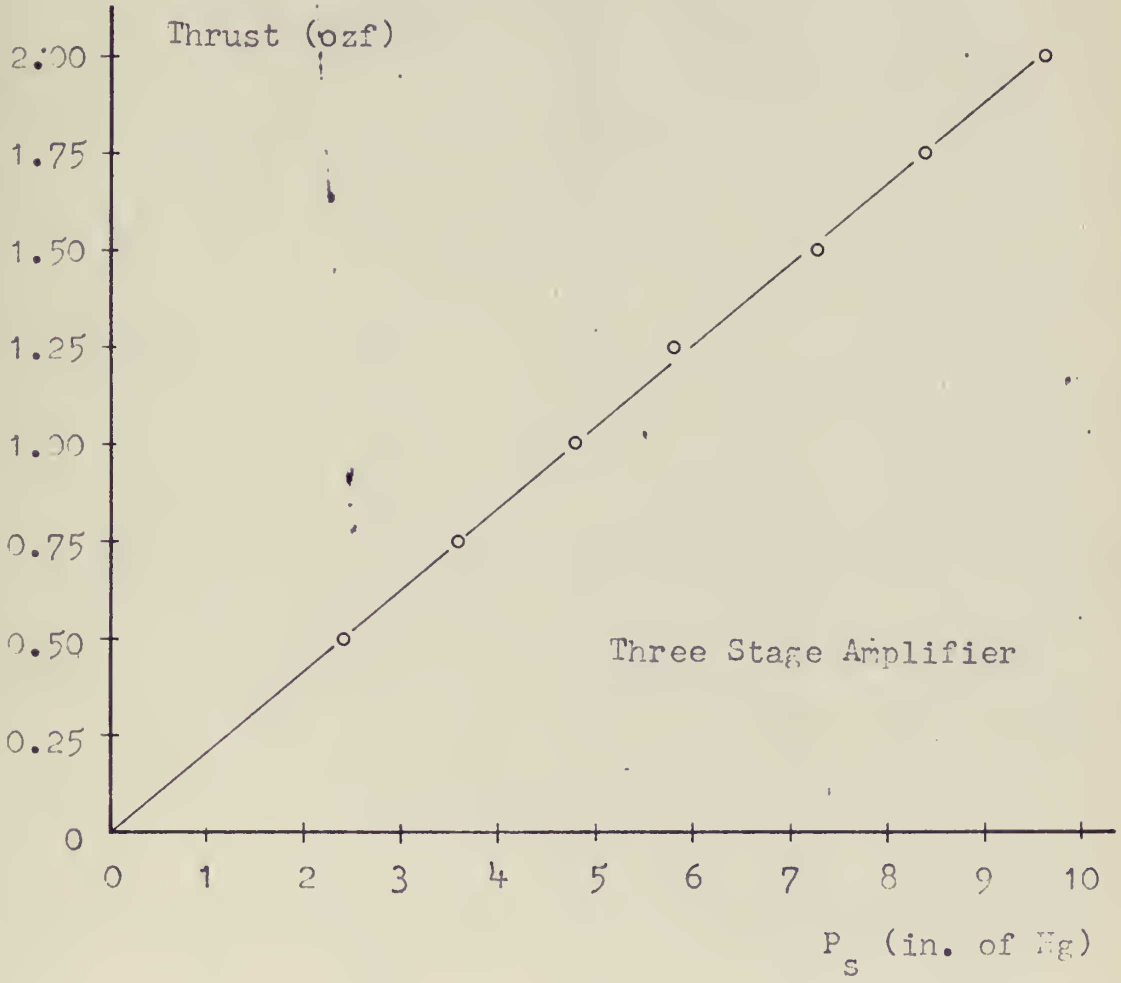

Figure 6.4

Reaction Jet Thrust Versus Supply Pressure

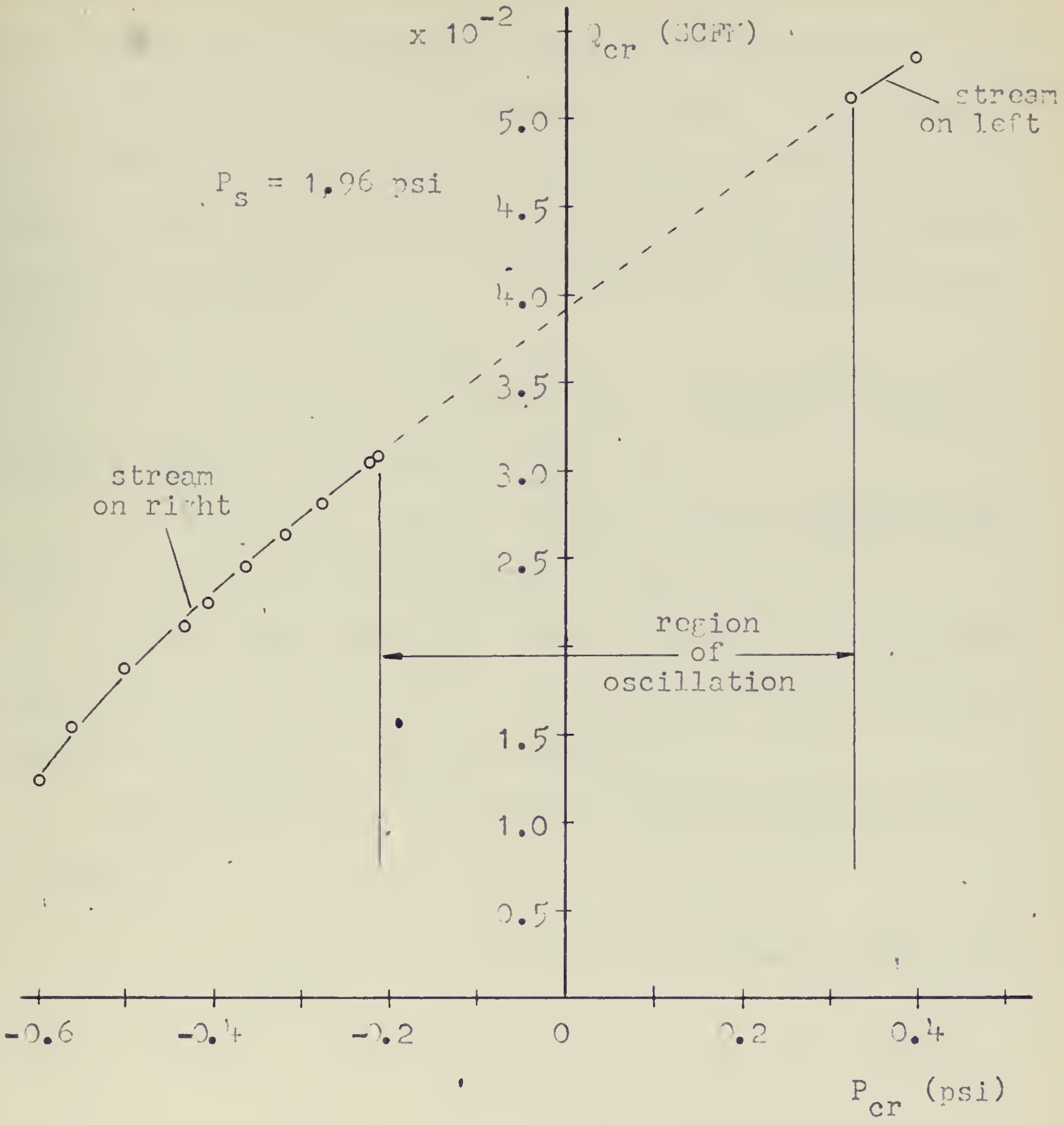

Figure 6.5

Reaction Jet Input Characteristics

bistable devices requiring a finite flow and pressure differential to exist across the control ports to effect switching. The half width of the hysteresis band was determined from actual measurements with the summer-amplifier set at its proper supply pressure and driving the reaction jet cascade. The half width was found to be 0.0685 psi. The time delay involves two major phenomena:

1) The time it takes the fluid streams to traverse physical distances (transport time) and

2) The time it takes to charge the interconnecting volumes to the required switching levels.

Actual measurements of this time delay were not made. From theoretical calculations in Appendix B the time delay constant was found to be 0.022 seconds.

The transfer function of the reaction jet cascade is thus given by

$$\frac{\pm T}{\Delta P} = e^{-\tau_3 s} \quad \text{with hysteresis of} \pm 0.0685 \text{ psi} \tag{6.12}$$

CHAPTER VII

CONTROL SYSTEM SYNTHESIS, PERFORMANCE AND ANALYSIS

7.1 System Synthesis

A major part of the problem of synthesizing the system components has been accomplished by careful consideration of the role each of these components was to play in the final system. However, in order to finally bring these components together into a working system it is necessary to know how each component will behave when actively loaded into the component it is to drive in the final design.

Of critical importance is the setting of the power supply pressure to the summer-amplifier. This pressure must be high enough to prevent the reaction jet cascade from oscillating and, at the same time, allow for maximum amplification of the rate and position control signals. It can readily be seen that had the reaction jet cascade been designed with no consideration for this supply pressure setting, that the magnitude of the control signal required for switching the jets might have been so large as to preclude the operation of the system.

The rate sensor had been tested with its outputs loaded into passive orifices approximating the control orifices of the summer-amplifier. It was thus necessary to recalibrate the rate sensor with its outputs loaded into the summer-amplifier.

For accurate results the summer-amplifier must be set at its proper supply pressure and, in addition, must have the second set of controls activated. This is necessary as the input impedance of the control nozzles is slightly affected by the supply pressure and bias level at the other controls. The steady state results of these calibration tests on the rate sensor are shown in Figure 7.1. For these tests, the rate sensor output was loaded into the summer-amplifier with the power supply pressure set at its operating level. The second set of controls were not activated. The results shown in this figure were not obtained from an accurate rate table and are considered reasonably accurate only in the range ± 0.5 radians per second.

In order to set the maximum pressure signal from the position sensor*, it was necessary to know:

1) The gain ratio of the two summer-amplifier control ports and
2) The final system T/J ratio.

As was pointed out in the discussion of the signal comparator, the gain ratio depends on the summer-amplifier power supply pressure setting and control bias levels. Thus, to obtain the correct gain ratio, a new set of curves similar to those shown in Figure 4.1 were constructed for the proper supply pressure setting and control bias levels.

---

* The maximum signal occurs at ±90 degrees of angular rotation.

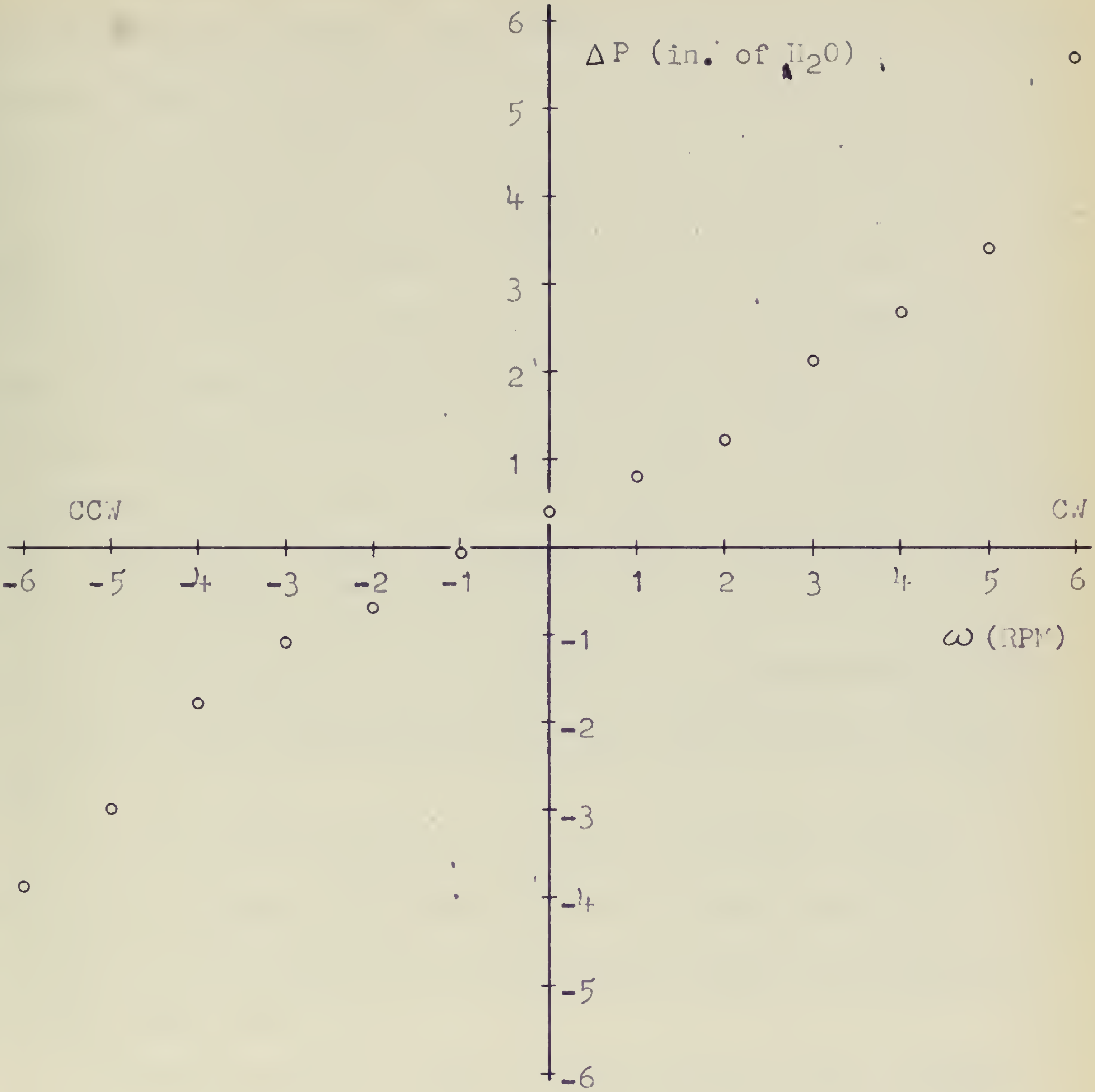

Figure 7.1

Steady State Angular Rate Sensor Output

While Loaded into the Summer-Amplifier

As shown in Appendix C.1, the T/J ratio defines the switching curve equation. The criteria used to set the maximum pressure signal from the position sensor was as follows: If the system starts with an initial error of θ = 90 degrees and $\dot{\theta}$ = 0 radians per second, the maximum rate signal at the point of theoretical optimum switching will occur at θ = 45 degrees. To effect switching of the jets, the position signal should then equal the rate signal at this point. The T/J ratio defines the value of this peak $\dot{\theta}$. From Figure 7.1, the pressure signal corresponding to this value of $\dot{\theta}$ is determined. This then is the value that the position signal must have at 45 degrees. Knowing the shape of the real switching curve and the value of the gain ratio of the summer-amplifier, the value of the maximum position signal can readily be determined.

In the final system, a pair of adjustable orifices were placed between the output of the position sensor and the input to the summer-amplifier to make fine adjustments of the switching curve.

Figure 7.2 shows a block diagram of the final control system composed of the various transfer functions from the previous chapters. A summary of the numerical values for the parameters is given below:

$$^{*}K_1 = 1.19 \ \frac{\text{psi}}{\text{rad/sec.}}$$

$$^{*}K_2 = 1.14 \ \frac{\text{psi}}{\text{rad}}$$

---

*These gains have included the gains of the summer-amplifier. The summer amplifier multiplied the rate signal by six and the position signal by 4.5

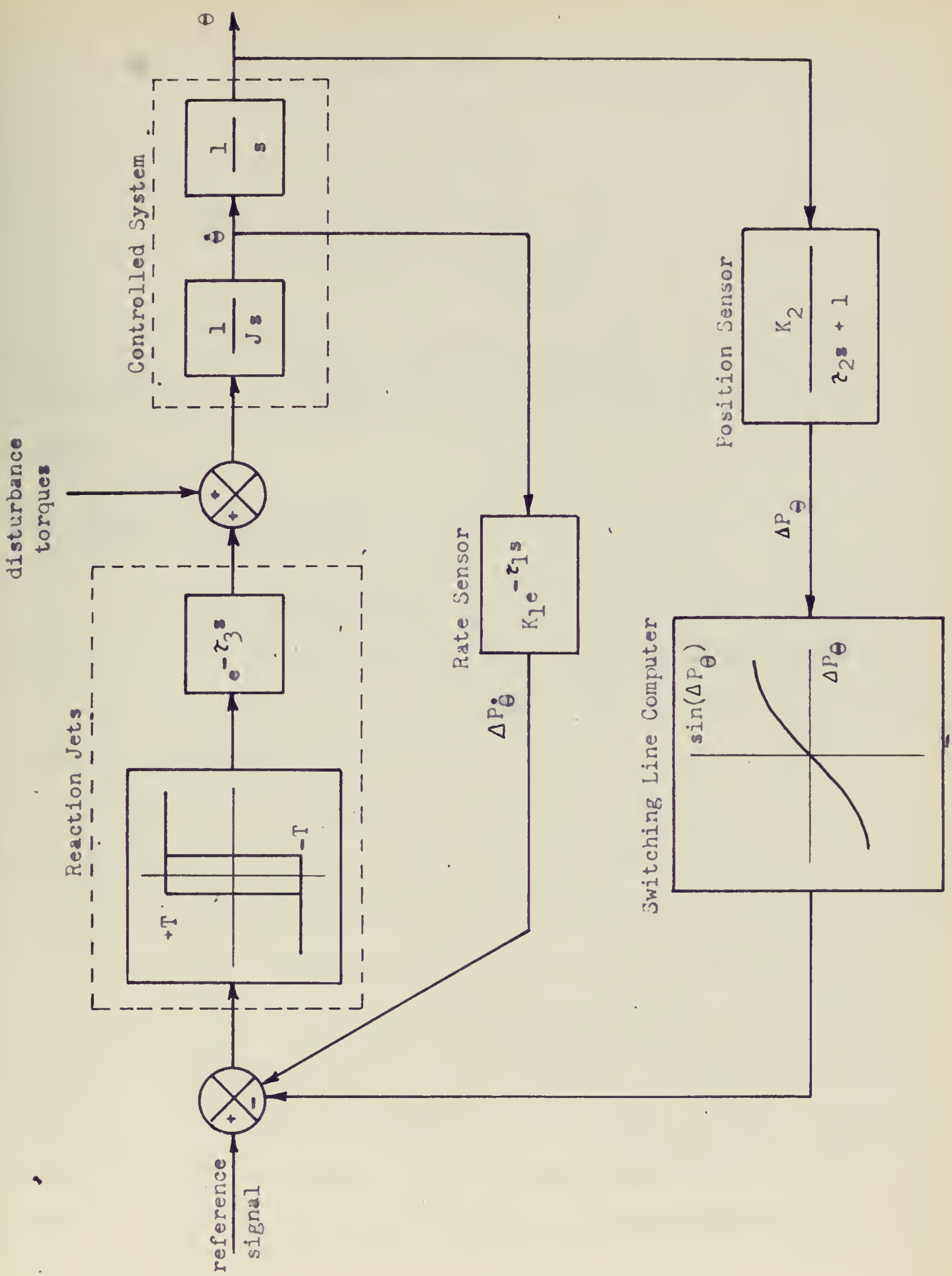

Figure 7.2

Block Diagram of Complete Control System

τ_1 = 0.055 sec.

τ_2 = 0.04 sec.

τ_3 = 0.022 sec.

T = 7.72 in-ozf

hysteresis = ±0.0686 psi

J = 9.60 in-ozf-sec^2

Figure 7.3 shows the same system in circuit diagram form*. A photograph of the complete control system is shown in Figure 7.4.

7.2 System Performance

To obtain performance data on the system, a rotary potentiometer was connected to the control system and the output signal displayed on an X-Y recorder. The results are shown in Figures 7.5 thru 7.9.

Figure 7.5 shows the response of the system to a number of position errors. The reaction jets switched in a nearly perfect manner when responding to counter clockwise errors. The response to clockwise errors, however, resulted in a slight amount of "after end point chattering". The magnitude of the limit is seen to be erratic, averaging roughly 8.5 degrees at approximately 0.5 cps. This erratic response is due to noise from the proportional amplifiers in the system. Considering the T/J ratio of this system, the

---

* The symbols used in this figure follow those recommended by Boothe[16].

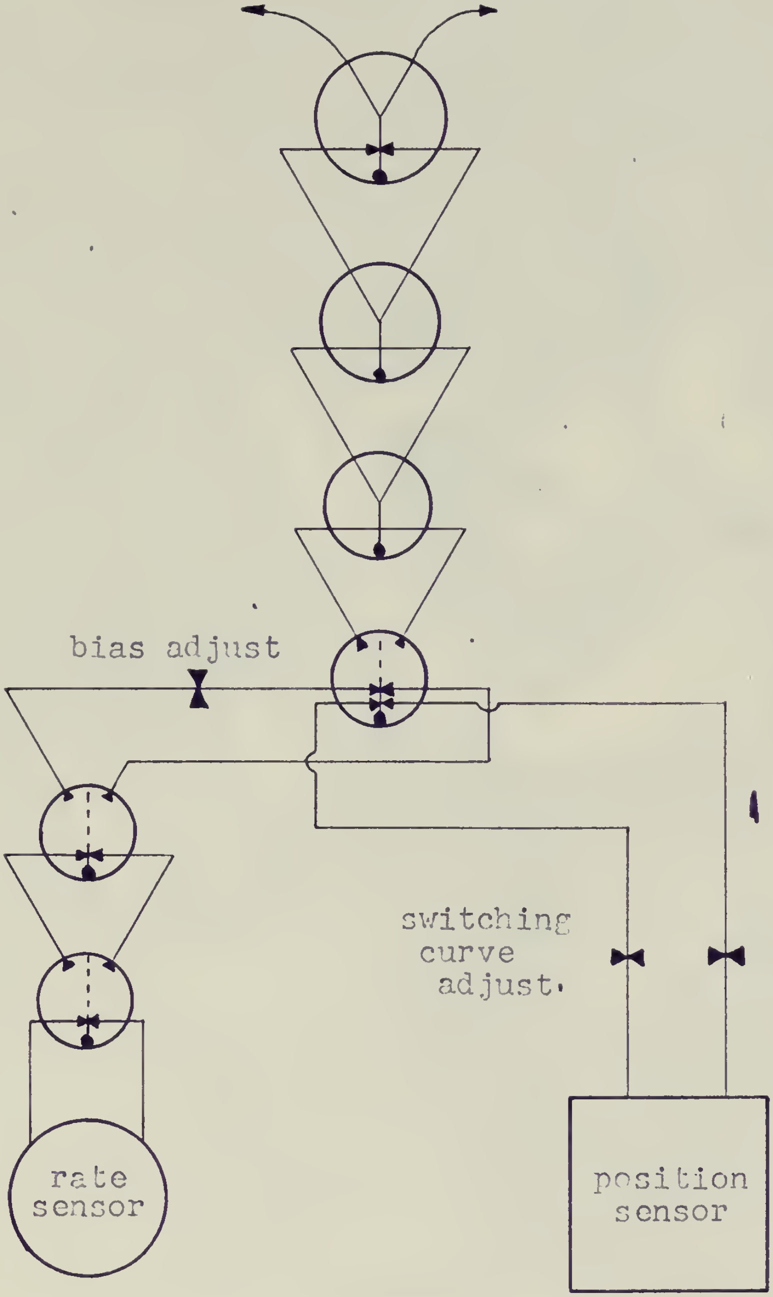

Figure 7.3

System Circuit Diagram

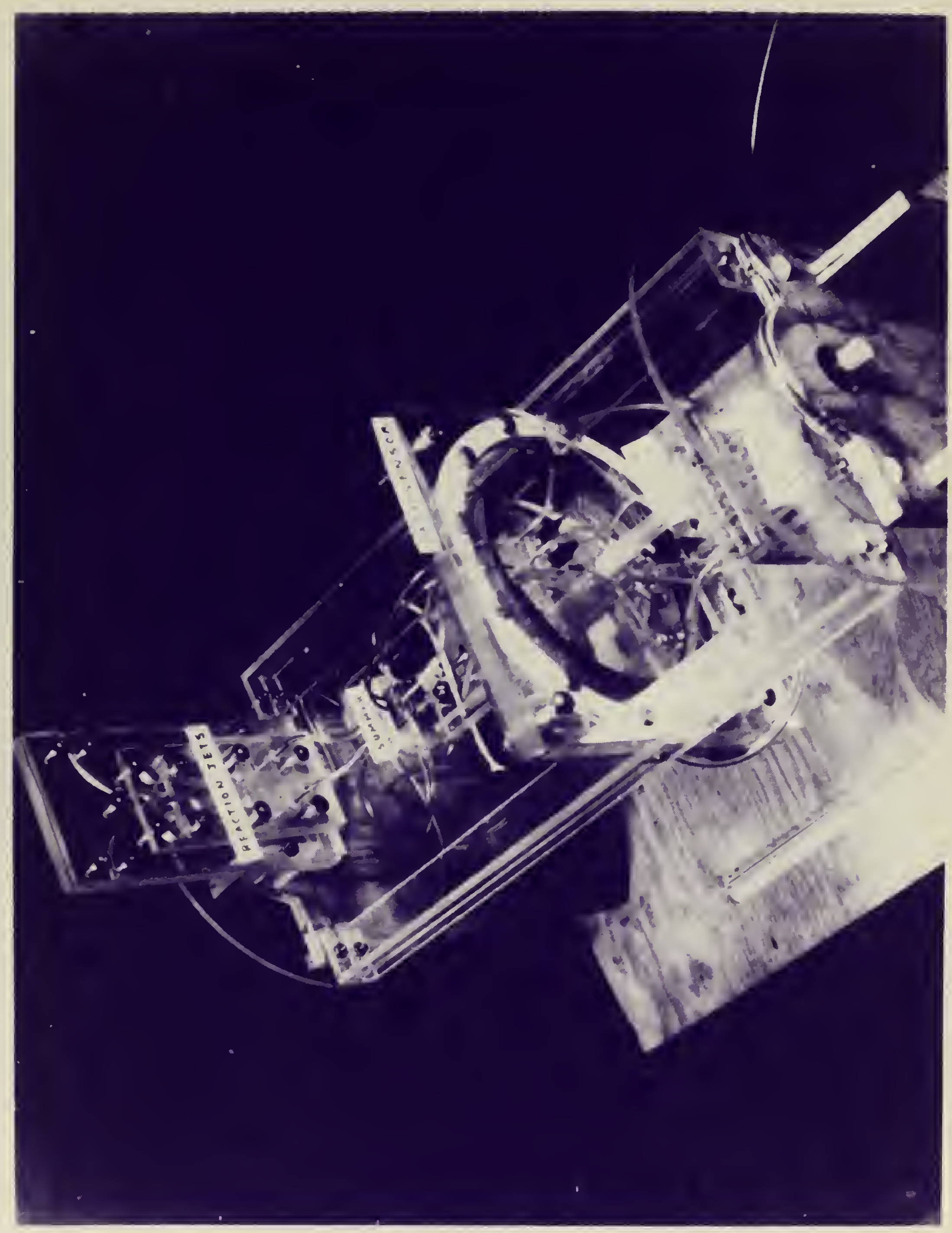

Figure 7.4

Complete Control System and Demonstration Model

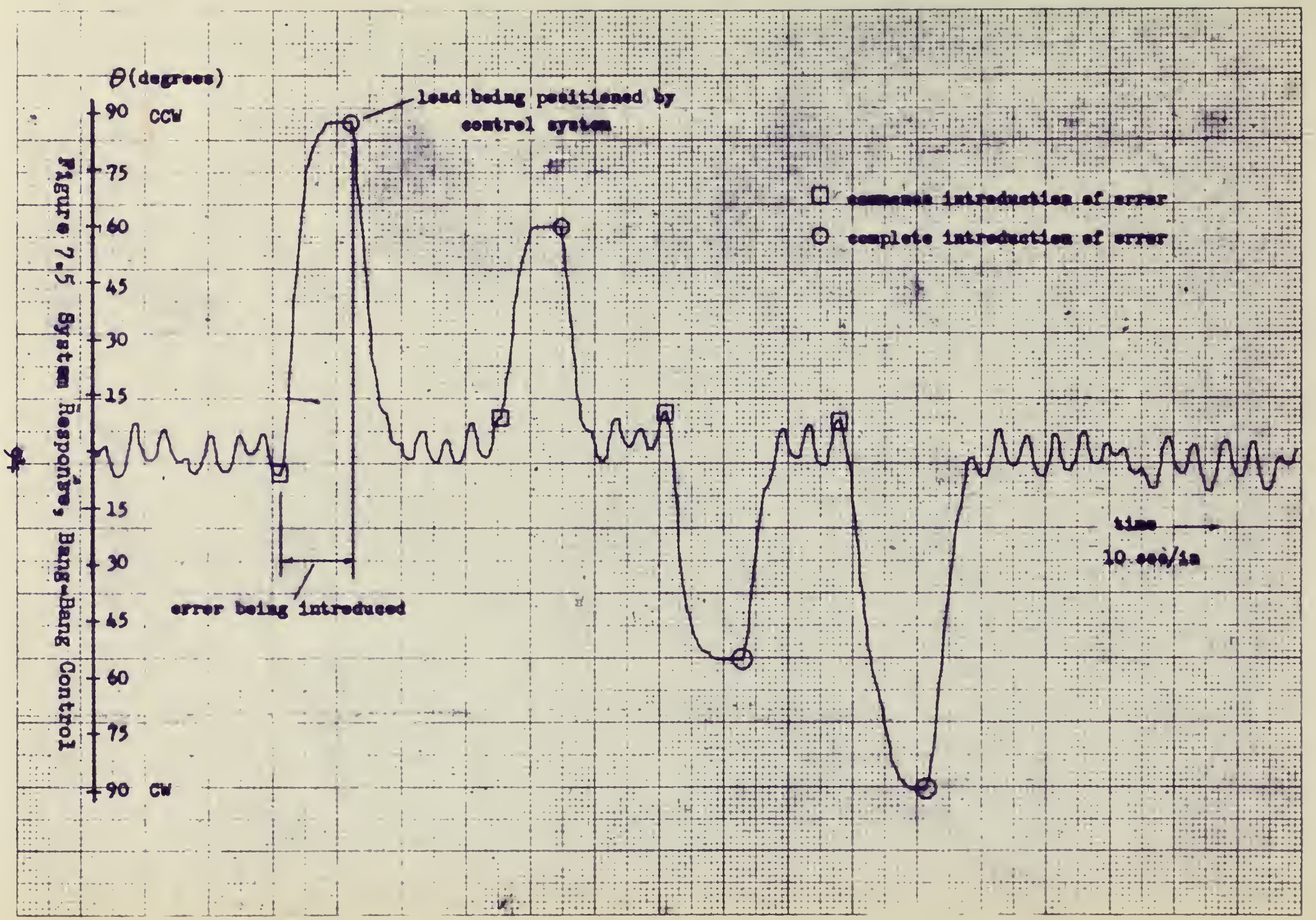

Figure 7.5 System Response, Bang-Bang Control

response time for the errors shown was found to be nearly optimal.

Figure 7.6 shows the system operation with a slightly lower summer-amplifier supply pressure setting. By lowering the supply pressure, the magnitude of the hysteresis band was decreased, resulting in the marked decrease in the magnitude of the limit cycle. Unfortunately, the noise present in the system could then switch the reaction jets more readily resulting in a slightly less optimal time response to large errors because of random switching.

Figure 7.7 shows the system performance with the rate sensor disconnected from the control loop. As pointed out more clearly in Appendix C.2, the control system should, theoretically, be completely unstable. Because of the finite damping in the system, in practice a new limit cycle was reached at a much higher amplitide and lower frequency.

Figures 7.8 and 7.9 show an interesting mode of operation possible with this system. As pointed out in the preceding chapter, the reaction jet cascade is unstable unless driven, due to the heavy loading on the output legs of the last stage. This back pressure is so high that it causes the first and second stage amplifiers also to oscillate. Introducing small control flows into one side of the first stage cause the pulsing to occur more often on one side than on the other in direct proportion to the magnitude of the input signal. Thus the system effectively operates in a pulse

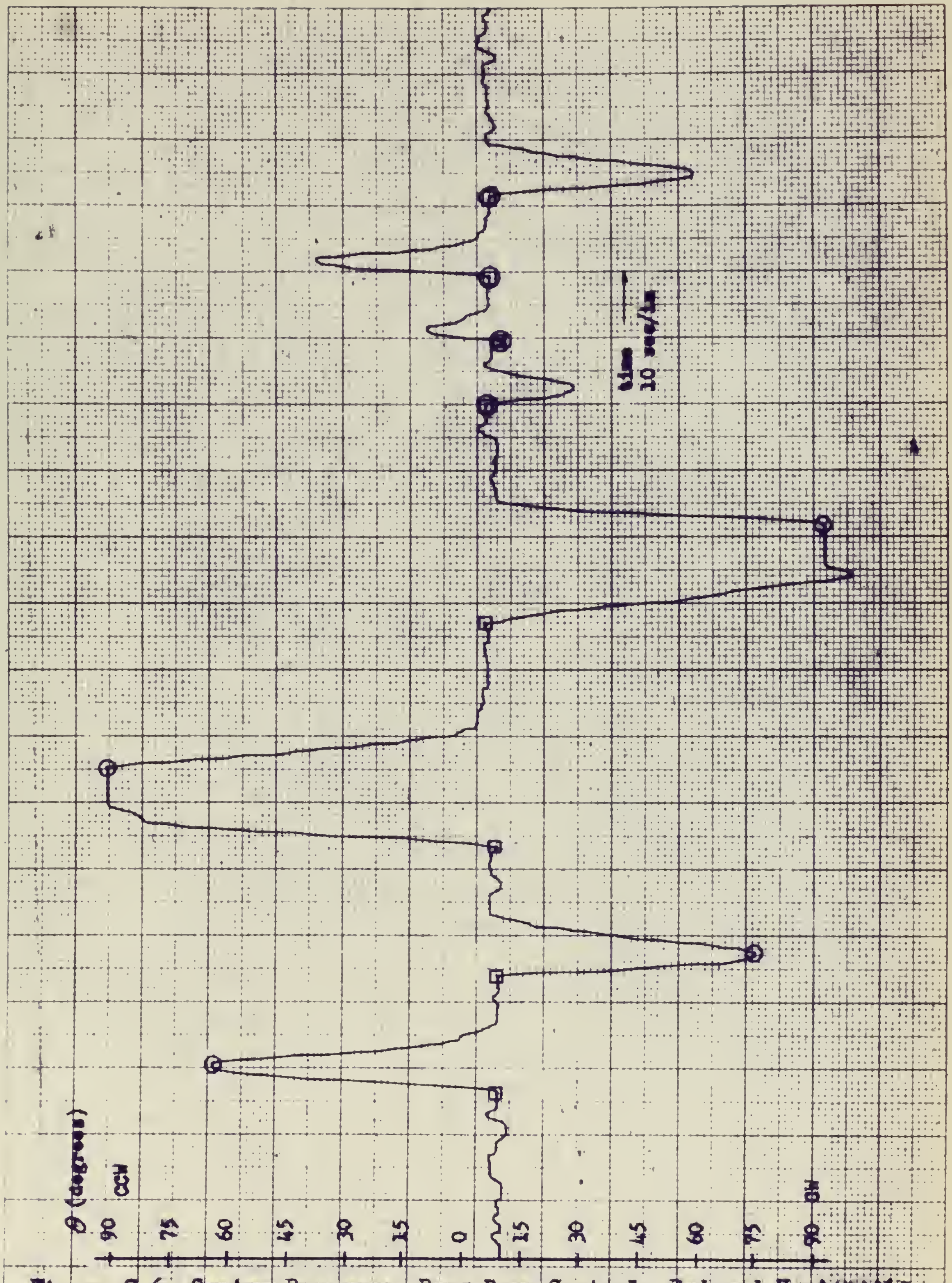

Figure 7.6 System Response, Bang-Bang Control, Reduced Hysteresis

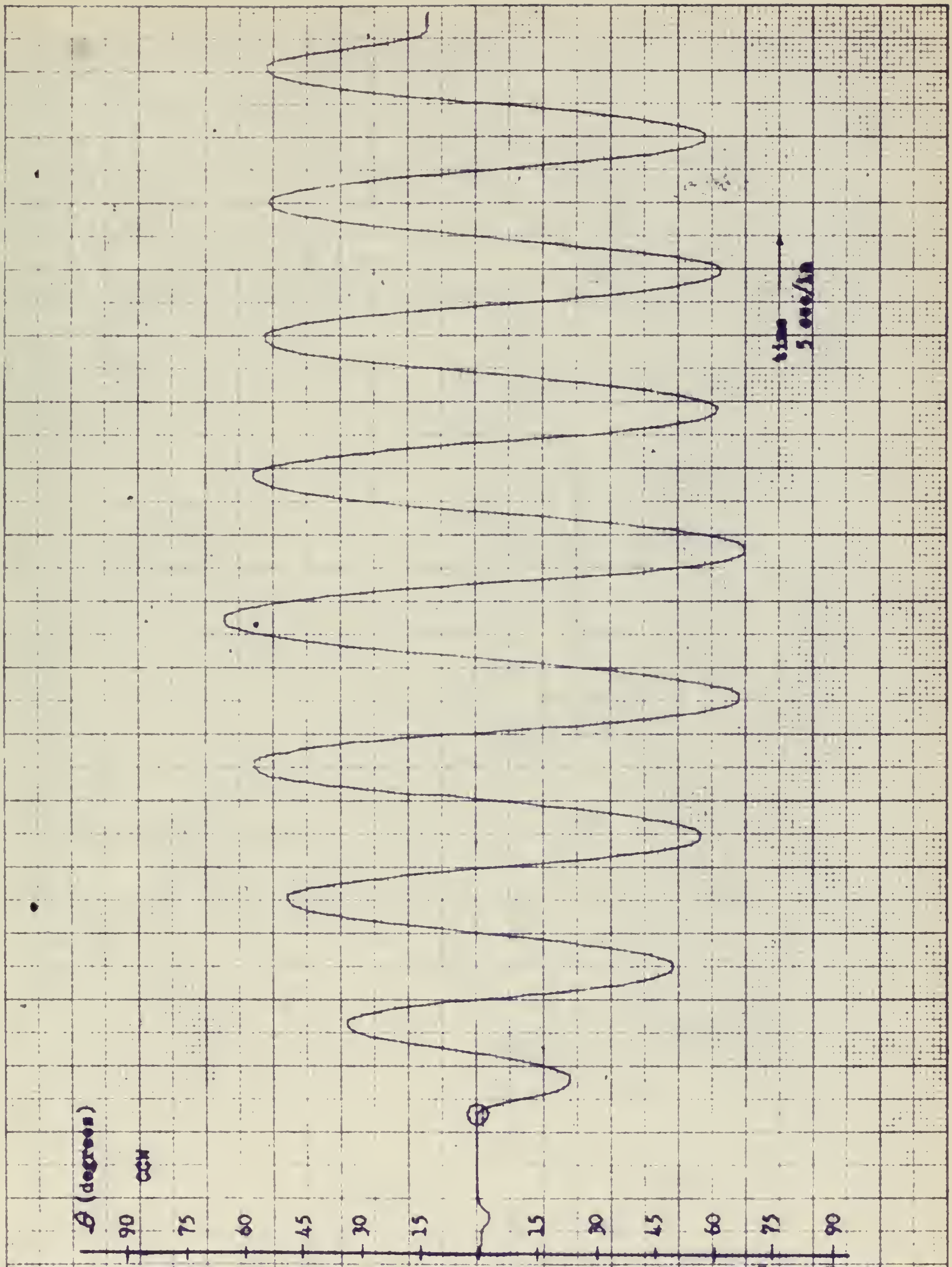

Figure 7.7 System Response, Bang-Bang Control, Without Rate Feedback

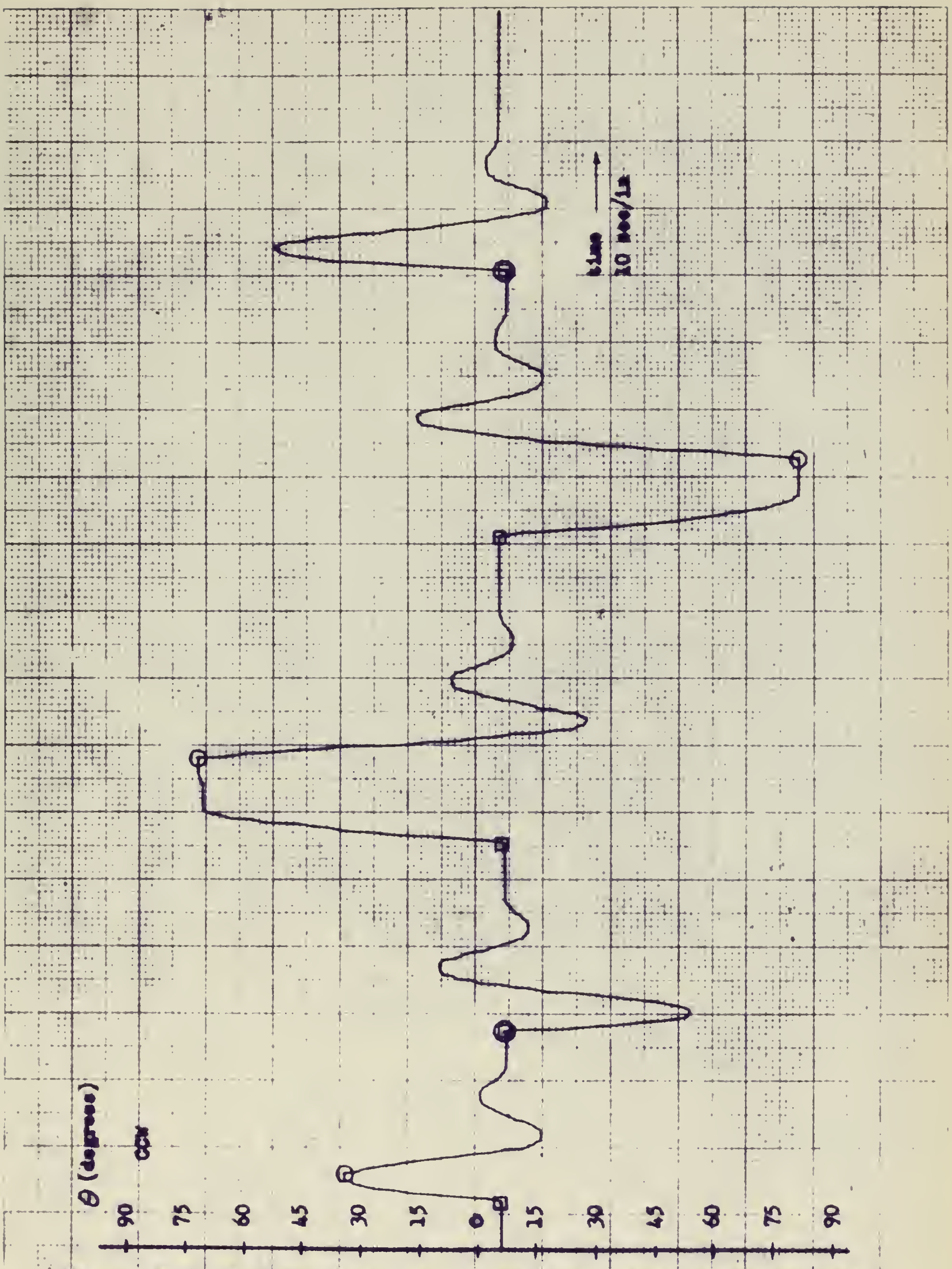

Figure 7.8 System Response, Pulse Width Modulation Control

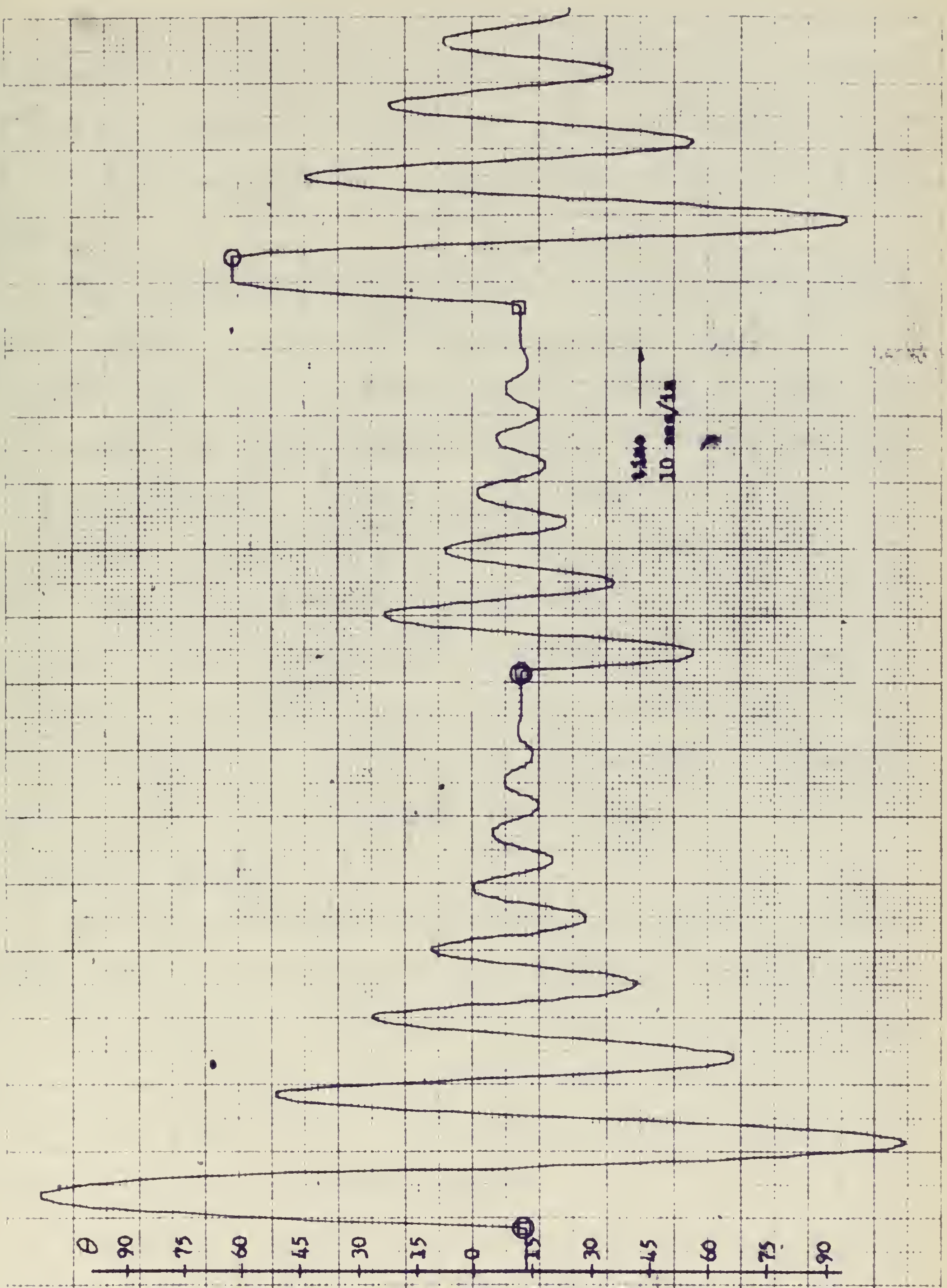

Figure 7.9 System Response, PWM Control, Without Rate Feedback

width modulation mode*.

In Figures 7.8 and 7.9 this pulse width modulation mode was obtained by lowering the summer-amplifier supply pressure. The frequency of oscillation is too high (approximately 100 cps) for the system to respond to the individual torque pulses.

Figure 7.8 shows the response to various disturbances while operating in this pulse width modulation mode. Of particular note is the disappearance of random fluctuations due to noise. A certain amount of stiction is noted caused by the potentiometer attached to the system.

Figure 7.9 shows the system response with the rate sensor disconnected from the control loop. If the load were completely free of damping, the response, of course, would not damp out. A comparison of this figure with Figure 7.7 shows the functioning of the vortex rate sensor and the part it plays in the stabilization of the system.

7.3 System Analysis

This control system falls into the category of nonlinear control systems because of the bang-bang method of controlling the load. The most convenient way of analyzing this system, in order to predict the magnitude and frequency of the limit cycle and the stability of the system, is by using the describing-function method.

Gibson[1] points out that this approximation method is

---

*For a more complete explanation of this mode of operation see reference 17.

quite accurate in systems containing sufficient low pass filtering. The nature of an inertial load amply fulfills this requirement as it refuses to respond (filters) to high frequency signals.

This method essentially consists of assuming that the input to the non-linear element is sinusoidal. The resulting output is then written in the form of a Fourier series. Then it is assumed that only the fundamental component of this series is important in relation to the response. The coeficient of this fundamental frequency, which is dependent on the magnitude of input signal but independent of the frequency, is used as an equivalent gain (K_{eq}) of the non-linear element. The rest of the system being linear is frequency dependent but not dependent on the magnitude of the input signal. By plotting the equivalent gain function of the non-linear element and the frequency response of the linear elements on a polar plot, a point of intersection may be found which represents a possible point of operation. If the point is found to be a stable point, then the frequency and magnitude of oscillation can readily be determined.

This method is applied to the analysis of this system in Appendix C.2 The results closely predict both the magnitude and frequency of the limit cycle shown in Figure 7.5*.

---

*The data on which the calculations were based was obtained from the system just after Figure 7.5 was recorded.

APPENDIX

APPENDIX A

RATE SENSOR CALCULATIONS

A.1 Rate Sensor Design Calculations

Given $R_o = 3$ in.

$$\omega_{max} = 70^{\circ}/\text{sec} = 1.221 \text{ rad/sec}$$

$$\Delta P \text{ @ } \omega_{max} = 0.1 \text{ lbf/in}^2$$

$$\Delta \theta \text{ @ } \omega_{max} = 3^{\circ} = 0.0523 \text{ rad.}$$

$$\rho = 2.34 \text{X} 10^{-3} \ \frac{\text{lbf-sec}^2}{\text{ft}^4}$$

$$\nu = 1.623 \text{X} 10^{-4} \ \text{ft}^2/\text{sec}$$

From equation (2.19)

$$U_s = \sqrt{\frac{144 \Delta P}{4 \rho \Delta \theta}} = \sqrt{\frac{(144)\ (0.1)}{4(0.00243)(0.0523)}}$$

$$U_s = 171.2 \ \text{ft/sec}$$

From equation (2.21)

$$Q = 2\left[\pi r_s^{\,2} - 4 c r_s\right] U_s$$

$$= \frac{2\left[\pi(0.1562)^2 - 4(0.0212)\ (0.1562)\right]171.2}{144}$$

$$Q = 0.151 \ \text{ft}^3/\text{sec} \quad 9.05 \ \text{ft}^3/\text{min.}$$

From equation (2.22)

$$Re = \frac{Q\ h/2}{\nu\ R_o^{\ 2}}$$

$$Re = \frac{(0.151)\ (0.0281)}{(1.623\times 15^4)\ (0.0625)} = 310$$

From reference 3, page 327, we find that this value of Re is off the scale but E is leveling off to roughly 0.66. A "factor of safety" was introduced here and E was taken to be 0.5.

Rearranging equation (2.20) gives

$$r_{po} = \frac{Ro^2\ \omega\ E}{\Delta\theta\ U_s}$$

$$r_{po} = \frac{(0.0625)\ (1.221)\ (0.5)}{(0.0523)\ (171.2)}$$

$$r_{po} = 4.27 \times 10^{-3} \text{ft.} \qquad 5.12 \times 10^{-2} \text{ inc.}$$

Rearranging equation (2.23) gives

$$a = \sqrt{r_{po}^{\ 2} - c^2/2}$$

$$a = \sqrt{(5.12 \times 10^{-2})^2 - \frac{(0.0212)^2}{2}}$$

$$a = 0.0475 \text{ in.}$$

A.2 Calculation of First Stage Supply Pressure

From Figure 2.8, $Q_{c\ max} = 0.107$ in^3/sec and take $Q_{c\ min} = 0$.

Then $\quad V_c = \frac{Q_c}{A_c} = \frac{0.107}{3.75\times 10^{-4}} = 285$ in/sec

From equation (2.24), $V_p = \sqrt{\frac{w_c \; V_c^2}{w_p \; \tan\theta}}$

where $\tan\theta = \frac{w_p/2}{L} = \frac{0.005}{0.1} = .05$

$w_c = 0.015$ in.

$w_p = 0.010$ in.

Therefore, $V_p^2 \quad 2.43 \times 10^6$ in^2/sec^2

From equation (2.28)

$$A_p V_p = Q_p = C_{dp} \; A_p \sqrt{\frac{2}{\ } \; P_p}$$

or

$$P_p \quad \frac{V_p^2}{C_{dp}^2} \qquad \rho/2$$

From Corning design data sheets, $C_{dp} \cong 0.70$.

Thus $P_p = 0.28$ psi = 7.7 inches of water.

APPENDIX B

CALCULATION OF THE REACTION JET TIME DELAY CONSTANT

The time required for the power jet to traverse the distance between the nozzle and the receiver ports is given by

$$t = \frac{l}{V_{avg}}$$

where l = splitter distance

V_{avg} = the average velocity of a particle while traveling between the power nozzle exit and the receiver.

Reference 19 gives the dynamic pressure profile of a submerged jet at various distances from the power nozzle. If it is assumed that the velocity decreases linearly from nozzle exit to the receiver, then V_{avg} is given by

$$V_{avg} = \frac{V_j + V_s}{2}$$

where $V_j = \sqrt{\frac{2}{\rho} P_j}$ = nozzle exit velocity

V_s = jet velocity at the entrance to the splitter

The value of V_s can be determined from the graphs given in reference 19 if the splitter distance is known. For the first stage:

splitter distance $= 18w = 0.36$ in $= l$

$$V_j = \sqrt{\frac{2}{\rho} P_j} = \sqrt{\frac{(2)\ (1.96)}{(1.129 \times 10^{-7})}} = 5.9 \times 10^3 \text{ in/sec}$$

$$\frac{\rho/2\ V_{18}^2}{\rho/2\ V_j^2} = 0.45$$

$$\therefore \quad V_{18} = V_s = 3.96 \times 10^3 \text{ in/sec}$$

$$V_{avg} = \frac{V_j + V_s}{2} = 4.93 \times 10^3 \text{ in/sec}$$

$$t_1 = \frac{1}{V_{avg}} = \frac{0.36}{4.93 \times 10^3} = 73 \times 10^{-6} \text{ secs.}$$

Similarly for the second and third stages:

$$t_2 = 197 \times 10^{-6} \text{ secs.}$$

$$t_3 = 137 \times 10^{-6} \text{ secs.}$$

The time required for the flow in the control nozzle of an intermediate stage to build to that flow level necessary for switching can be approximated from the time constant associated with the volume connecting the two stages and the resistance of the control port. The time constant is given by

$$\tau = RC$$

where R = impedance of the control port lbf-sec/in^5

C = capacitance due to the interconnecting volumes in^5/lbf

The value of R was determined by linearizing the input impedance

curves of each nozzle about an assumed operating point. The value of C is given, for adiabatic conditions, by

$$C = \frac{v}{\rho K \mathcal{R} T}$$

where v = connecting volume (in^3)

ρ = mass density ($lbf\text{-}sec^2/in^4$)

K = adiabatic constant = 1.4

$\mathcal{R}$ = gas constant = 2.48×10^5 (in^2/sec^{-oR})

T = temperature (^oR)

For lines connecting the first and second stage:

$$R = 0.287 \quad lbf\text{-}sec/in^5$$

The value of v was found to equal 0.279 in^3. Therefore

$$C = \frac{v}{\rho K \mathcal{R} T} = \frac{(0.279)}{(1.129 \times 10^7)(1.4)(2.48 \times 10^5)(550)}$$

$$C = 0.013 \quad in^5/lbf$$

Hence

$$\tau = .00372 \text{ secs.}$$

The relationship between the flow into the connecting volume (assumed constant) and the flow through the control nozzle (variable) is given by

$$\frac{q_o}{q_{in}} = \frac{1}{\tau s + 1}$$

The value of q_{in} is known from the nozzle geometry of the first stage. q_o is zero before switching occurs. After

switching Q_o increases until it reaches the value required for switching. The value required for switching was taken to be nearly equal to Q_{in}. Therefore, the time required for the flow to build to the switching level is approximately four time constants, or t= 0.0149 seconds. In a similar manner the buildup time between the second and third stage was found to equal 0.006 seconds. The final time delay is due to the time required for the output flow to traverse the length of the output leg. By an elementary calculation this was found to equal 636×10^{-6} seconds.

The total time delay is equal to the sum of all the time delays discussed above, 0.022 seconds.

APPENDIX C

SYSTEM ANALYSIS

C.1 Determining the Equation of the Switching Curve

Consider a bang-bang control system as shown in Figure C.1. The equation of motion describing the operation of this system is given by

$$\ddot{\theta} = \left[\text{Sign}\,\theta\right]\frac{T}{J} \qquad (C.1)$$

If $\ddot{\theta}$ is rewritten as

$$\ddot{\theta} = \frac{d\omega}{dt} = \frac{d\omega}{d\theta}\,\frac{d\theta}{dt} = \omega\,\frac{d\omega}{d\theta}$$

and substituted for $\ddot{\theta}$ in equation C.1 one obtains

$$\omega\,\frac{d\omega}{d\theta} = \left[\text{sign}\,\theta\right]\frac{T}{J} \qquad (C.2)$$

Equation C.2 can now be integrated resulting in

$$\frac{\omega^2}{2} = -\frac{T}{J}\theta + C_1 \quad \text{for} \quad (-)\;\theta \qquad (C.3a)$$

$$\frac{\omega^2}{2} = \frac{T}{J}\theta\;C_2 \quad \text{for} \quad (+)\;\theta \qquad (C.3b)$$

These curves represent two families of parabolas in the phase plane (ω vs θ) where C_1 and C_2 determine the values of the initial conditions. If these curves are plotted in the phase plane, it will be found that the curves corresponding to $C_1 = C_2 = 0$ pass through the origin. They represent trajectories

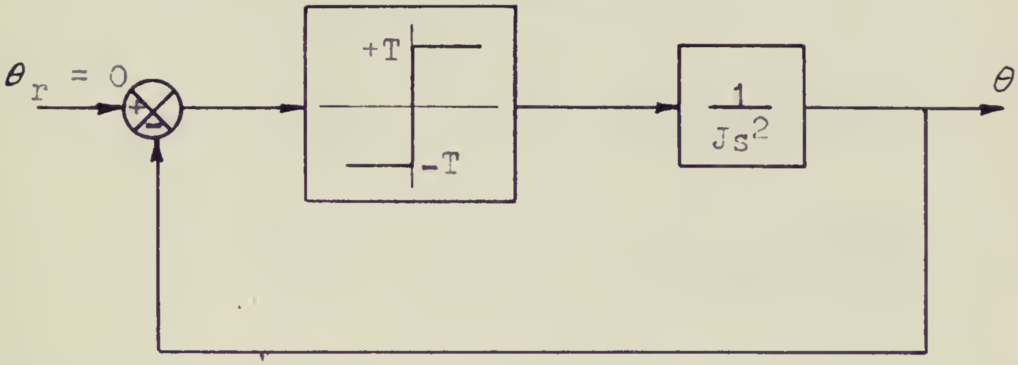

Figure C.1

Idealized Contactor Servomechanism Controlling an Inertia Load

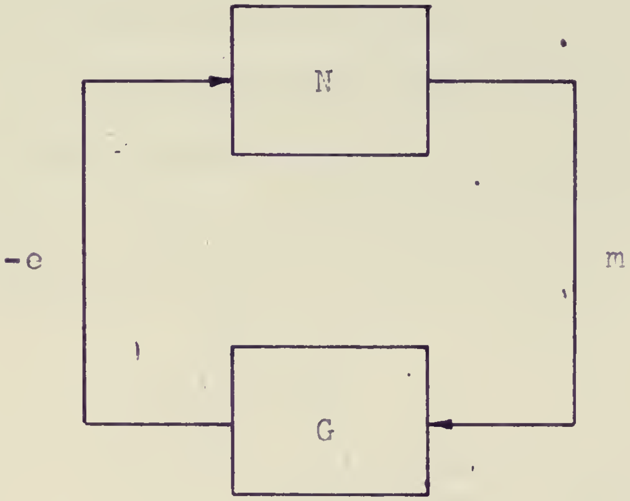

Figure C.2

Generalized Autonomous Control System Containing a Nonlinear Element

such that, if the system is switched at the time one or the other curve is intersected, a time optimal reduction of errors introduced into the system will result.

Thus the switching line equations are given by

$$\frac{\omega^2}{2} = -\frac{T}{J}\theta \quad = \text{second quadrant switching curve}$$

$$\frac{\omega^2}{2} = +\frac{T}{J}\theta \quad = \text{fourth quadrant switching curve}$$

C.2 Limit Cycle Analysis

The block diagram shown in Figure 7.2 can be reduced to the form shown in Figure C.2 if the following conditions exist:

1) The reference signal is zero

2) The magnitude of the position signal stays within the linear region of the switching curve.*

In the figure, N represents the nonlinear element in the system and G is the combination of all the linear elements.

Gibson[1] shows that a sufficient condition for the existence of sustained oscillation is

$$G(j\omega) = -\frac{1}{Keq}$$

where Keq = the equivalent gain of the nonlinear element, which is a function of the magnitude of the input signal to the nonlinear element.

---

* This condition is satisfied as shown by the results in Figure 7.5.

Keq for a contactor with hysteresis is given by Gibson as

$$K_{eq} = g(E) + j\, b(E) \,^{*}$$

where E = the magnitude of the input to the contactor represented by $\Delta P_\theta + \Delta P_{\dot\theta}$

and

$$g(E) = \frac{4T}{\pi E} \sqrt{1 - \left(\frac{a}{E}\right)^2}$$

$$b(E) = -\frac{4T}{\pi E} \quad \frac{a}{E}$$

where a = the half width of hysteresis band (psi)

T = the magnitude of the torque output (in-ozf)

For this system,

a = 0.0686 psi

T = 7.72 in-ozf

By assuming values for $E = \Delta P_\theta + \Delta P_{\dot\theta}$, various values of $-1/K_{eq}$ may be obtained. For example

Assume E = 3 inches of water 0.1082 psi.

$$g = \frac{4T}{\pi E} \sqrt{1 - \left(\frac{a}{E}\right)^2}$$

$$g = \frac{4\,(7.72)}{\pi(0.1082)} \sqrt{1 - \left(\frac{0.0686}{0.1082}\right)^2}$$

---

[*] These values are normalized Fourier coeficients. The term b(E) is needed to take care of phase distortion of the fundamental harmonic.

$$g = 70 \quad \frac{\text{in-ozf}}{\text{psi}}$$

$$b = \frac{4Ta}{\pi E^2} = -\frac{4(7.72)(0.0686)}{\pi\ (0.1082)^2} = -57.6 \ \frac{\text{in-ozf}}{\text{psi}}$$

$$K_{eq} = 89.5 \angle -39.4^\circ$$

$$-\frac{1}{K_{eq}} = 0.0112 \ \frac{\text{psi}}{\text{in-ozf}} \angle 39.4^\circ$$

The linear transfer function G(s) is given by

$$G(S) = \frac{\left[K_1 S e^{-\mathcal{T}_1 S} + \frac{K_2}{\mathcal{T}_2 S + 1}\right] e^{-\mathcal{T}_3 S}}{JS^2} \qquad (C.4)$$

Assume that the time delay of the rate sensor ($\mathcal{T}_1$) is zero in order to see what effect rate feedback has on the system. For this case, the linear transfer function becomes

$$G(S) = \frac{K_2}{J} \frac{\left(\frac{K_1 \mathcal{T}_2}{K_2} S^2 + \frac{K_1}{K_2} S + 1\right)}{S^2 (\mathcal{T}_2 S + 1)} e^{-\mathcal{T}_3 S} \qquad (C.5)$$

By substituting actual numerical values gives

$$G(S) = (0.1188) \frac{\left[\frac{S^2}{(4.89)^2} + \frac{2(2.55)}{4.89} S + 1\right]}{S^2 \ (0.04S + 1)} e^{-0.022S} \qquad (C.6)$$

To show the effect of rate feedback on the stability of this system, disconnect the rate feedback ($K_1 = 0$). For this case equation (C.6) becomes

$$G(S) = 0.1188 \quad \frac{e^{-0.022S}}{S^2 \ (0.04S + 1)} .$$

By substituting $s = j\omega$, the values for the magnitude and phase of $G(j\omega)$ as ω varies from zero to infinity are obtained. If this frequency response data is plotted on a polar plot along with the magnitude and phase of $-\frac{1}{K_{eq}}$, a plot similar to that shown in Figure C.3 will be obtained. It can be seen that no intersection of the two plots occur and hence the system is unstable.

Substituting $s = j\omega$ into equation (C.6) and plotting this function on a polar plot (Figure C.4) shows the stabilizing effects of rate feedback. It can be seen that a point of intersection now occurs and a stable limit cycle results. The effect of rate feedback is to introduce phase lead into the system which "pulls" the $G(j\omega)$ curve away from the -180 degrees phase shift line a sufficient amount to allow this intersection to occur. To investigate what effects the time delay in the rate feedback will have on the system, Equation (C.4) may be written in the following form

$$G(S) = \frac{K_2}{J} \; \frac{\left(\frac{K_1 \tau_2}{K_2} S^2 e^{-\tau_1 S} + \frac{K_1}{K_2} S e^{-\tau_1 S} + 1 \right)}{S^2(\tau_2 S + 1)} \, e^{-\tau_3 S}$$

If the rate sensor time delay term is factored out of the quadratic term and combined with the reaction jet time delay, the result is

$$G(S) = \frac{K_2}{J} \; \frac{\left(\frac{K_1 \tau_2}{K_2} S^2 + \frac{K_1}{K_2} S + e^{\tau_1 S} \right)}{S^2 \, (\tau_2 S + 1)} \quad e^{-(\tau_1 + \tau_3) S} \tag{C.7}$$

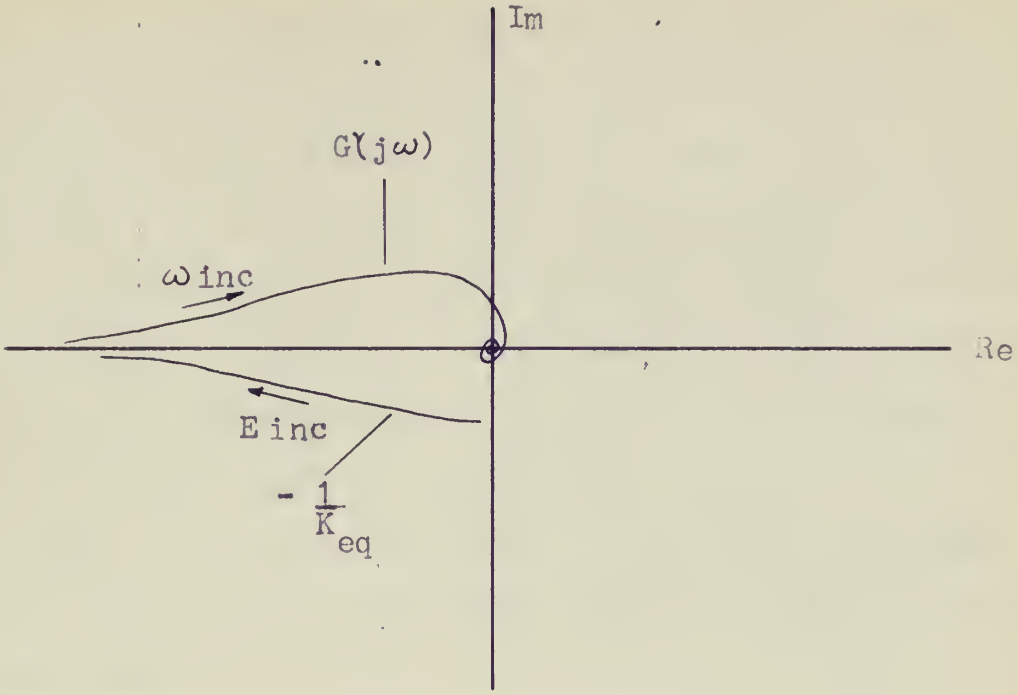

Figure C.3

Polar Plot of G(jω) and $-\frac{1}{K_{eq}}$ Without Rate Feedback

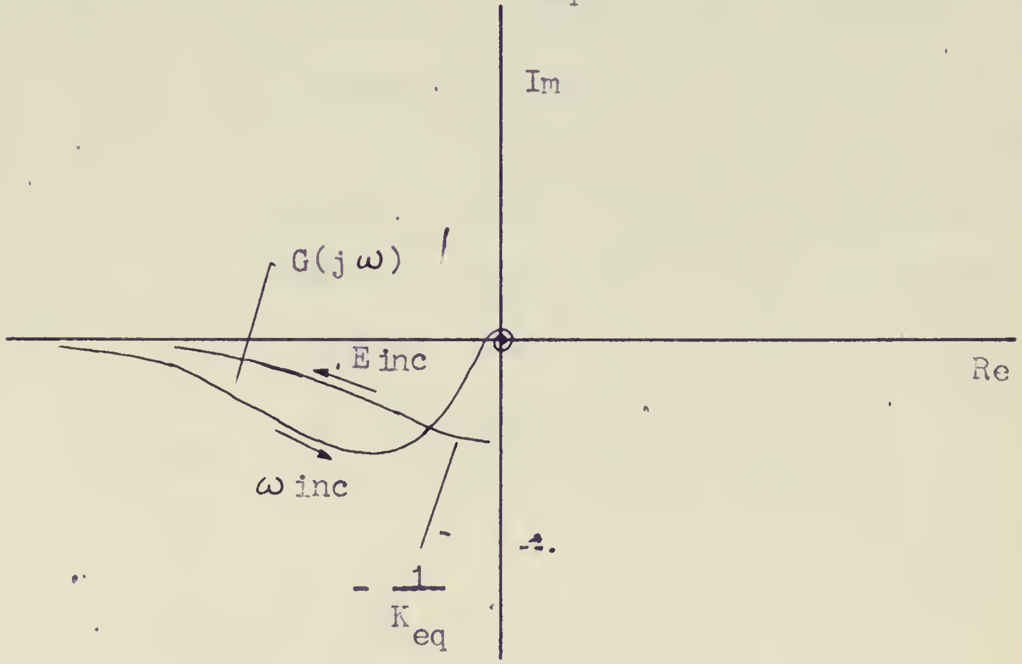

Figure C.4

Polar Plot of G(jω) and $-\frac{1}{K_{eq}}$ With Rate Feedback

Comparing equation (C.7) with equation (C.5), the first major effect to be noted is the increased transport time delay given by the term $e^{-(\tau_1+\tau_2)s}$. The other effect to be noted occurs in the quadratic term. If the quadratic terms given in these two equations are plotted over the frequency range $0 < \omega < \infty$, it will be found that they differ in magnitude and phase only by a very slight amount around the break frequency. Thus, the major effect of the rate sensor time delay is to increase the transport time delay of the over all system.

Figure C.5 shows a Bode plot of equations (C.5) and (C.7) where the effect of the rate sensor time delay can be seen more clearly.

Figure C.6 shows polar plots of $G(j\omega)$ and $-\frac{1}{K_{eq}}$. The effect of the rate sensor time delay is to increase the magnitude of the limit cycle and decrease the frequency. From this figure, the frequency of the limit cycle for the system is predicted to be 9.5 radians per second or 1.51 cps.

The predicted magnitude can be found by working backwards through the linear transfer function to get an expression for θ. This procedure gives

$$\theta_{max} = \frac{E_o}{K_2} \frac{\tau_2(j\omega_o)+1}{\left[\frac{K_1\tau_2}{K_2}(j\omega_o)^2 + \frac{K_1}{K_2}(j\omega_o)+1\right]}$$

where at the point of intersection

$$E_o = 0.1082 \text{ psi}$$

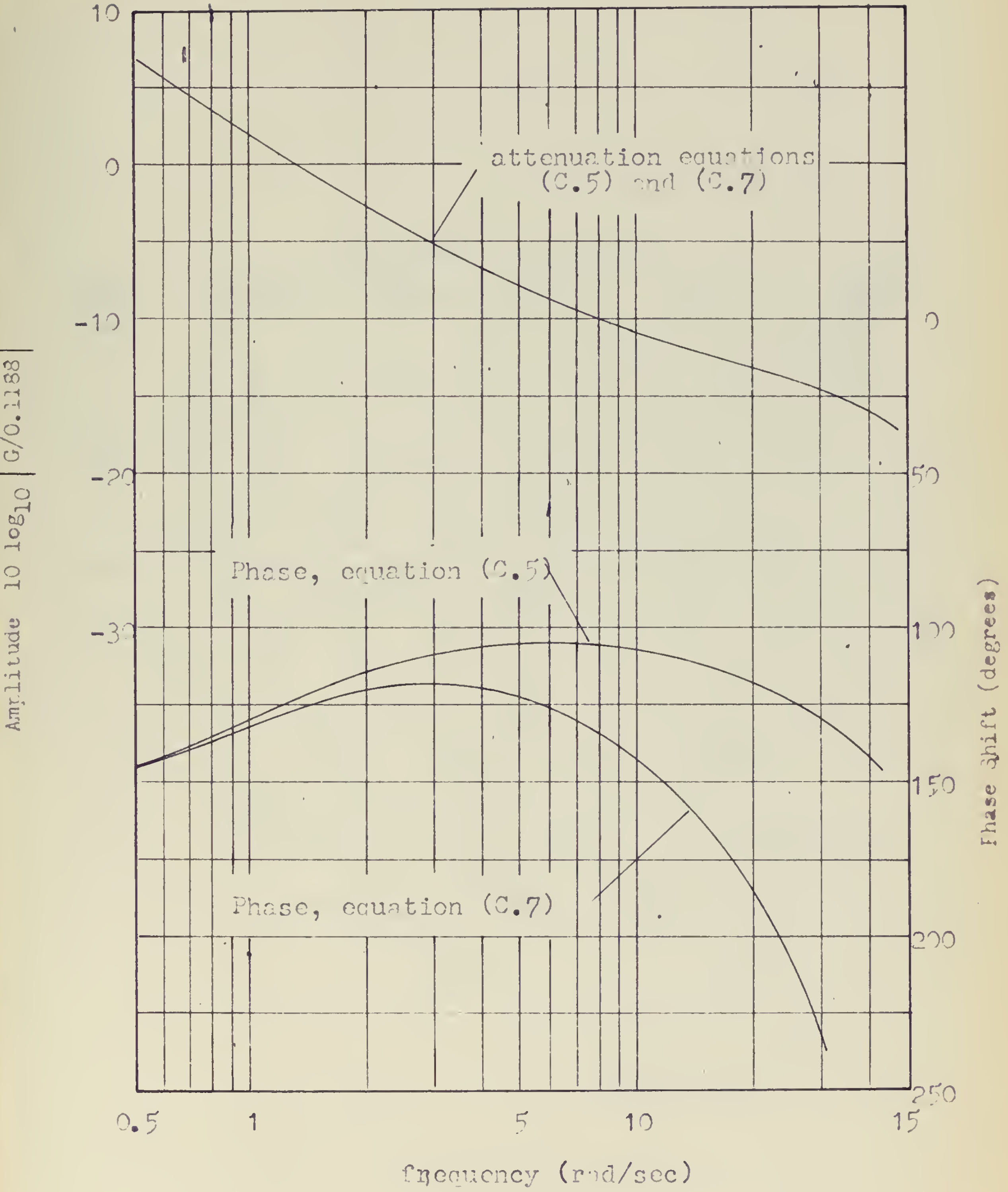

Figure C.5

Bode Plots of Linear Transfer Function $G(j\omega)$

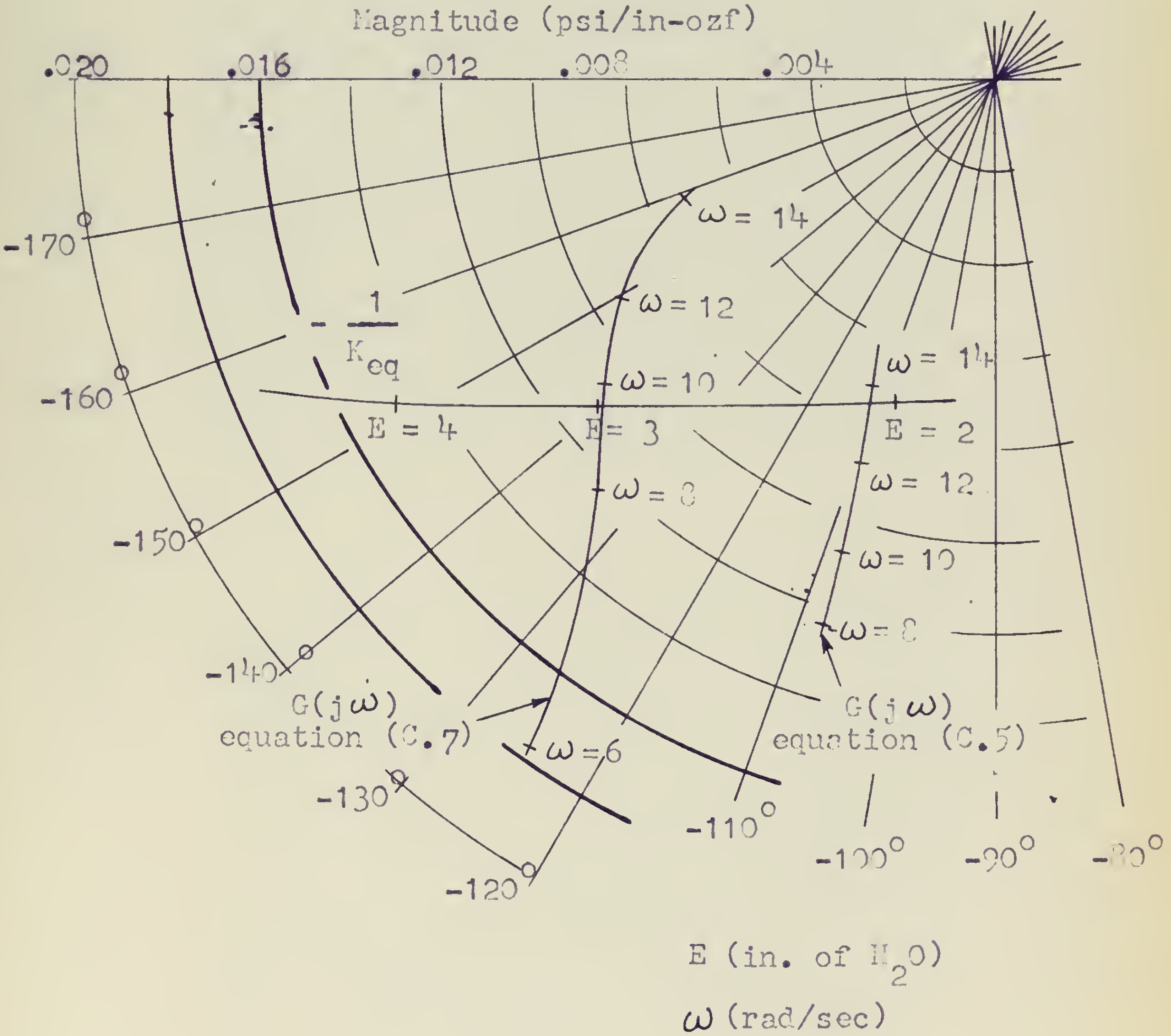

Figure C.6

Polar Plot of G(jω) and $-\frac{1}{K_{eq}}$

$$\omega_0 = 9.5 \text{ radians per second.}$$

Making these substitutions and carrying out the indicated calculation gives

$$\theta_{max} = 5.68 \text{ degrees}$$

APPENDIX D

PHOTOGRAPHS OF COMPONENTS

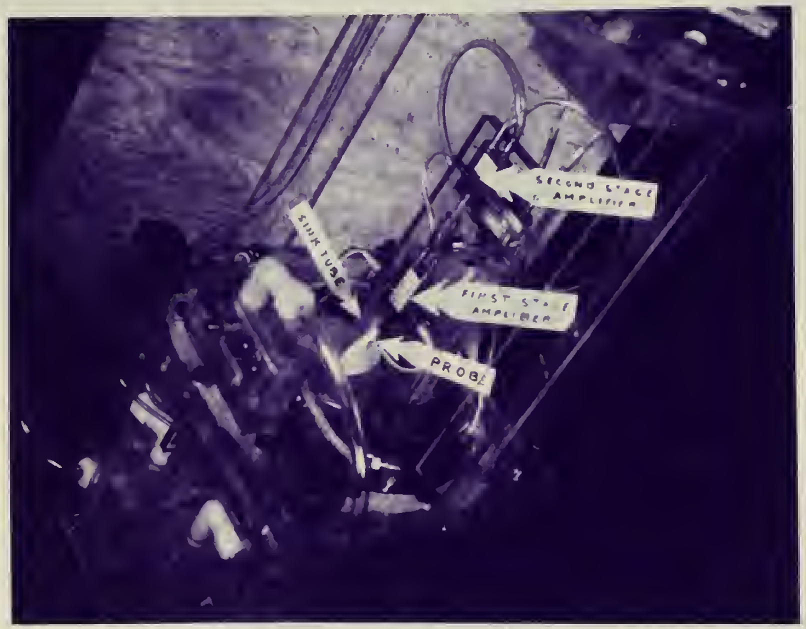

Figure D.1

Vortex Rate Sensor Showing Details of Signal Amplification

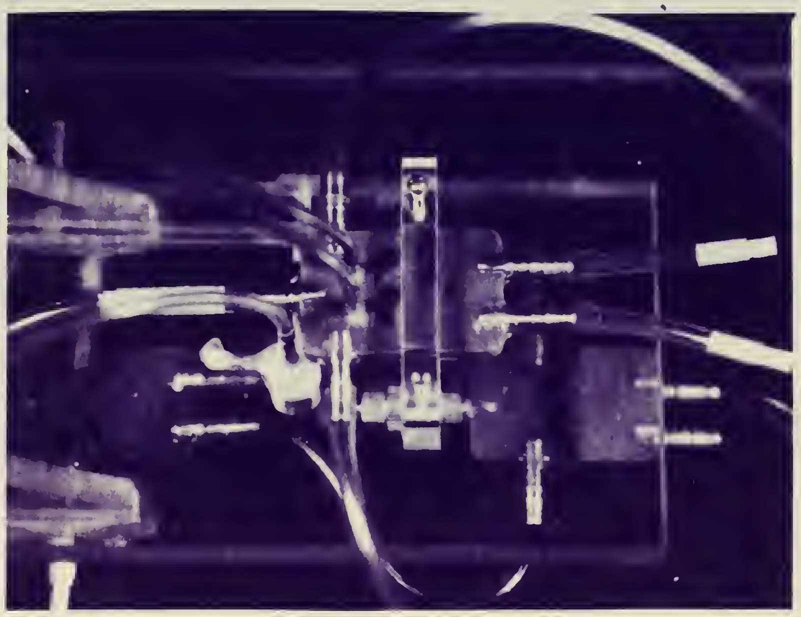

Figure D.2 Summer-Amplifier

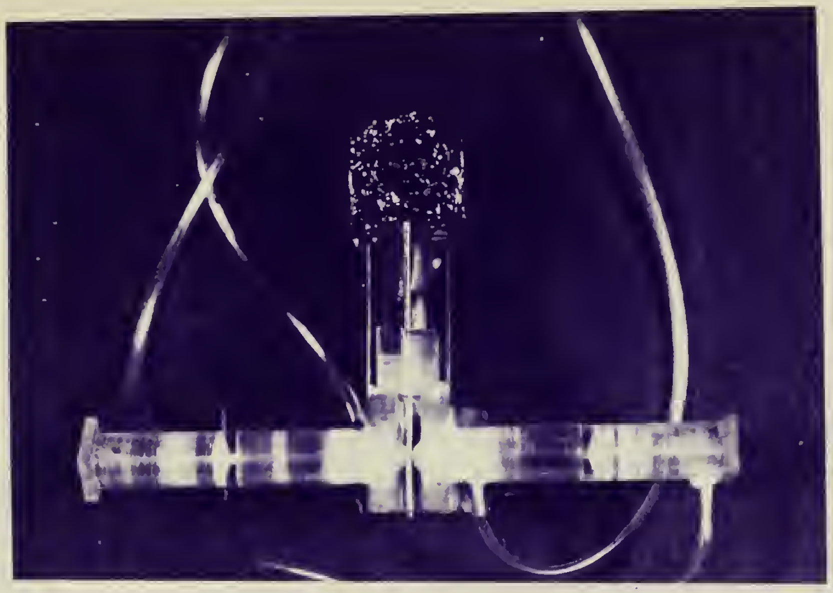

Figure D.3

Angular Position Sensor

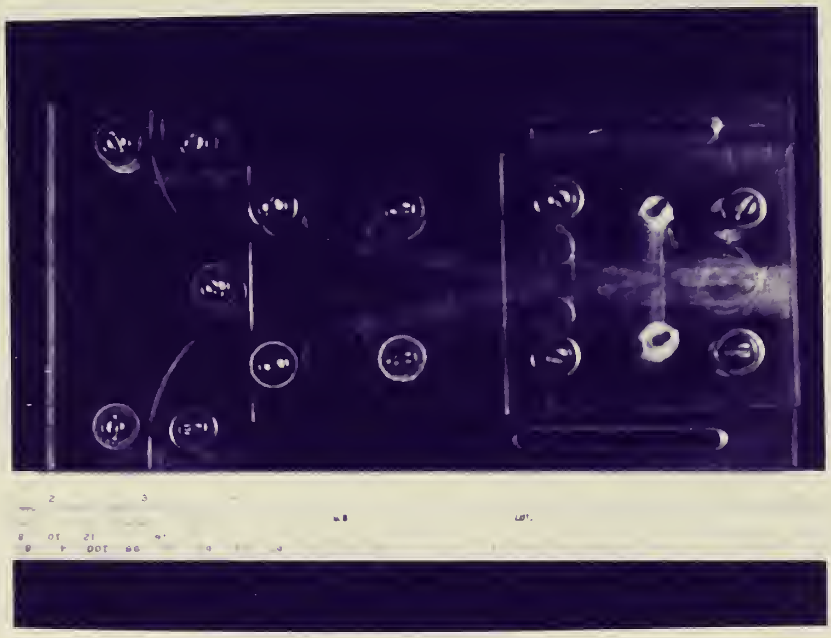

Figure D.4

Power Amplifier Cascade and Reaction Jets

BIBLIOGRAPHY

1. Gibson, J. E., Nonlinear Automatic Control, McGraw-Hill Book Company, New York, 1963.

2. Taplin, L. B. "Phenomenology of Vortex Flow and its Applications to Signal Amplification," Summer Engineering Seminars, Pennsylvania State University, Fluid Control Systems, July 6-16, 1965.

3. Taplin, L. B. and J. F. Hall, "Synthesis of a Pure Fluid Flight Control System," AIAA/ION Guidance and Control Conference, August 16-18, 1965.

4. Sarpkaya, S., "A Theoretical and Experimental Investigation of the Vortex-Sink Angular Rate Sensor," Proceedings of the Fluid Amplification Symposium, Volume 11, Harry Diamond Laboratories, Washington, D.C., October, 1965.

5. Dexter, E. M., "An Analog Pure Fluid Amplifier," Symposium on Fluid Jet Control Devices, ASME, November 28, 1962.

6. Belsterling, C. A. and K. Tsui, "A Proved Technique for Analyzing Proportional Fluid Amplifier Circuits," Control Engineering, August, 1965.

7. Boothe, W. A., "A Lumped-Parameter Technique for Predicting Analog Fluid Amplifier Dynamics," ISA Transactions, Vol. 4, No. 1, January, 1965.

8. Katz, S., J. M. Goto and R. J. Dockery, "Experiments in Analog Computation With Fluids," Proceedings of the Fluid Amplification Symposium, Volume 11, Harry Diamond Laboratories, Washington, D.C., May, 1964.

9. Bowles, R. E. and E. M. Dexter, "A Second Generation of Fluid System Applications," Proceedings of the Fluid Amplification Symposium, Volume 111, Harry Diamond Laboratories, Washington, D.C., October, 1965.

10. Blackburn, J. F., G. Reethof and J. L. Shearer, Fluid Power Control, The M.I.T. Press, Massachusetts Institute of Technology, Cambridge, Massachusetts, 1960.

11. Bowles Engineering Corporation, "Elements of Pure Fluid Systems," Loan Copy from Bowles Engineering Corporation, 1965.

12. Warren, R. W., "Bistable Fluid Amplifiers," Seminar on Fluid Amplification, The Catholic University of America, Washington, D.C., June 15-19, 1964.

13. Campagnulo, C. J., "A Three Stage Digital Amplifier," Proceedings of the Fluid Amplification Symposium, Volume I, Diamond Ordnance Fuze Laboratories, Washington, D.C., October, 1962.

14. Campagnulo, C. J. and L. M. Sieracki, "A Digital-Proportional Fluid Amplifier for a Missile Control System," Proceedings of the Fluid Amplification Symposium, Volume III, Harry Diamond Laboratories, Washington, D.C., October, 1965.

15. Hayes, W. F. and C. Kwok, "Impedance Matching in Bistable and Proportional Fluid Amplifiers Through the Use of a Vortex Vent," Proceedings of the Fluid Amplification Symposium, Volume I, Harry Diamond Laboratories, Washington, D.C., October, 1965.

16. Boothe, W. A. and J. N. Shinn," A Suggested System of Schematic Symbols for Fluid Amplifier Circuitry," Proceedings of the Fluid Amplification Symposium, Diamond Ordnance Fuze Laboratories, Volume I, Washington, D.C., October, 1962.

17. Warren, R. W., "Pulse Duration Modulation," Proceedings of the Fluid Amplification Symposium, Diamond Ordnance Fuze Laboratories, Volume 1, Washington, D.C., October, 1962.

18. Reilly, R. J. and F. A. Moynihan, "Notes on a Proportional Fluid Amplifier," Symposium on Fluid Jet Control Devices, ASME, November 28, 1962.

19. Peperone, S. J., J. Katz and J. M. Goto, "Gain Analysis of the Proportional Fluid Amplifier," Proceedings of the Fluid Amplification Symposium, Volume I, Diamond Ordnance Fuze Laboratories, Washington, D.C., October, 1962.

thesL608
Analysis and synthesis of a pure fluid s

3 2768 002 11881 2
DUDLEY KNOX LIBRARY